FINAL REPORT

The Detection and Discrimination of Small Munitions using Giant Magnetoresistive (GMR) Sensors

SERDP Project MR-1639

SEPTEMBER 2010

Janet E. Simms
Hollis H. Bennett, Jr.
Ricky A. Goodson
Tere A. DeMoss
Morris P. Fields
John C. Morgan
U.S. Army Engineer Research and Development Center

A Lloyd Riggs
Auburn University

Dwain K. Butler
Applied Geophysics Consultancy, LLC

REPORT DOCUMENTATION PAGE

Form Approved
OMB No. 0704-0188

PLEASE DO NOT RETURN YOUR FORM TO THE ABOVE ORGANIZATION.

1. REPORT DATE *(DD-MM-YYYY)* 01-09-2010	**2. REPORT TYPE** Final	**3. DATES COVERED** *(From - To)*

4. TITLE AND SUBTITLE
The Detection and Discrimination of Small Munitions using Giant Magnetoresistive (GMR) Sensors

5a. CONTRACT NUMBER

5b. GRANT NUMBER

5c. PROGRAM ELEMENT NUMBER

6. AUTHOR(S)
Janet E. Simms, Hollis H. Bennett, Jr., Ricky A. Goodson, Tere A. DeMoss, Morris P. Fields, John C. Morgan, Lloyd Riggs, Dwain K. Butler

5d. PROJECT NUMBER

5e. TASK NUMBER

5f. WORK UNIT NUMBER

7. PERFORMING ORGANIZATION NAME(S) AND ADDRESS(ES)
US Army Engineer Research and Development Center, 3909 Halls Ferry Road, Vicksburg, MS 39180-6199
Elec. and Computer Eng. Dept., 200 Brown Hall, Auburn University, AL 36849

8. PERFORMING ORGANIZATION REPORT NUMBER

9. SPONSORING/MONITORING AGENCY NAME(S) AND ADDRESS(ES)

10. SPONSOR/MONITOR'S ACRONYM(S)

11. SPONSOR/MONITOR'S REPORT NUMBER(S)

12. DISTRIBUTION/AVAILABILITY STATEMENT
Approved for public release; distribution is unlimited

13. SUPPLEMENTARY NOTES

14. ABSTRACT

This effort focused on characterizing the noise floor of giant magnetoresistive (GMR) sensors and evaluating their performance in detecting small (<81 mm) munitions. A GMR sensor allows data acquisition over a broadband frequency spectrum in a single coverage, thus providing the capability of measuring responses presently requiring both a magnetometer and frequency domain or time domain electromagnetic induction sensor. Both the Honeywell and NVE GMR sensors studied have similar operating range, sensitivity, and noise levels. The additional features available on the Honeywell sensors make them the GMR sensors of choice. The performance characteristics of a single GMR sensor were studied, both as a static magnetic field sensor and time domain electromagnetic induction field sensor. In passive mode, the GMR sensor, which has a resolution of less than 10 nT, performed similarly to a cesium vapor magnetometer. When tested in dynamic mode for measuring the response of a single-turn copper coil, multi-turn copper coil, and solid copper sphere, the GMR sensor measured a distinct decay response for each target.

15. SUBJECT TERMS

giant magnetoresistive sensor, GMR, small munitions, total field magnetometry

16. SECURITY CLASSIFICATION OF:			**17. LIMITATION OF ABSTRACT**	**18. NUMBER OF PAGES**	**19a. NAME OF RESPONSIBLE PERSON**
a. REPORT	**b. ABSTRACT**	**c. THIS PAGE**		69	Janet E. Simms
					19b. TELEPHONE NUMBER *(Include area code)* 601-634-3493

Reset

Standard Form 298 (Rev. 8/98)
Prescribed by ANSI Std. Z39.18

Table of Contents

List of Acronyms

AC	alternating current
A/D	analog-to-digital
CW	continuous wave
dB	decibel
DC	direct current
EM	electromagnetic
EMI	electromagnetic induction
f_O	break frequency
FS	full scale
G	gauss
GMR	giant magnetoresistive
Hz	hertz
$I_T(j\omega)$	frequency-dependent transmitter current
L	length
L_O	q-coil inductance
L_T	transmitter coil inductance
M_{OR}	magnetic coupling (mutual inductance) between the object and receiver
M_{TO}	magnetic coupling (mutual inductance) between the transmitter and object
M_{TR}	magnetic coupling (mutual inductance) between the transmitter and receiver
nT	nanoTesla
Oe	oersted
$Q(j\omega)$	q-coil response
r	radius
rms	root mean square
R_O	q-coil resistance
R_T	transmitter coil resistance
RPM	revolutions per minute
SERDP	Strategic Environmental Research and Development Program
SNR	signal-to-noise ratio
sps	samples per second
S/R	set/reset
UXO	unexploded ordnance
V	volt
$V_{OUT}\,(j\omega)$	q-coil output

List of Figures

List of Tables

Keywords

Giant Magnetoresistive Sensor, GMR, Small Munitions, Total Field Magnetometry

Acknowledgements

The authors would like to acknowledge Deepthi Gautam, PhD graduate student at Auburn University, for her efforts in assisting Dr. Lloyd Riggs with the laboratory study of the GMR sensors.

Executive Summary

The detection of small munitions is particularly difficult because of the fine spatial sampling required to detect them. The geophysical systems typically used for ordnance detection generally are not deployed in an array adequate for detecting small targets or do not have the necessary resolution. Giant magnetorisitive (GMR) sensors are small (order of one centimeter) and could be combined in a compact, lightweight array. This study focused on characterizing the fundamental capabilities of GMR sensors, particularly the noise floor, and determining the expected performance in terms of signal-to-noise at specified distances for a variety of munitions types.

GMR sensors manufactured by Honeywell and NVE were evaluated to identify differences in performance characteristics (sensitivity, bandwidth, saturation, hysteresis, etc.) and features. The sensors chosen to evaluate are the Honeywell HMC100x series and the NVE AA00x series. These GMR sensors have similar operating range and sensitivity specifications that are suitable for geophysical applications. Both the Honeywell and NVE GMR sensors tested exhibited similar noise levels and have a minimum detectable magnetic field change, i.e., sensitivity of approximately 24 μGauss rms (2.4 nT rms). Regardless of sensor type, there is a tradeoff between linear operating range (or dynamic range) and sensitivity; increased sensitivity is associated with decreased dynamic range. The sensitivity of a GMR sensor operating in passive mode can be enhanced by use of a flux concentrator (a strip of high permeability material that aids in channeling magnetic flux into the sensor).

The GMR sensors were evaluated for use as both static (magnetometer) and pulsed magnetic field measurements. As passive magnetometers, both the Honeywell and NVE sensors performed similarly and, performance-wise, there is no preference for one over the other. However, the Honeywell GMR sensor does offer two features which make it desirable, Set/Reset strap and OFFSET strap. These features aid with, among other things, improving linearity and sensor biasing. Also, Honeywell offers the HMR2300 Smart Digital Magnetometer, a three-component sensor, which incorporates the HMC100x GMR sensors. The HMR2300 package is compact and has an onboard analog-to-digital converter, serial interface, and selectable sample rate. The additional features the Honeywell sensors offer make it the preferred GMR sensor for magnetic measurements. For passive magnetic measurements, the HMR2300 is the chosen GMR sensor package. It is important to note that because of the signal attenuation feature offered by the Honeywell HMR2300, the *HMR2300 can only be used for passive measurements and not for active GMR measurements*.

It is shown that a GMR sensor can be used in active mode (pulsed or continuous wave), i.e., as a receiver sensor in combination with a coil transmitter, to measure the eddy current response of a target. The late-time response of a single-turn copper wire, multi-turn wire, and solid copper sphere were measured. Three distinct decay rates were observed. The sensitivity of a GMR sensor operating in active mode can be biased by using a static (permanent magnet) or time varying magnetic field, or combination of the two. It is important to note that measuring the eddy current response of ferrous targets with a GMR sensor is more difficult than measuring the eddy current response of non-ferrous targets because ferrous targets, in general, have a non-zero DC response. A ferrous target near the GMR sensor will upset the bias, making stable eddy current measurements more difficult. We did not explore ways to mitigate this problem, however a high-pass filter with a suitably low 3 dB cutoff frequency is a possible method for resolving this issue.

The Honeywell HMR2300 was used to collect static or passive total magnetic field measurements over four ordnance (20-mm projectile, 40-mm projectile, 60-mm mortar, and 81-mm mortar) and three clutter targets. The targets were oriented at azimuths of 0º and 60º, and dip angles of 0º, 28º down, and 62º up. The GMR sensor response is similar to that of other magnetometers. The GMR sensor has a resolution of approximately 7 nT, compared to 0.01 nT (at 1 second cycle rate) for a cesium vapor magnetometer. Measurements were acquired over two proximal 20-mm projectiles at two sensor-target separations (multiples of the target length L). At a horizontal separation of 1.0L, there is a slight indication in the positive signature response that two targets might be present. As the horizontal separation increases, two distinct dipole responses are observed as expected.

The performance of GMR sensors is comparable to magnetometers typically used for geophysical applications. The GMR sensor studied has a resolution < 7 nT, which is generally suitable for near-surface geophysical purposes. A unique feature of a GMR sensor is its ability to detect magnetic fields over a wide frequency range, from DC to several megahertz. Thus, a single GMR sensor is capable of measuring responses presently requiring both a magnetometer and a frequency domain or time domain electromagnetic induction sensor. Further research is required to evaluate the combined static and dynamic aspects of a GMR sensor, and to evaluate its use in arrays for unexploded ordnance discrimination and identification.

Abstract

This effort focused on characterizing the noise floor of giant magnetoresistive (GMR) sensors and evaluating their performance in detecting small (≤ 81 mm) munitions. The munitions were positioned (a) with no influence from other objects, (b) close to each other in a horizontal plane, and (c) vertically over another. A GMR sensor allows data acquisition over a broadband frequency spectrum in a single coverage, thus providing the capability of measuring responses presently requiring both a magnetometer and a frequency domain or time domain electromagnetic induction sensor. Both the Honeywell and NVE GMR sensors studied have similar operating range, sensitivity, and noise levels. The additional features available on the Honeywell sensors make them the GMR sensors of choice. The performance characteristics of a single GMR sensor were studied, both as a static magnetic field sensor (magnetometer) and time domain (continuous wave or pulsed) electromagnetic induction magnetic field sensor. In passive mode, the GMR sensor, which has a resolution of less than 10 nT, performed similarly to a cesium vapor magnetometer. When tested in dynamic mode for measuring the response of a single-turn copper coil, multi-turn copper coil, and solid copper sphere, the GMR sensor measured a distinct decay response for each target. Further research is needed to test a GMR sensor for (1) measuring ferrous targets in dynamic mode, (2) simultaneously acquiring static and dynamic magnetic field measurements, and (3) array configurations in both passive and dynamic modes.

Objective

The focus of this study is to characterize the fundamental detection capabilities of giant magnetoresistive (GMR) sensors. In particular, the noise floor and signal-to-noise ratio of GMR sensors available from NVE and Honeywell are investigated. Because of their extremely wide bandwidth, a GMR sensor can be used as a magnetometer to measure the earth’s magnetic field (passive mode) or to measure the magnetic field produced by a transient or continuous wave magnetic source (active mode). Our intent is to measure, in both passive and active modes, the response of canonical targets (loops, spheres, cylinders, etc.) and standard UXO in different orientations and at different target-to-sensor distances, so as to thoroughly characterize the sensitivity and overall utility of GMR sensors.

Background

Recent advances in inversion algorithms for the discrimination and identification of UXO suggest that data density on a grid scale less than 10 cm is necessary for more reliable inversion results, particularly for the smaller UXO. The cost and size of geophysical sensors typically employed for UXO detection surveys tend to prohibit their placement at a relatively small spacing. The implementation of giant magnetoresistive (GMR) sensors may be the solution to this data acquisition dilemma. These sensors measure approximately 0.5 cm by 0.2 cm and can be placed millimeters apart. The small size and low power requirements of the GMR sensor makes it well suited for array applications. The close spacing allowed by these sensors presents an opportunity to study the detection and discrimination of munitions, and munitions proximal to one another, both horizontally and vertically, which have overlapping signatures.

The GMR sensor exploits thin-film magnetic technology. GMR films have two or more magnetic layers separated by a non-magnetic layer. These layers are on the order of a few nanometers thick. The alternating layers allow magnetic modulation of the electron spin in the materials. The GMR phenomenon is a result of a large decrease in the electrical resistance when a magnetic field is applied to the films and the spin dependence of conduction electrons in the magnetic materials. GMR sensors directly detect the magnetic field rather than the rate of change in magnetic field. They can detect magnetic fields over a wide frequency range—from DC to several megahertz. Thus, *a single GMR sensor is capable of measuring responses presently requiring both a magnetometer and a frequency domain or time domain electromagnetic induction (EMI) sensor*. Multi-axis data can be obtained by orienting the sensors along the three principal axes. GMR gradiometer sensors are also available. The cost of a single GMR chip is less than $10, and the cost per chip is even less if bought in bulk quantity, so cost is not a limiting factor when constructing arrays.

Over the past 20 years the use of GMR sensors has been incorporated into a variety of applications, including the detection of magnetic ink for validating currency and documents, medicine (sensing body position, biological diagnostics, biological assays), vehicle detection, magnetic stripe reading, crack/corrosion detection in materials, and subsurface detection. Applications to subsurface detection primarily have been focused on the detection of landmines/UXO (SERDP; Dalichaouch et al., 2003; Dalichaouch et al., 2004) and subsurface water (McGlone, 1998). The presentation of data relative to UXO detection with GMR sensors ERDC is sparse. This effort addresses smaller ordnance (≤ 81 mm) which is typically found at shallow depths.

Preliminary measurements were conducted to become familiar with some of the fundamental operating characteristics of GMR sensors. Described below is a method for using a GMR sensor to measure the continuous wave (CW) eddy current response of a simple wire loop (sometimes referred to as a q-coil). It will be shown that *we have been able to use an NVE GMR sensor to measure the eddy-current response of a simple q-coil to within 2% of its exact theoretical value.* Figure 1 shows a schematic diagram of the experimental setup along with a digital photograph of the test equipment. The HP-89410A vector signal analyzer forms the heart of the measurement system. The analyzer is programmed to provide excitation in the form of a periodic chirp over the frequency range from 500 Hz to 10 kHz. The analyzer's source feeds the power amplifier (instrument with yellow front panel) which in turn drives current through the 1-m × 1-m transmitter coil. A Tektronix current probe is used to measure the transmitter coil current and its output feeds channel 1 of the analyzer. Channel 2 of the analyzer is used to measure the amplified GMR output. The oscilloscope is only used to monitor the transmitter coil current and GRM output voltage and does not affect the measurement in any way.

Referring to Fig. 2, the GMR sensor (this experiment uses a NVE AA004-02 Bridge sensor – see www.NVE.com) is placed at the approximate center of the 1-m × 1-m transmitter coil. Shown near the GMR is a small permanent magnet that is used to bias the sensor part way up its output curve (Fig. 3). The GMR sensor output is amplified by an instrumentation amplifier (INA118/BB) according to the circuit shown in Fig. 4. The 9-volt battery provides power to the GMR and instrumentation amplifier. A q-coil (30-cm circumference 18 AWG copper loop), whose eddy-current response is to be measured, is shown placed beneath the GMR sensor (Fig. 2).

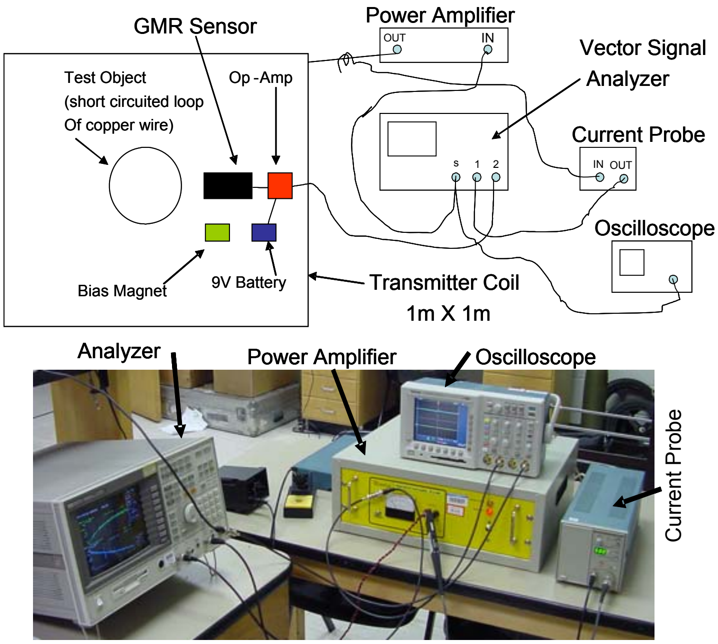

Figure 1. Schematic diagram and of the experimental setup used to measure the q-coil response with a GMR sensor.

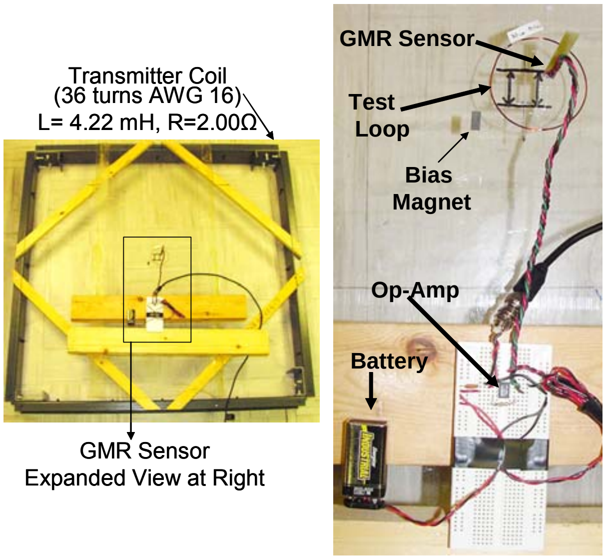

Figure 2. Photograph showing the GMR sensor (positioned at approximately the center of the 1-m × 1-m transmitter coil), bias magnet, operational amplifier, and 9-volt battery power supply. The copper test loop can be seen in the expanded view at the right just below the GMR sensor.

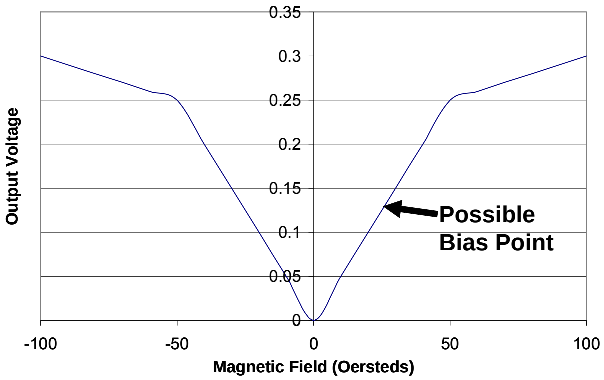

Figure 3. Representative GMR response characteristics.
For the experiments conducted here the bias point is achieved by placing a small permanent magnet near the GMR sensor.

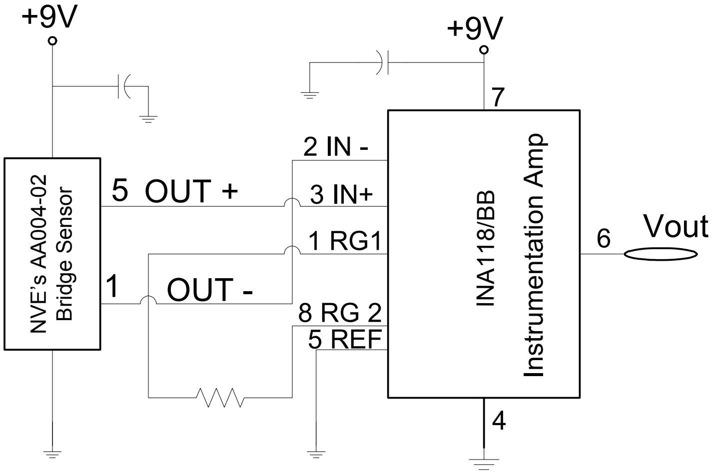

Figure 4. Circuit diagram showing instrumentation amplifier connected to the GMR sensor.

The circuit diagram in Fig. 5 can be used to develop the frequency domain transfer function for the q-coil. Under the assumption of weak magnetic coupling between transmitter and q-coil and between q-coil and GMR sensor, the q-coil output can be written:

$$V_{OUT}(j\omega) = \frac{j\omega M_{TO} M_{OR} I_T(j\omega)}{R_O + j\omega L_O} + M_{TR} I_T(j\omega) \quad , \tag{1}$$

or equivalently

$$\frac{V_{OUT}(j\omega)}{I_T(j\omega)} = \frac{j\omega M_{TO} M_{OR}}{R_O + j\omega L_O} + M_{TR} \quad , \tag{2}$$

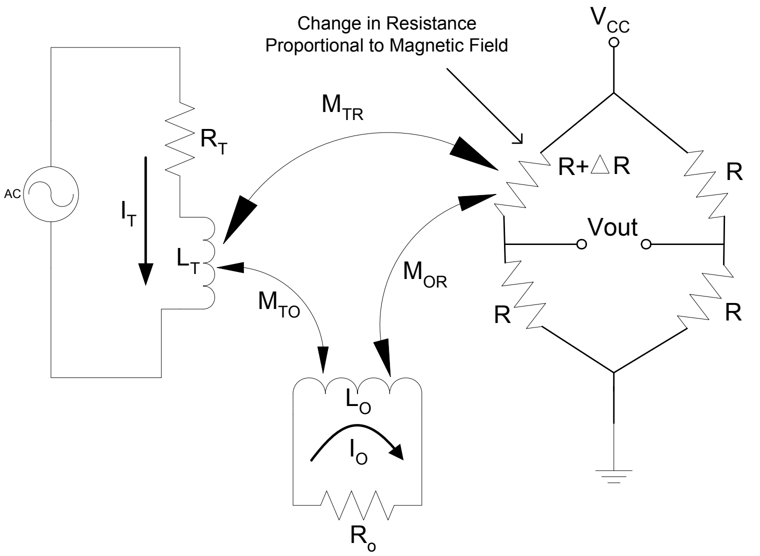

Figure 5. Circuit diagram of the electromagnetic induction system shown in Fig. 2. The GMR sensor is represented by the bridge circuit on the right.

where M_{TO}, M_{OR}, and M_{TR} represent magnetic coupling (mutual inductance) between the transmitter and object, object and receiver, and transmitter and receiver, respectively. R_O and L_O are the q-coil's resistance and inductance, respectively, and $I_T(j\omega)$ is the frequency-dependent transmitter current.

The transmitter current decreases with increasing frequency (single pole low-pass response) according to

$$I_T(j\omega) = \frac{V_S(j\omega)}{R_T + j\omega L_T} \quad , \tag{3}$$

where R_T and L_T are the transmitter coil resistance and inductance, respectively. The objective of the experiment is to measure only the q-coil's response, which is

$$Q(j\omega) = \text{q-coil response} = \frac{j\omega}{R_O + j\omega L_O} \quad . \tag{4}$$

According to Eq. 2, in the absence of a target

$$\frac{V_{OUT}(j\omega)}{I_T(j\omega)} = M_{TR} \quad , \tag{5}$$

since $M_{TO} = M_{OR} = 0$.

Procedurally, $\frac{V_{OUT}(j\omega)}{I_T(j\omega)}$ is measured in the absence of a target and then stored in the analyzer's memory. Next, with the target in place, the analyzer is programmed to subtract the no-target measurement (Eq. 5) from the target-plus-no-target measurement (Eq. 2) yielding

$$\frac{V_{OUT}(j\omega)}{I_T(j\omega)} = \frac{j\omega M_{TO} M_{OR}}{R_O + j\omega L_O} \ , \tag{6}$$

a quantity with the same frequency dependence as Eq. 4. It is a simple matter to manipulate Eq. 6 into the form

$$\frac{V_{OUT}(j\omega)}{I_T(j\omega)} = \frac{M_{TO} M_{OR}}{L_O} \frac{j\frac{f}{f_O}}{1 + j\frac{f}{f_O}} \ . \tag{7}$$

In the vernacular of electrical system theory, Eq. 7 is referred to as a high-pass filter term and $f_O = R_O/(2\pi L_O)$ is the break frequency where the magnitude of the response is 3 dB below its high frequency asymptotic value of $M_{TO}M_{OR}/L_O$. At the break frequency, f_O, the real and imaginary parts of Eq. 7 are equal and therefore the phase must be 45 degrees.

Figure 6 shows the analyzer output with the q-coil in place near the GMR sensor after subtracting the no-target response. The upper curve (green) is the amplitude response while the lower curve (blue) is the phase response. Note that the marker (small triangle) is placed at the 45 degree phase point (f_O in Eq. 7) which occurs at 3,132 Hz. The 20-cm circumference 18 AWG copper q-coil's inductance L_O and resistance R_O can be computed from simple formulas (see for example *Antenna Theory and Design* by Stutzman and Thiele, pages 74 and 75), leading to a theoretical break frequency of 3,173 Hz. *Therefore, our measurement is within 1.3% of the exact theoretical value*! The experience gained during this effort allows us to proceed with confidence toward the goal of detecting small, shallow munitions.

Several remarks are in order regarding the experiment described above. To measure the response of the q-coil it was necessary to subtract the no-object response from the response with the q-coil in place, essentially removing (or at least minimizing) direct coupling between the transmitter and GMR sensor from the measurement. This is certainly not the only method, or necessarily the best method, of eliminating direct coupling. Alternatively, one can arrange the transmitter coil in such a way so that at some position a field "null" will exist. One such arrangement used by others (see for example www.Geophex.com) is shown in Fig. 7. Here the GMR would be placed at the center of the coils (at the null position). In the absence of a target, the data acquisition computer would be programmed to adjust the coil bias currents so as to produce zero output from the GMR sensor. After zeroing, each subsequent measurement should (theoretically) be caused by the object's eddy current response. A deep null (i.e., a value of

Magnitude and Phase Response of a 20 cm Circumference
18 AWG Wire Loop (Q-Coil)

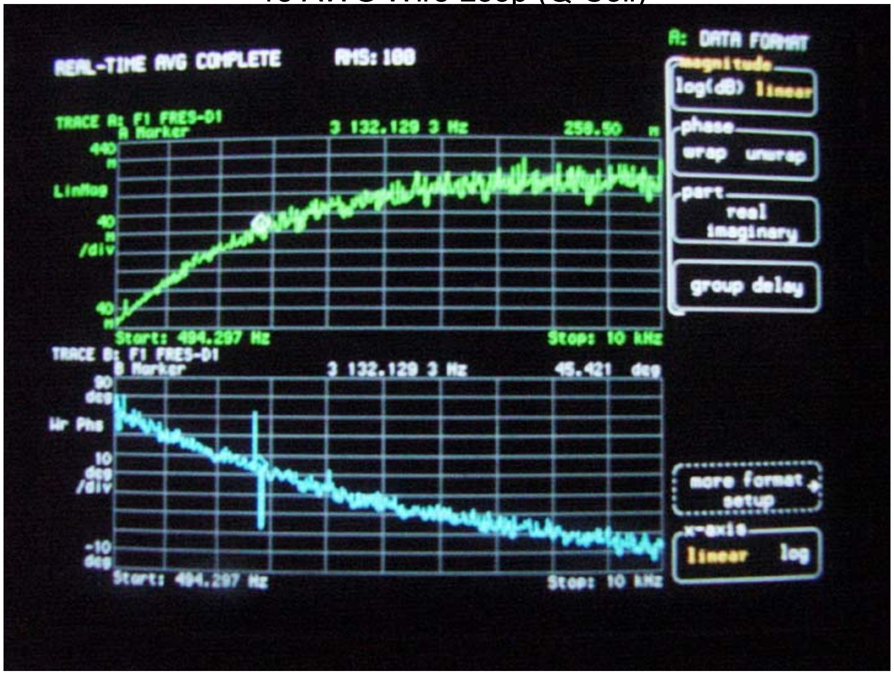

Figure 6. Measured response of a 20-cm circumference 18 AWG copper loop (q-coil). Top curve (green) is the magnitude response while the bottom curve (blue) is the phase response. The measured q-coil response shows high-pass characteristics with a measured 3 db frequency (or 45 degree phase frequency) of 3,132 Hz (location of triangular marker). The measured 3 db frequency is within 1.3% of the theoretical value. The spikes in the phase (bottom) response near the triangular marker are caused by harmonics of the line frequency (N×60) or some other interference signal.

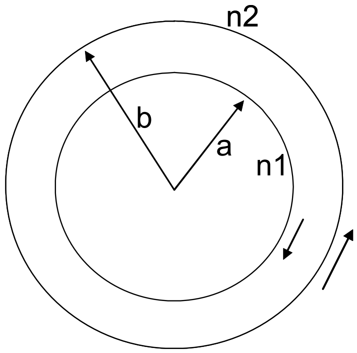

Figure 7. Transmitter coil designed to produce a null field at the center of the two coils. The null field is produced by properly adjusting the turns ratio of the two coils n2/n1 and the ratio of their radii b/a. The currents in the two concentric loops must flow in opposite directions.

magnetic field at the center of the coils that is very small in comparison to the amplitude of magnetic field being measured) is required to achieve good sensitivity, and a deep null can only be achieved through careful control of the bias currents. Therefore, the data acquisition computer would need a digital-to-analogue converter with sufficient resolution (a 12 or 16 bit DA would probably suffice) to produce a very small field at the center of the transmitter coils.

Materials and Methods—GMR Sensors

A typical GMR sensor and its functional block diagram are shown in Fig. 8. An applied magnetic field along the sensitive axis of the sensor (parallel to the length of the ruler in Fig. 8) will lower the resistance of the two unshielded resistors resulting in a differential output voltage between pins 1 and 5 that is proportional to the applied magnetic field. If necessary, amplification of the detected signal can be provided using a signal conditioning circuit like the one depicted in Fig. 9.

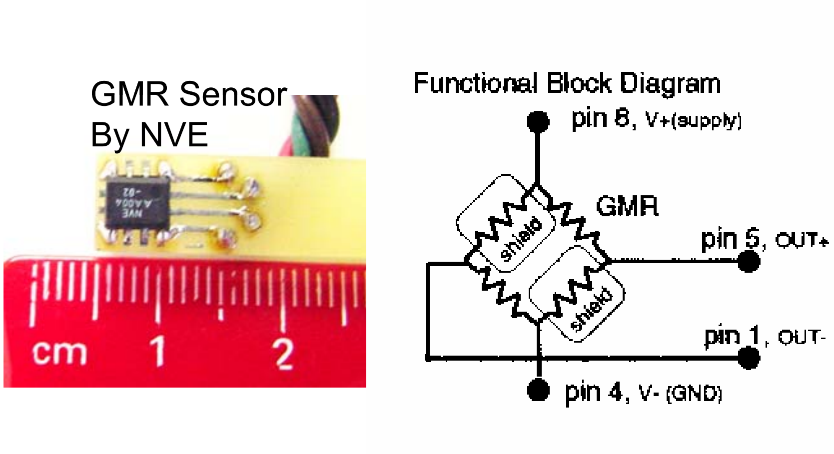

Figure 8. GMR sensor manufactured by NVE (www.nve.com) and corresponding functional block diagram.

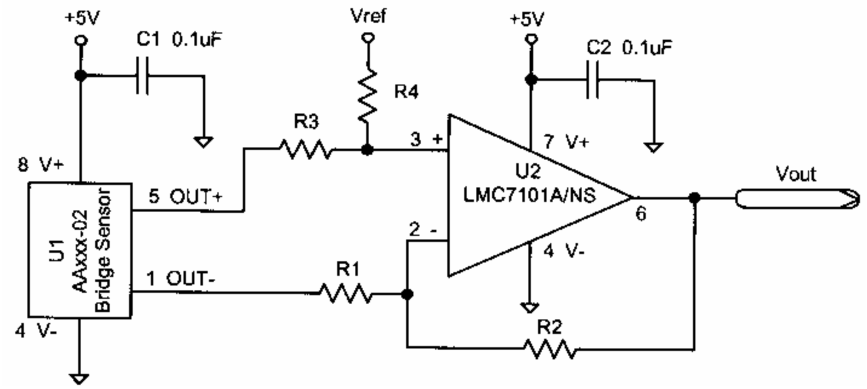

Figure 9. Signal conditioning circuit used to amplify signals received by a GMR sensor. (Taken from NVE Sensor Engineering and Application Notes (9-10-98 revision).doc revised – 9/10/98; www.nve.com.)

The two primary providers of GMR sensors are Honeywell and NVE. The performance of the NVE and Honeywell sensors is compared and measured in terms of overall sensitivity, signal-to-noise ratio, bandwidth (probably not much of an issue with either sensor), dynamic range, versatility, ease of use, and costs. The Honeywell and NVE sensors are tested in both the dynamic (CW and pulsed) and static operational modes. As discussed above, an important issue with CW operation is how effectively the direct coupling between the transmitter and GMR sensor can be canceled. It is anticipated that the Honeywell sensors, with their on-chip Set/Reset and OFFSET straps, may have an inherent advantage over the NVE sensors for CW operation. In the pulsed operational mode it is necessary to take a careful look at dynamic range issues. For example, the EM-63 manufactured by Geonics Ltd. can, in a suitably quiet electromagnetic environment, measure the eddy current response of a target over 5 orders of magnitude (from 10,000 mV to 0.1 mV). The EM-63's performance could serve as a bench mark against which to compare both the NVE and Honeywell GMR sensors. This effort will lead to a decision on whether or not the GMR sensor can be operated in a combined dynamic/static mode, or whether it will need to operate in one mode or the other.

Regarding the anticipated success of the proposed effort, precedence exists indicating that the GMR sensor and flux-gate magnetometers are similar. According to McGlone (1998)

> "The basic result is that both instruments are very similar in that they are about the same size, they have similar minimum resolution, the vector response is about the same, the SNR appears similar; the only significant difference is the much greater frequency response of the SCIMAG (GMR sensor). And the SCIMAG is likely to be considerably less expensive."

Furthermore, Dalichaouch et al. (2003, 2004) have successfully developed a GMR system to measure the in-phase and quadrature components of low metallic content landmines (CW system). Their work demonstrates that it is definitely possible to buck out the direct coupled field using small coils located near the sensor and driven by a voltage controlled current source. It appears however, that GMR sensors have not been successfully employed in time domain electromagnetic induction (EMI) systems, and so an opportunity exists to further the state of the art in this area.

Honeywell GMR Sensors

There are six Honeywell GMR sensors that would be suitable for use in geophysical surveying. Table 1 lists their operating characteristics. The HMC1001 is a single axis magnetic sensor, whereas the HMC1002 is a two-axis sensor. Similarly, the HMC1021 and HMC1022 are single and dual axis sensors, respectively. The primary differences between these four GMR sensors are their range and sensitivity. The HMC2003 is a three-axis hybrid sensor, incorporating the HMC1001 and HMC1002. The HMR2300 Smart Digital Magnetometer is a three-axis sensor that also incorporates the HMC1001 and HMC1002. It includes a RS-232 or RS-485 serial interface, 16-bit A/D converter, and has a selectable sample rate of 10 to 154 samples per second. The block diagram (Honeywell, 2004) in Fig. 10 shows the configuration of the HMC-1001 and HMC-1002 sensors in the HMR2300.

Table 1. Honeywell GMR sensor characteristics (taken from Honeywell literature, http://www.ssec.honeywell.com/magnetic/products.html).

Part Number	**Field Range (Gauss[1])**		**Sensitivity (mV/V/Gauss[1])**		**Maximum Linearity Error (% FS[2])**	**Maximum Hysteresis (% FS[2])**	**Maximum Operating Temp. (ºC)**	**Bridge Resistance (Ohms)**
	Min	Max	Min	Max				
HMC1001	-2	+2	2.5	4.0	0.5	0.1	150	1200
HMC1002	-2	+2	2.5	4.0	0.5	0.1	150	1200
HMC1021	-6	+6	0.8	1.25	0.05 (typical)	0.08 (typical)	150	1300
HMC1022	-6	+6	0.8	1.25	0.05 (typical)	0.08 (typical)	150	1300
	Field Range (Gauss[1])		**Sensitivity (V/Gauss[1])**		**Maximum Linearity Error (% FS[2])**	**Maximum Hysteresis (% FS[2])**	**Maximum Operating Temp. (ºC)**	
	Min	Max	Min	Max				
HMC2003	-2	+2	0.98	1.02	2	0.1	85	
HMR2300	-2	+2	NA	NA	0.5	0.02	85	

[1] In SI, 1 Tesla=10^4 Gauss

[2] FS=full scale, total applied field

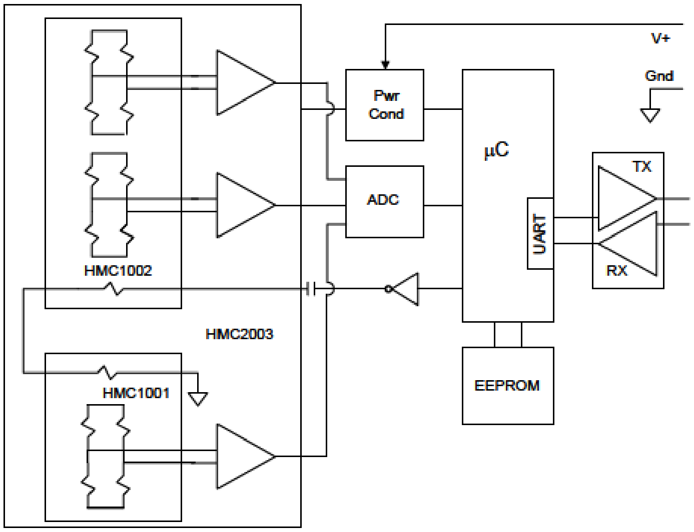

Figure 10. Block Diagram for Honeywell HMR2300.

The Honeywell GMR sensor has two features that may be particularly useful. Firstly, the Honeywell GMR sensor has a Set/Reset (S/R) strap that can be pulsed with a high current to: 1) force the sensor to operate in the high sensitivity mode, 2) flip the polarity of the output response curve, and 3) be cycled during normal operation to improve linearity and reduce cross-axis and temperature effects. Secondly, it provides an OFFSET strap that allows: 1) cancellation of an unwanted magnetic field, 2) setting the bridge offset to zero, 3) using the bridge output to drive the OFFSET strap to cancel out the field being measured in a closed loop configuration, and 4) auto-calibrating the system by adjusting the bridge current gain. Feature (3) associated with the OFFSET strap is particularly attractive. According to Honeywell,

> "In this mode of operation the GMR's output amplifier is connected to a current source that drives the OFFSET strap. Using high gain and negative feedback in the loop will drive the GMR bridge output to zero. This method gives extremely good linearity and temperature characteristics. The idea here is to always operate the GMR bridge in the balanced resistance mode. *That is, no matter what magnetic field is being measured, the current through the OFFSET strap will cancel it out.* The bridge always "sees" a zero field condition. The resultant current used to cancel the applied field is a direct measure of that field strength and can be translated into the field value."

NVE GMR Sensors

Table 2, taken from the NVE literature, can be used to compare the performance of a number of different AA-series and AAH-series GMR sensors offered by NVE. This table is quite instructive and indicates some of the important engineering trade-offs faced in the selection of a GMR sensor for a particular application. Note especially the columns labeled Linear Range (Oe) and Sensitivity (mV/V-Oe). (One Oersted (Oe) is equal to one Gauss in air. The earth's magnetic field is about 0.5 Gauss.) Of the AA-series sensors, the AA0002-02 GMR has the highest sensitivity, but the lowest linear range. This is a general characteristic among GMR sensors, with the sensors having a higher sensitivity exhibiting a narrower linear range. Note further that the AAH series (H stands for high) has very high sensitivity compared to the AA series, but has a linear range much smaller than a typical AA series GMR sensor.

GMR sensors offered by Honeywell perform similarly to those offered by NVE. In particular, the Honeywell HMC1001/1002 has a typical sensitivity of 3.2 mV/V/Gauss, which is comparable to NVE's AA002-02 (see Table 2). The Honeywell HMC1021/1022 has a sensitivity of 1mv/V/Gauss and, as expected, a wider linear range than the HMC1001/1002 (Table 1).

Table 2. NVE GMR sensor characteristics (taken from NVE literature, www.NVE.com).

Magnetometers									
Part Number	**Linear Range (|Oe[1]|)**		**Sensitivity (mV/V/Oe[1])**		**Maximum Nonlinearity (% Uni.[2])**	**Maximum Hysteresis (% Uni.[2])**	**Maximum Operating Temp. (ºC)**	**Typical Resistance (Ohms)**	**Package**
	Min	Max	Min	Max					
AA002-02	1.5	10.5	3.0	4.2	2	4	125	5K	SOIC8
AA003-02	2.0	14	2.0	3.2	2	4	125	5k	SOIC8
AA004-00	5.0	35	0.9	1.3	2	4	125	5K	MSOP8
AA004-02	5.0	35	0.9	1.3	2	4	125	5K	SIOC8
AA005-02	10.0	70	0.45	0.65	2	4	125	5K	SIOC8
AA006-00	5.0	35	0.9	1.3	2	4	125	30K	MSOP8
AA006-02	5.0	35	0.9	1.3	2	4	125	30K	SIOC8
AAH002-02	0.6	3.0	11.0	18.0	6	15	150	2K	SIOC8
AAH004-00	1.5	7.5	3.2	4.8	4	15	150	2K	MSOP8
AAL002-02	1.5	10.5	3.0	4.2	2	2	150	5.5K	SIOC8
Gradiometers									
	Linear Range (|Oe[1]|)		**Resistor Spacing (mm)**		**Maximum Nonlinearity (% Uni.[2])**	**Maximum Hysteresis (% Uni.[2])**	**Maximum Operating Temp. (ºC)**	**Typical Resistance (Ohms)**	**Package**
	Min	Max							
AB001-02	20	200	0.5		2	4	125	2.5K	SOIC8
AB001-00	20	200	0.5		2	4	125	2.5K	MSOP8
ABH001-00	5	40	0.5		4	15	150	1.2K	MSOP8

[1] Oersted (Oe) = 1 Gauss in air

[2] Unipolar operation means exposure to magnetic fields of one polarity, for example 0 to +30 Guass, or -2 to -50 Guass. Bipolar operation (for example, -5 to +10 Guass) will increase nonlinearity and hysteresis.

Results and Discussion of GMR Sensor Characteristics

Noise Comparison of the Honetwell HMC1021Z and NVE AA004-02

In this section we address noise and signal-to-noise ratio (SNR) measurements with GMR sensors. Several good references are available on the general topic of noise including chapters in the book *Noise Reduction Techniques in Electronic Systems* by Ott (Chapters 8 and 9) (Ott, 1976) and *The Art of Electronics* by Horowitz and Hill (Chapter 7) (Horowitz and Hill, 1999). Also, Honeywell provides a brief discussion on GMR noise on page 6 of their application note titled *1- and 2-Axis Magnetic Sensors HMC1001/1002HMC1021/1022* (http://www.magneticsensors.com/datasheets/hmc1001-2_1021-2.pdf).

Based on the theory presented in the above three references, measurements were made of noise and SNR for several different GMR sensors, including the AA004-02 manufactured by NVE and the HMC1021Z manufactured by Honeywell. It should be noted that these two sensors have nominally the same sensitivity, approximately 1 mV/V/Gauss.

In the experimental set up shown schematically in Figure 11, the HP 89410A Vector Network Analyzer is used to drive current through the transmitter coil, which in turn applies an excitatory magnetic field at the location of the GMR sensor. The strength of the magnetic field at the position of the GMR sensor can be adjusted by adjusting the strength of the source voltage at port S of the analyzer. Output from the GMR sensor is amplified with gain=100 by the Burr-Broun INA118 instrumentation amplifier and then measured on channel B of the analyzer. Sources of noise in the experimental setup include noise from the GMR sensor, as well as noise contributed by the amplifier.

Using an NVE AA004-02 GMR sensor, a noise voltage output of 2.4 µV rms was measured with the sensor disconnected from the input to the amplifier, while with the GMR connected a noise voltage of 14.0 µV rms was measured, indicating that the GMR sensor, as expected, is the dominate contributor to the output noise (by 15 dB=20log$_{10}$(14/2.4)). The measurement was made with a continuous wave source set to a nominal frequency of 5 kHz using a measurement bandwidth of 5 kHz.

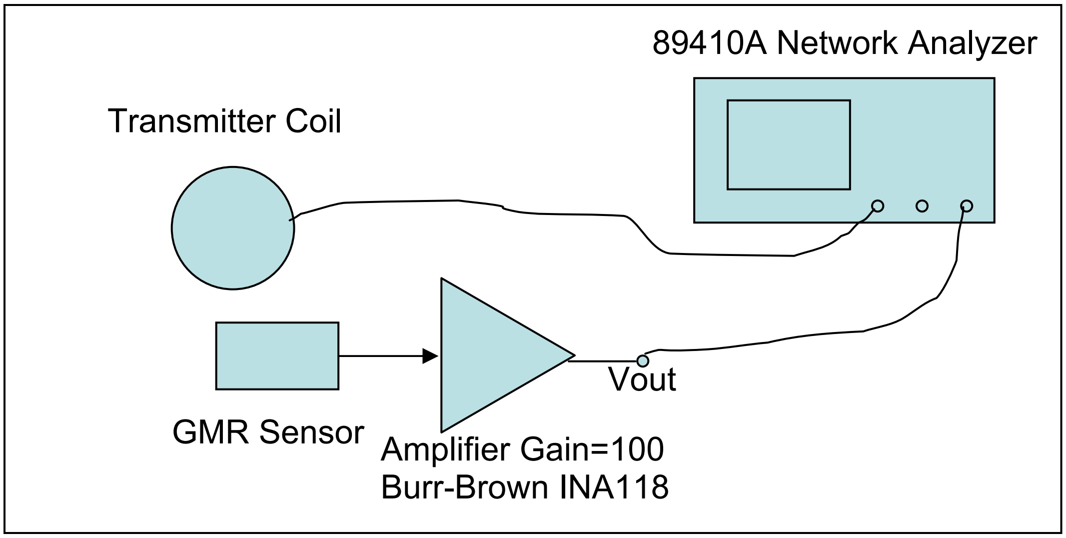

Figure 11. Experimental setup to evaluate noise and SNR of GMR sensors.

Knowing the sensitivity of the GMR and the gain of the amplifier, one can easily compute the input magnetic field strength that will provide a given SNR. For this study we assume that a minimum SNR of 2 is necessary for reliable detection. First, we take the output noise voltage with the GMR sensor connected and divide by the amplifier gain (100) to determine an equivalent input noise of 14.0 µV rms /100 = 140 nV rms. This value can be expressed in terms of magnetic field strength by dividing by the nominal sensitivity of the GMR sensor, yielding 11.7 µGauss rms (=140 nV rms ÷12 mV/Gauss). (Note that the sensitivity of the GMR sensor must be multiplied by the power supply voltage 12 V.) Finally, we can conclude that the noise floor of the GMR sensor plus amplifier combination (referred to the input) is around 12 µGauss rms. This results in a minimum detectable magnetic field of 24 µGauss rms (2.4 nT rms) at 5 kHz (assuming a SNR of 2 and a measurement bandwidth of 5 kHz).

The above measurements were repeated by replacing the NVE AA004-02 GMR sensor with the Honeywell HMC1021Z, which has a nominal sensitivity of 1 mV/V/Gauss (same as the NVE AA004-02). Noise amplitudes measured with the HMC1021Z were very close to those measured for the NVE AA004-02 indicating that, for a minimum acceptable SNR of 2, both sensors have a minimum detectable magnetic field of approximately 24 µGauss rms (2.4 nT rms). The earth's magnetic field of nominally 0.5 Gauss (50,000 nT) is 20,833 times larger (86 dB) than the minimum detectable field of 24 µGauss rms (2.4 nT rms) for the HMC1021Z and AA004-02 GMR sensors.

Sensitivity of the Honeywell HMC1001 and NVE AAH002

A comparison was made of the sensitivity of the Honeywell HMC1001 and NVE AAH002 GMR sensors. These sensors have a greater sensitivity, but reduced range than those used in the noise comparison. Based on design attributes, one would expect the HMC1001 to saturate at a higher field strength, but be less sensitive than the AAH002. Each GMR sensor was connected to the same instrumentation amplifier (fixed gain of 100) and the sensor output voltage was measured with an oscilloscope with a fixed vertical sensitivity setting (1V/division). A small permanent magnet was moved along the sensitive axis of each sensor and the output voltage recorded (Fig. 12). Observe that the HMC1001 just begins to register a deflection on the oscilloscope when the magnet is about 70-cm away (Fig. 12a). The AAH002 begins to register a deflection on the oscilloscope when the magnet is about 150-cm away (Fig. 12b)–more than twice the distance as that for the HMC1001. Observe further that the AAH002 saturates at around 0.225 volts, whereas the HMC1001 saturates at around 3 volts. Again we observe that increased sensitivity is associated with decreased linear operating range (or dynamic range.)

Using flux concentrators to enhance the sensitivity of a GMR sensor. One way to enhance the sensitivity of a GMR sensor is to use what is referred to as a flux concentrator. A flux concentrator is a strip of high permeability material that aids in channeling magnetic flux into the sensor. Figure 13 shows a GMR sensor (NVE AA002-02) fixed between two boards with two flux concentrators, 0.64-cm (0.25-in.) wide by 6.35-cm (2.5-in.) long, positioned along the sensitive axis of the GMR. It is important that the end of the flux concentrator be in contact with the end of the GMR, as even a small gap may significantly compromise performance. Notice the small magnet fixed with putty in Fig. 13 (left side) that is used to bias the sensor in the middle of its linear region. With no flux concentrators, and using a 5.08-cm (2-in.) diameter ferrous sphere as a target, we were able to just detect the ferrous sphere at a distance of 15.24 cm (6 in.) directly above the GMR. The detection distance doubled to 30.48 cm (12 in.) when the flux concentrators were in place. We then increased the length of the flux concentrator to a little over 7.62 cm (3 in.) (still 0.64-cm (0.25-in.) wide), but observed little improvement in overall sensitivity.

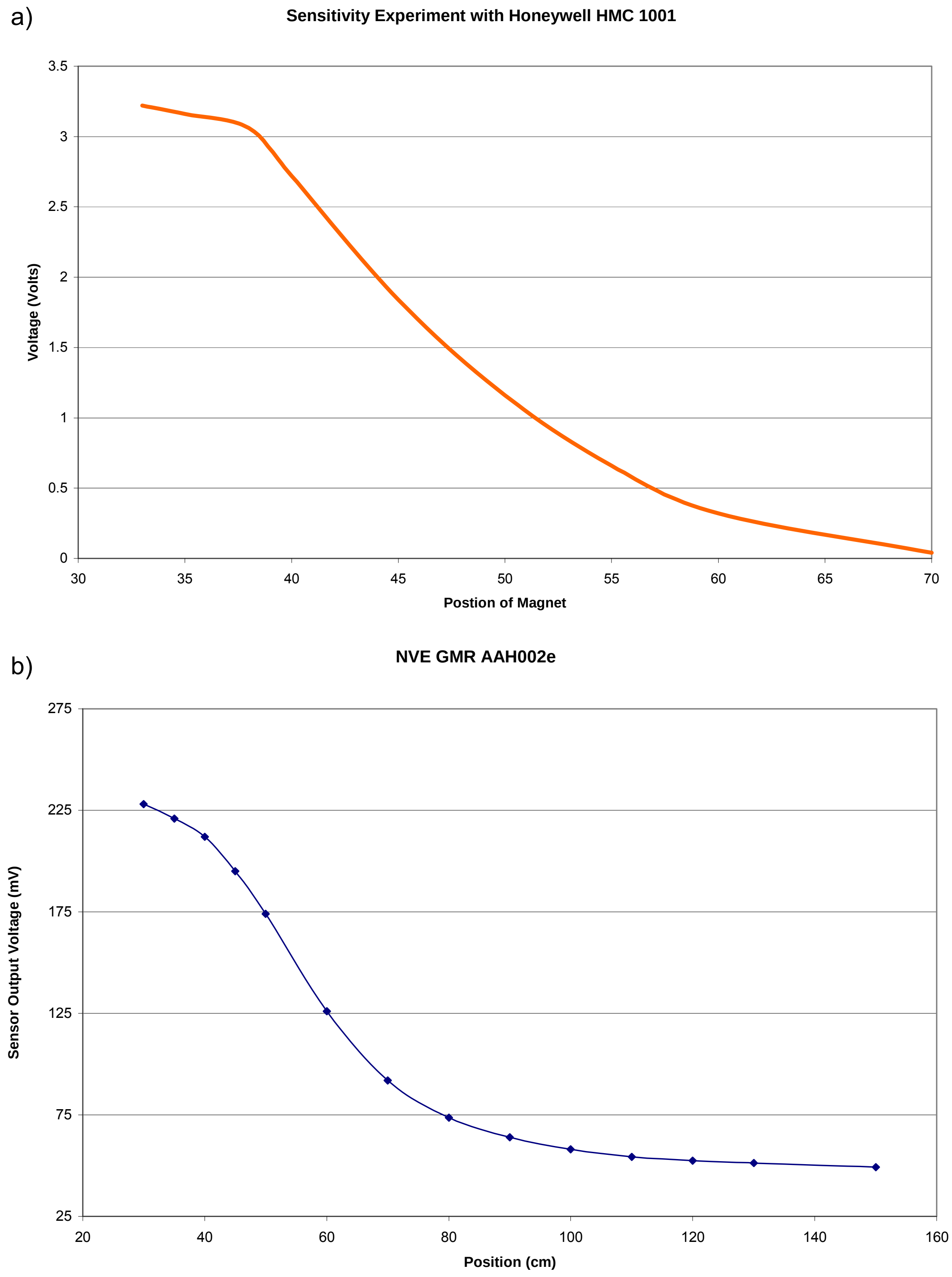

Figure 12. Output voltage as a function of distance a small magnet is from a (a) Honeywell HMC1001 and (b) NVE AAH002e GMR sensor. The magnet is moved along the sensitive axis of the sensor.

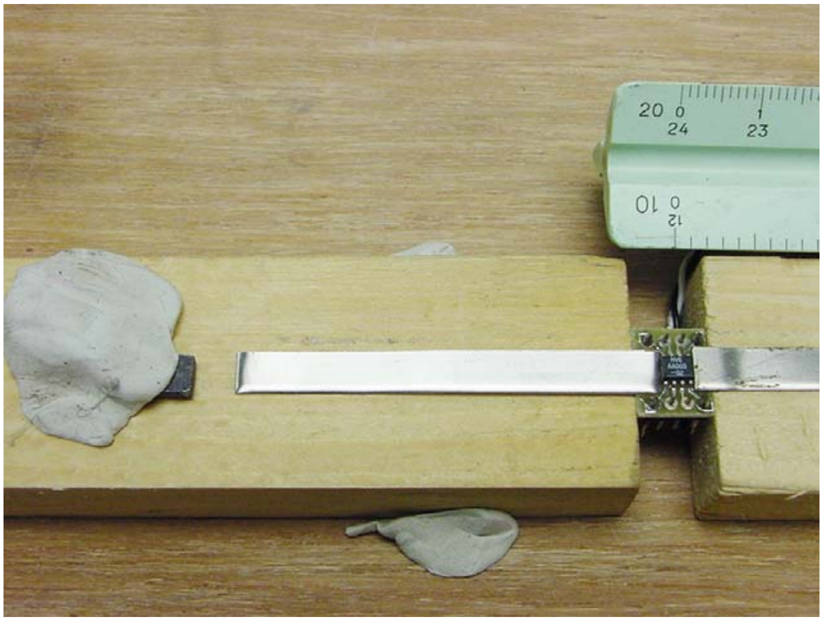

Figure 13. GMR sensor with flux concentrator and small magnet to bias the sensor. The flux concentrator serves to enhance the sensitivity of the GMR over what could be achieved without the flux concentrator.

Hysteresis and Latch-up in GMR Sensors

Two observations made during the experiments described above are worth discussing. As the small permanent magnet is moved back and forth along the sensitive axis of the sensor, and fairly close to the sensor (about 10 to 15 cm), it is easy to observe a deflection of the oscilloscope trace. However, the output voltage of the GMR will saturate if the magnet gets too close to the GMR. In other words, the GMR output voltage will reach some maximum value (less than that of the power supply) when the magnet is a given distance from the sensor, but moving the magnet even closer will not result in a further increase in GMR output voltage. (Note that this effect is not caused by saturation of the GMR preamplifier since the maximum GMR output voltage observed is less than the supply voltage!) Essentially, this means that the magnetic field at the sensor is large enough to "push" the sensor out of its linear operating range (linear part of the sensor's characteristic curve in Fig. 3). Furthermore, after the GMR sensor has been pushed into saturation and then the magnet removed to a location further from the sensor, the measured voltage will not return to the value observed when the magnet was previously at the same position. This phenomenon is referred to as hysteresis – the GMR sensor "remembers" that it was earlier forced into saturation.

The second observation involves the extreme case when the GMR sensor is pushed "hard" into saturation. When this occurs, the sensor may "latch-up", meaning that its output voltage remains fixed independent of the position of the magnet. Once latch-up has occurred, the sensor can usually be returned to its original linear operating state by forcing a large magnetic field through the sensor in the opposite direction to the magnetic field that caused the sensor to latch-up. It has been observed that certain GMR sensors can be permanently damaged by exposing them to very strong magnetic fields. This situation was observed only for the most sensitive NVE GMR sensor, the AAH002. Latch-up is a common problem with GMR sensors, but fortunately it can be easily corrected by momentarily exposing the sensor to a strong magnetic field of the proper polarity. The Honeywell GMR sensors have a set/reset pin on the GMR IC that can be conveniently used to reset (fix latch-up) the GMR. In the case of a NVE GMR sensor, a small external coil placed near the sensor can be used to force a reset.

Using a GMR Sensor in Active Mode—Measuring the Eddy Current Response of a Copper Wire Loop (q-coil)

The discussion so far has focused on the use of the GMR sensor as a magnetometer or as a static earth's magnetic field sensor (passive mode). In this section we examine the possibility of using a GMR sensor in active mode, i.e., to measure the eddy current response of a target under pulsed magnetic field excitation. Figure 2 shows the setup used. Short pulses of current are driven into the transmitter coil (instead of a CW signal as was done for the data presented in the "Background" section) and, once properly biased (i.e., so that the range of input magnet fields do not saturate the sensor) by the small permanent magnet, the GMR sensor is used to measure the total magnetic field. The total magnetic field is that resulting from the transmitter current flowing in the transmitter coil, plus that from eddy currents induced into any nearby target. Since the eddy current response of a target will usually persist long after the transmitter current "turns off," the late time response recorded by the GMR sensor should be that caused by only the eddy currents induced in the target. Note that the GMR sensor is oriented so as not to be influenced by the earth's magnetic field.

A NVE AA003 (similar operating characteristics as the AA002) sensor was used with the experimental setup described above to measure the eddy current response of a 30-cm circumference 18 AWG copper loop. The loop response should be in the form of a pure exponential decay with a time constant equal to the ratio of loop inductance to loop resistance. Since the response is exponential ($e^{(-t/\tau)}$, where τ is a time constant), the GMR voltage plotted using a logarithmic ordinate and linear abscissa scale should be a straight line. As observed in Fig. 14, the measured loop response is indeed linear, indicating that the GMR sensor does a good job capturing the late time loop response.

The same experimental setup was also used to measure the eddy current response of a 5.08-cm (2-in.) diameter solid copper sphere and a multi-turn wire loop. The late time response of all three targets is displayed in Fig. 15. Three distinct decay rates are observed from the three non-ferrous targets. Thus, the GMR sensor is able to measure the late time response with sufficient fidelity to facilitate discrimination.

It is important to note that measuring the eddy current response of ferrous targets with a GMR sensor is more difficult than measuring the eddy current response of non-ferrous targets. The reason for this is that ferrous targets, in general, have a non-zero DC response. A ferrous target near the GMR sensor will upset the bias, making stable eddy current measurements more difficult. It may be possible to AC couple the output of the GMR sensor to the preamplifier to help mitigate this problem; however, this was not attempted.

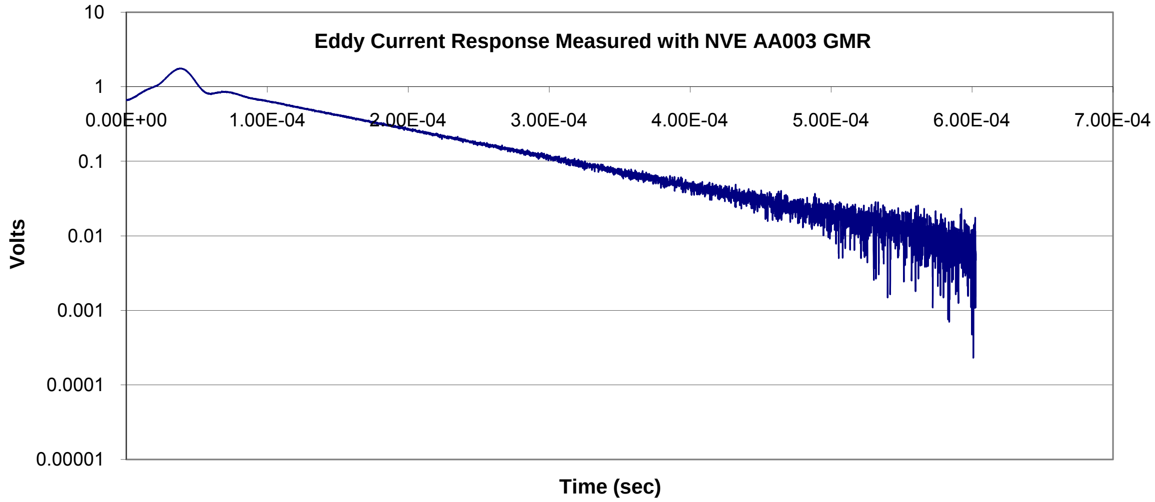

Figure 14. Eddy current response of a wire loop (q-coil) measured using a NVE AA003 GMR sensor. The late time response of the wire loop is of the form of a decaying exponential and should therefore be a straight line when plotted using a logarithmic ordinate and linear abscissa axis.

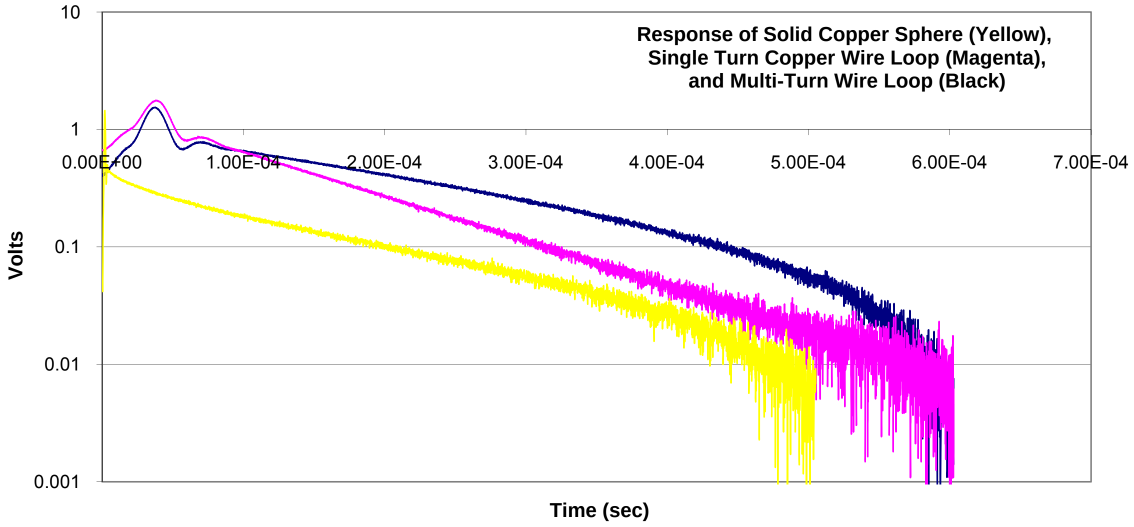

Figure 15. Eddy current response of a wire loop, multi-turn coil, and 5.08-cm (2-in.) diameter copper sphere measured using a NVE AA003 GMR sensor. The late time response of the wire loop is of the form of a decaying exponential and should therefore be a straight line when plotted using a logarithmic ordinate and linear abscissa axis. Note that the three targets have distinct decay rates, indicating that the response measured with the GMR sensor has sufficient fidelity to be used for purposes of discrimination.

Nonlinear biasing of a GMR sensor to enhance sensitivity. One interesting observation made during the course of this research was that increased sensitivity could be achieved by biasing the GMR sensor using a combination of static and time varying magnetic fields. Figure 16 depicts the general setup where a small permanent magnet and multi-turn loop are proximal to a GMR sensor. The magnet serves to bias the sensor part way up its response curve, while the coil simultaneously provides an alternating sinusoidal magnetic field. A target (not shown in Fig. 16) near the GMR sensor will perturb the biasing so that at a negative or positive peak of the alternating field the sensor will either be biased very near zero or where the GMR sensor saturates. In either case, the GMR will essentially rectify the input sinusoidal component of the magnetic field. The oscilloscope trace of the GMR output voltage (lower trace) corresponding to three different target positions is shown in Fig. 17. The change in GMR sensor response from Fig. 17a to Fig. 17c is a result of the target getting closer to the GMR sensor and the sensor is driven further into saturation or nonlinear operation.

Consider the following example of the increased sensitivity over the linear biasing technique provided by the nonlinear biasing method described above. Using the Honeywell HMC1001 GMR sensor statically biased (without any AC biasing), a small magnet target could be just detected at approximately 10 cm from the sensor. Using the same HMC1001 GMR sensor, but this time with both static and dynamic biasing (10 kHz sine wave driving current into the biasing coil), the same small magnet target could be just detected at 34 cm from the sensor. In this experiment, the nonlinear biasing technique results in more than a three-fold increase in detection distance over the standard linear static biasing technique.

Figure 16. Configuration for non-linear biasing of a GMR sensor. A small magnet biases the GMR sensor part way up the linear portion of its operating curve (see Fig. 3). The coil adds further CW (AC) biasing so that any small perturbation of the biasing conditions causes a large change in GMR sensor output voltage.

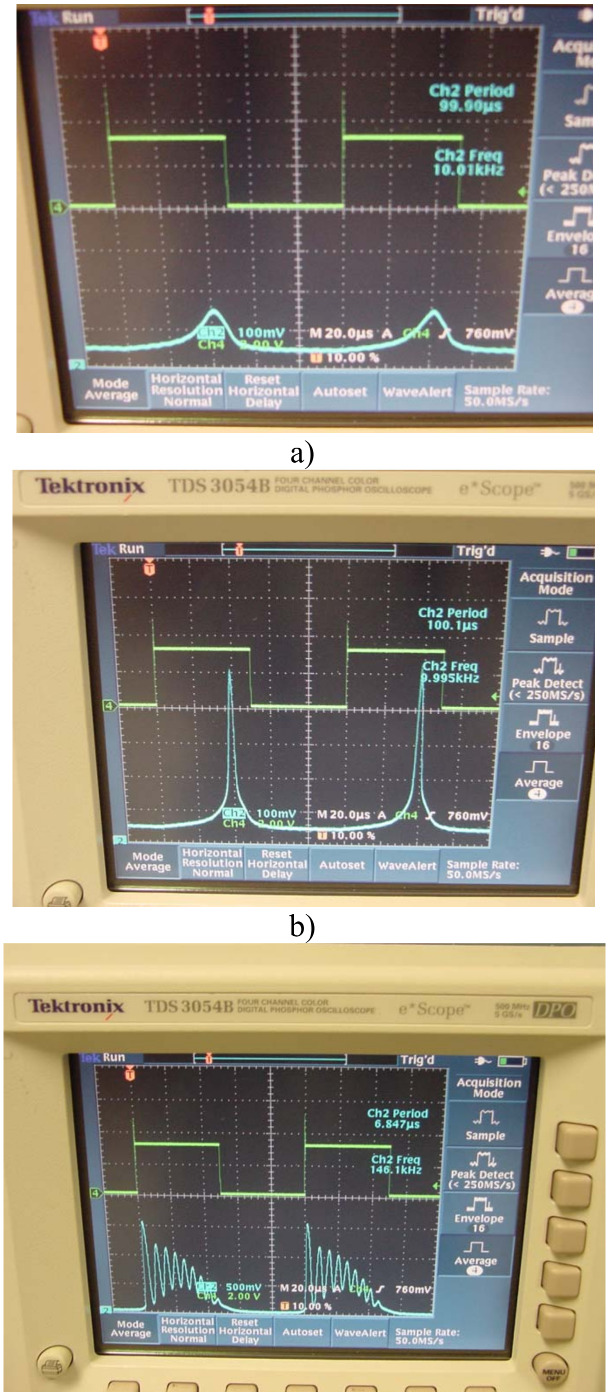

a)

b)

c)

Figure 17. Oscilloscope output when the target is at different distances from the GMR sensor: a) close, b) closer, and c) closest. The GMR sensor was nonlinearly biased resulting in a significant increase in sensitivity over what could be achieved with linear biasing methods. In all photos, the top curve is the AC nonlinear drive voltage, and the bottom curve is the GMR sensor response.

Influence of the primary magnetic field. As discussed previously with reference to Fig. 7, the magnetic field generated by the transmitter may need to be reduced to a small (relative to the magnitude of the field being measured) value at the location of the GMR sensor. An appropriately designed transmitter coil could be used to provide the required null at the location of the sensor. If CW excitation is chosen, a small biasing coil (for the NVE GMR sensors) or an appropriately adjusted nulling current through the offset strap (for a Honeywell GMR sensor) could be used to cancel (or buck out) the primary magnetic field.

Final Sensor Selection

Passive mode. After evaluating the various features among the NVE and Honeywell GMR sensors and doing some preliminary measurements, our research indicates that the HMC1001/1002 housed in the Honeywell HMR2300 Smart Digital Magnetometer is a good choice for investigating the *passive* mode sensitivity of GMR sensors. The HMR2300 is a microcontroller-based smart sensor with a range of ±2 Gauss with less than 7 nT resolution (the average strength of the earth's magnetic field is on the order of 50,000 nT). The HMR2300 can be easily interfaced with a laptop PC for data acquisition purposes. The HMR2300 employs three of Honeywell's magnetoresistive sensors oriented in orthogonal directions to simultaneously measure the x-, y-, and z-vector components of the magnetic field. These sensor outputs are converted to 16-bit digital values using an internal delta-sigma A/D converter. Data output is serial full-duplex RS-232 or half-duplex RS-485 with 9600 or 19,200 data rates (we used the RS-232 mode of operation). Other convenient features of the HMR2300 include: 1) Zero Reading Command – a magnetic reading is stored in the microcontroller and this value is subtracted from subsequent readings as an offset (this feature is useful for nulling the earth's field before anomaly detection); 2) Set/Reset Command – this function generates a current/magnetic field pulse to each sensor to realign the permalloy thin film magnetization, thus insuring maximum output sensitivity by canceling out any temperature drift effects; 3) Average Command – fluctuations in the magnetic readings can be reduced by averaging which provides a low-pass filter effect on the output readings; 4) Output Sample Rates – the sample rate can be varied from 10 samples per second (sps) to 154 sps. A faster sample rate can be used provided the data is transferred in binary rather than ASCII; and 5) Input Signal Attenuation – magnetic signals being measured will be attenuated based on the sample rate selected. At the default rate of 20 sps, the instrument has a 3 dB point of 17 Hz. The digital filter inside the HMR2300 is the combination of a comb filter and a low pass filter. This provides a linear phase response with a transfer function that has zeros in it. When the 10 or 20 sps rate is used (default), the zeros are at the line frequencies of 50 and 60 Hz and therefore magnetic fields at power frequencies will not corrupt the measurement.

It is important to understand that because of input signal attenuation (feature (5) described above), the *HMR2300 can only be used for passive measurements and not for active GMR measurements*. In an active mode, pulsed or CW, much greater bandwidth is required so the GMR preamplifier must be configured accordingly.

Active mode. From a noise or sensitivity perspective, there is no compelling reason to choose the Honeywell GMR sensor over the NVE sensor. However, from an ease of implementation perspective, the Honeywell HMC100x series GMR sensors, with their patented set/reset and offset terminal pairs, offer an advantage over the simpler NVE GMR sensors.

Overall sensor selection. We have observed that the noise performance of the NVE and Honeywell GMR sensors are equivalent. Honeywell offers basically four raw (without support electronics) GMR sensors: the HMC1001 (single axis measurement) and HMC1002 (dual axis measurement) GMR, each with nominal 3.2 mV/V/Gauss sensitivity, and the HMC1021 (single axis measurement) and HMC1022 (dual axis measurement) GMR, each with nominal 1.0 mV/V/Gauss sensitivity. In comparison, with the exception of the AAH002-02, the sensitivities of the GMR sensors available from NVE are nominally equivalent to those available from Honeywell. Although the AAH002-02 has high sensitivity (nominally 14 mv/V/Gauss), it is less linear and suffers increased hysteresis in comparison to other NVE (and Honeywell) GMR sensors. Our experimentation also showed that the AAH002-02 could be permanently damaged, beyond normal latch up, by high intensity magnetic fields.

From the perspective of sensitivity and noise performance alone, there is no compelling reason to choose Honeywell GMR sensors over those offered by NVE. On the other hand, the Honeywell GMR sensors have certain features that are not available with the NVE GMR sensors. The NVE GMR sensors are simple 4-terminal bridge devices (two power terminals (plus and ground) and two output terminals), whereas the Honeywell GMR sensors have two additional terminal pairs over the usual power and bridge output pairs (namely the set/reset and offset pairs). By driving a pulse of current through the set/reset pairs, the sensor can be recovered from latch up conditions and linearly can be restored. By driving a steady current through the offset terminal pairs, the sensor bias point can be conveniently altered or, as discussed above, a feedback arrangement can be used in conjunction with the offset pins to always operate the sensor at a null field. With this latter arrangement, the feedback current needed to null the sensor is a direct measurement of the magnetic field along the sensitive axis of the sensor. The NVE GMR sensors do not have the convenient set/reset and offset features available with the Honeywell GMR sensors. For this reason, we recommend that future research efforts focus on using GMR sensors available from Honeywell.

Materials and Methods—Test Stand Data Collection

Data Acquisition Procedures

The free-air test stand located at the ERDC was used to collect the GMR sensor passive mode datasets. The test stand is aligned with magnetic north. The Honeywell HMR2300 Smart Digital Magnetometer was used to acquire the data. Ordnance ranging in size from 20 mm to 81 mm obtained from the APG standard set[1] were studied. Measurements over a steel sphere and ordnance scrap were also collected. Figures 18 and 19 show photographs of the ordnance and clutter targets, respectively. Measurements were acquired over a grid that encompassed the response of the target and background, with the targets oriented at two azimuths and two dip angles, and at different sensor-target distances. Table 3 lists the azimuth, dip, and depth combinations at which data were acquired, and Table 4 lists the specific sensor-target

---

[1] APG standard set is a set of standardized munitions that have the same model type, configuration, and relative magnetism to each other.

separations. For the 20 mm, these measurements were collected over the target alone and with other targets proximal to it, both horizontally and vertically. The 81-mm mortar was too long to rotate it at 0.5L and 1.0L separations, so shorter sensor-target separations were used. However, a

Figure 18. Photographs of ordnance used in study.

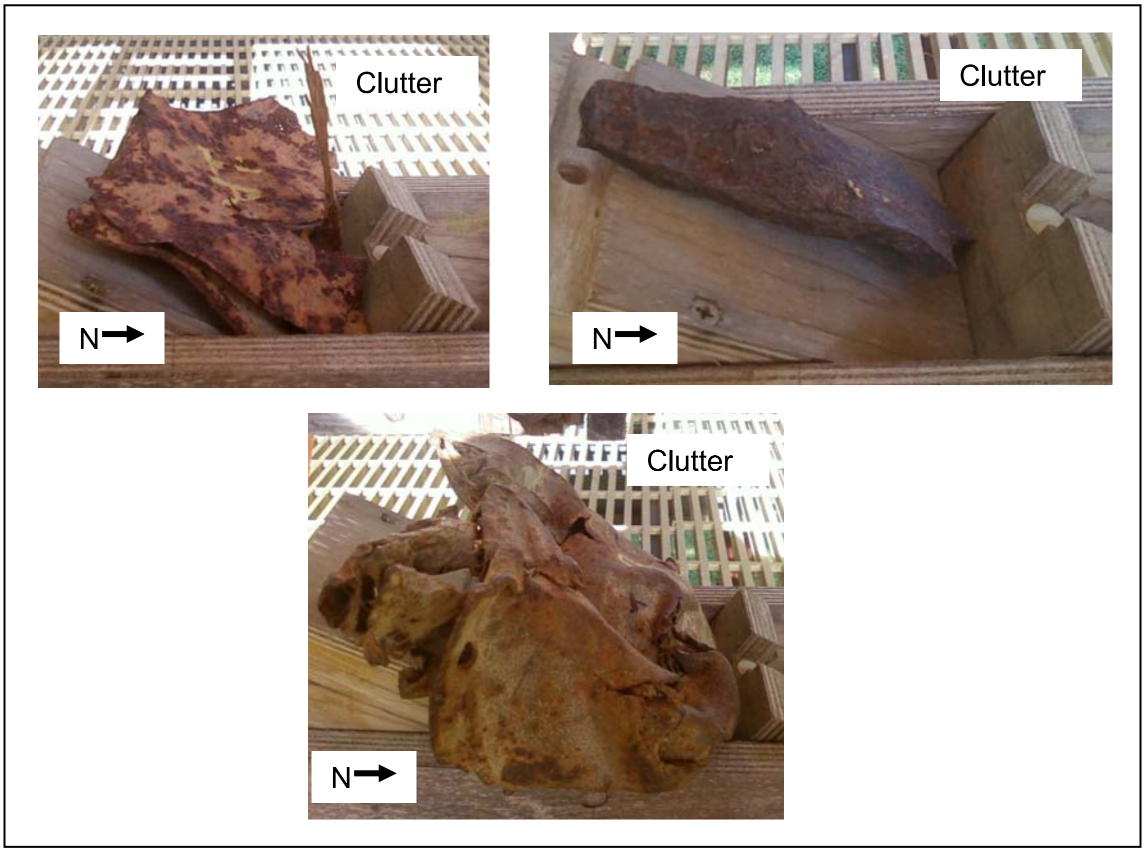

Figure 19. Photographs of side view of clutter targets positioned on target holder.

Table 3. Target orientation and relative separation distances used during data acquisition.

Azimuth[1] (deg)	Dip[2] (deg)	Relative Sensor-Target Separation[3]
0	0, 28, -62	20mm, 40mm, 60mm, clutter: 0.5L, 1.0L 81mm: 10cm, 15cm, 21cm
60	0, 28, -62	20mm, 40mm, 60mm, clutter: 0.5L, 1.0L 81mm: 10cm, 15cm, 21cm

[1] Relative to magnetic north

[2] Relative to horizontal, positive downward

[3] L is the length of the target

Table 4. Target parameters and actual sensor-target separations (0.5L, 1.0L).

Target	Length (L) (cm)	Diameter or Width (cm)	Thickness (cm)	0.5L (cm)	1.0L (cm)	Aspect Ratio
20-mm Projectile	7.5	2.0	--	3.75	7.5	0.27
40-mm Projectile	18.0	4.0	--	9.0	18.0	0.22
60-mm Mortar	24.5	6.0	--	12.25	24.5	0.25
81-mm Mortar	49.0	8.1	--	--[4]	--[4]	0.17
Clutter1	10.0[1]	11.5[2]	3.0[3]	5.0	10.0	1.15
Clutter2	12.5[1]	5.0[2]	0.75[3]	6.25	12.5	0.4
Clutter3	20.0[1]	15.0[2]	9.0[3]	7.5	15.0	0.75

[1] Length of the north-south axis of the clutter target as it was positioned on the target holder during data collection.

[2] Width of the east-west axis of the clutter target as it was positioned on the target holder during data collection.

[3] Typical thickness of the clutter target.

[4] 81-mm sensor-target separations were 10 cm, 15 cm, and 21 cm.

separation of 21 cm is close to the actual 0.5L of 24.5 cm. Regarding the choice of dip angles (28º and -62º), we had intended to align the targets in the direction of the earth's field (62º down) for maximum response and perpendicular (28º up) to the field for minimum response. This orientation would have agreed with that of the SERDP UX-1380 data collect. However, there was confusion regarding terminology so the GMR sensor data in this study was acquired using dip angles of 62º up and 28º down, rather than 62º down and 28º up.

Data collection on the test stand was performed using a standard routine with only minor modifications to account for sensor differences. The routine includes daily setup, warm up, background collect, data collect, background collect, and break down. At the beginning of the day, the sensors are set up on the test stand and secured to the shuttle (used to transport the sensor over the grid) (Fig. 20). Any wireless or wired data/control lines to and from the test stand are installed at this time. Once the sensor is set up, it is turned on and allowed to warm up. The warm up time depends on the system and environmental conditions, but is generally between 15 and 30 minutes. After warm up, the first data collect is a background collection to (1) check for any environmental changes either in the test stand or the surrounding environment that may affect the sensor, and (2) allow removal of that effect from the sensor data. Once the background collection is completed, data collections over targets are performed until the end of the daily target data collections, at which time another background data collect is performed, unless prohibited by a weather event.

Background and target data collections are performed using the same procedures. Typically, the data collection is started over the calibration point, which is located at the origin for the test stand. The origin is located in the southwestern corner of the test stand and is designated (0, 0). The target item is located on or over the target cradle, depending on the height/depth necessary for the target to be in relation to the sensor (Fig. 21). The target cradle center is located at grid coordinates x = 255 cm, y = 155 cm.

Figure 20. Photographs showing the test stand and a GMR sensor mounted on the test stand shuttle.

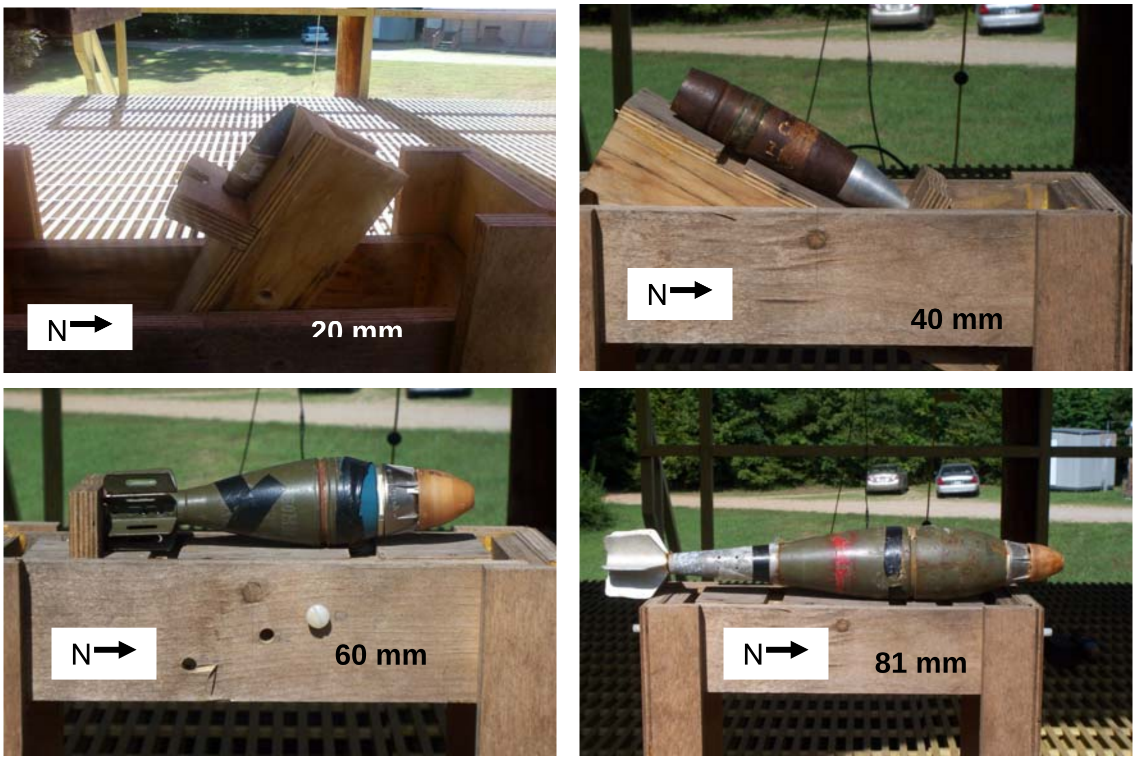

Figure 21. Photographs of the UXO targets in the target cradle used on the test stand.

The calibration target varies depending on the sensor type. For magnetometers and time domain EM (TDEM) devices, a standard 8 pound shot put is used. The calibration target has multiple uses during the data collect. Firstly, the calibration target is used to sync the sensor data and the position data if these two data streams are being stored on separate computers. Secondly, the calibration target is used to determine sensor drift during the data collection. The drift is determined by starting, ending and returning the sensor to the calibration target several times during the data collection. If there is no drift in the sensor, the data collected over the calibration target should be the same value each time. If there is drift in the sensor, the repeat values will not be the same, but the data can be leveled or normalized to the calibration target. During a typical test stand grid collection, 26 calibration grid points over the 8 pound shot put were collected. These calibration points are used to monitor and correct for the drift of the GMR sensor. The maximum drift recorded was 39 counts or approximately 2,546 μG=254.6 nT (1 count = 67 μG=6.7 nT), while the minimum drift recorded was five counts or approximately 335 μG=33.5 nT. The typical variation at any one data collection grid point was +/- one count or +/- 6.7 nT. Note that in the HMR2300 sensor, the analog voltages for the x-, y-, and z-axis magnetic fields are each digitized by 16-bit A/D converters. The conversion performed by the A/D converter is calibrated to +/- 2 Gauss for +/- 30,000 counts; therefore, one count equals 6.667 x 10^{-5} Gauss (66.67 μG=6.67nT) (Honeywell, 2004).

For each data collection, a grid file is created. This grid file contains all of the parameters for moving the shuttle on the test stand to the desired positions during the data collection. The parameters are x-position, y-position, z-position, speed of move (given in RPM for the SmartMotors) and dwell time at the given position. The x- and y-positions are given in centimeters from the origin. The z-position is given in height above the bottom of the target item cradle. The dwell time is determined based on how many data points need to be collected over a particular point; this can be shortened or lengthened as necessary.

Position files are generated by the Main Test Stand Control Software. This program reads the grid file and moves the sensor head to the specified grid point. Once the grid file has been selected and the data collection has started, a file is opened and actual position locations for the sensor head are stored. This file is named after the grid file to be consistent and allow for ease of use.

At the end of the day, the sensor is taken down and the data are stored. The sensor is placed back in either the storage building or the Test Stand Operations building. This is done to protect the sensor from the elements and to allow for the sensor batteries to be charged. Next, all of the data and positioning information are collected into a single directory on the data processing and storage computer. The data are given cursory examination for anomalies or bad data several times a day. Initial processing of these data is performed to check for problems with the sensor or test stand operation, and to reduce the collection of bad data.

Results and Discussion—Test Stand Data Collection

GMR Data Results

The GMR sensor response over both ordnance and clutter targets was acquired. Plots are constructed for the targets oriented at azimuths of 0º and 60º, and dips 0º, 28º down, and 62º up (-62º). Sensor-target separations are at 0.5L and 1.0L, where L is the length of the target. The 81-mm data were collected at separation distances of 10 cm, 15 cm, and 21 cm, rather than 0.5L and 1.0L, because the mortar was too long to achieve the dip angles at half and full length sensor-target separations. The 21-cm separation is close to the 0.5L separation of 24.5 cm.

The response of the GMR sensor as a passive magnetic sensor is similar to other magnetometers. Figure 22 shows plots of the 60-mm mortar at the various azimuth and dip combinations for the 0.5L and 1.0L separations. Similar plots for the 20 mm, 40 mm, and 81 mm are provided in Appendix A; plots for the clutter targets are in Appendix B. All plots represent the magnitude of the total magnetic field anomaly. At 60º azimuth, 0º dip and 0.5L (Fig. 22a, top right plot), the magnetic field response exhibits an actual rotation of approximately 41º. This is comparable with Altshuler (1996), who reported on the lag of the magnetization vector relative to the semi-major axis of the target. For the 60-mm mortar, as the dip angle varies from zero, the discrepancy between the magnetization vector and orientation increases. Similar behavior is observed as the sensor-target separation increases. However, the response to changing dip angle and target depth tends to vary among ordnance (see Appendix A). These differences are likely attributed to differences in the aspect ratio and Fe aspect ratio.

Plots of the individual x, y, and z magnetic field components are shown in Fig. 23 for the 60-mm mortar at 0º azimuth and 0º dip at 0.5L, along with the xy- and xz-component plots. The individual component plots show the expected response, although the y-component exhibits the affect of a much larger line spacing relative to the along-line spacing. The xy- and xz-component plots (Fig. 23, right side) are similar to what Simms et al. (2000) describe as a heart-shaped plot for the xz-component and tornado plot for the xy-component.

(a)

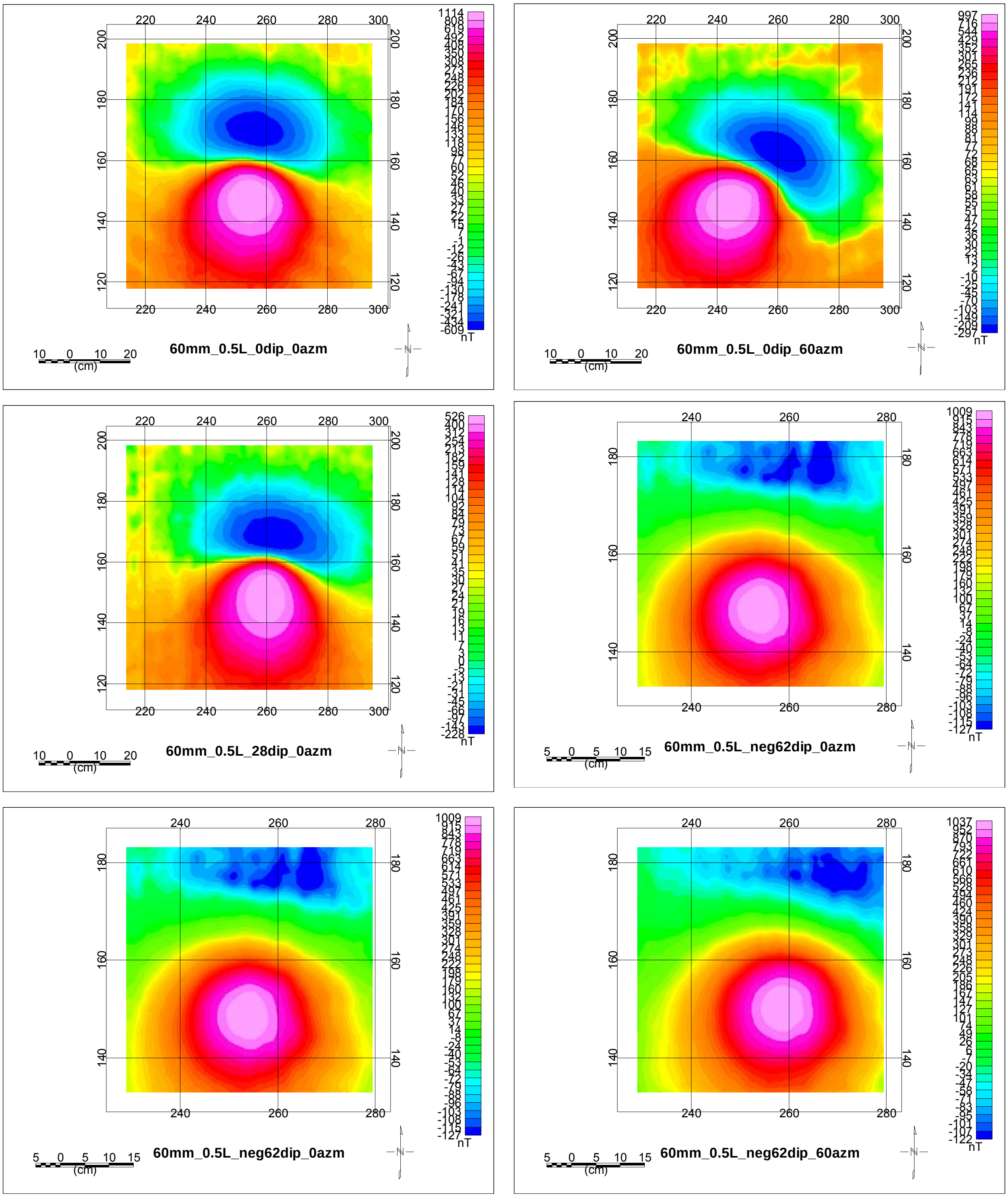

Figure 22. GMR sensor response for 60-mm mortar oriented at 0º azimuth (left) and 60º azimuth (right) for dip angles of 0º (top), 28º down (middle), and 62º up (bottom), at sensor-target separations of (a) 0.5L and (b) 1.0L.

(b)

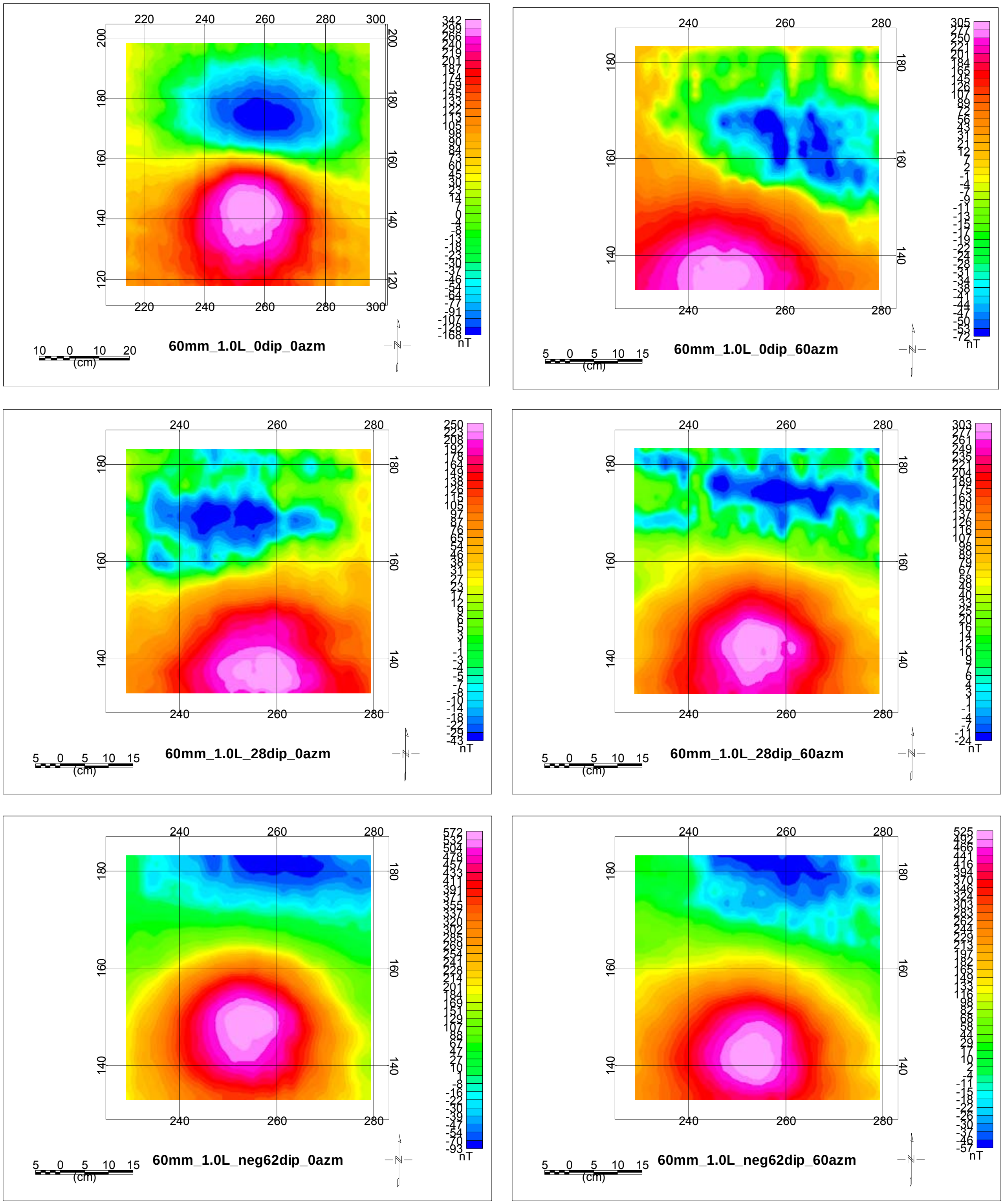

Figure 22. Concluded.

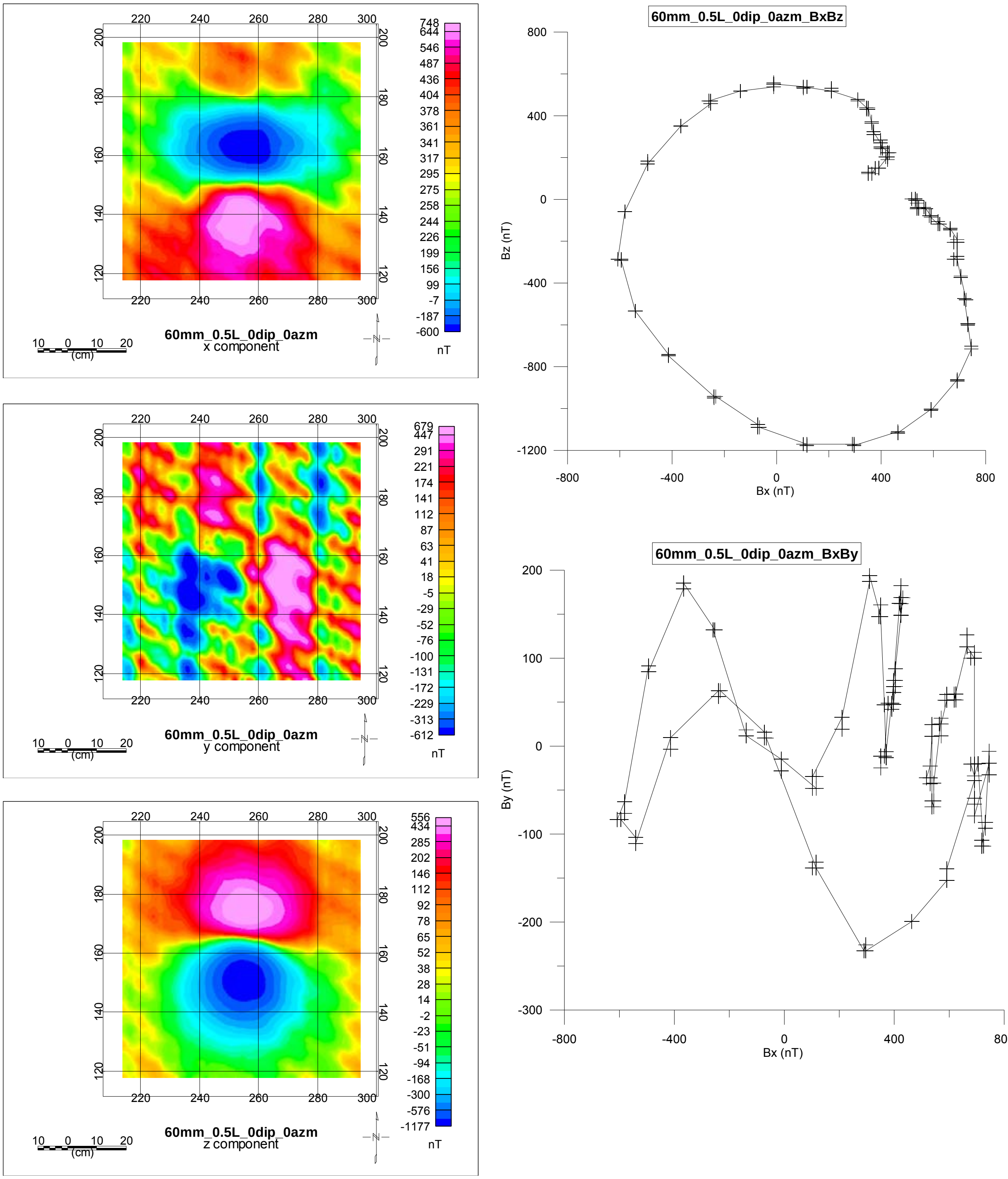

Figure 23. GMR sensor magnetic field component plots for 60-mm mortar at 0º azimuth, 0º dip, and 0.5L.

Comparison of Model and GMR Sensor Data

Modeling of the induced magnetic anomaly of UXO in the earth's magnetic field is useful for both forward and inverse modeling applications. Forward modeling is used to predict the magnetic signature of a given UXO to determine if it should be detectable by a given magnetic sensor at specified depths and orientations. Inverse modeling seeks to determine (recover) useful information about a target that produces a measured magnetic anomaly; and in the case of a UXO target, it is parameters like the magnetization vector, depth (z-coordinate), location (x-, y-coordinates), and size that are desired. The modeling can be as simple as a simple dipole model, which is equivalent to a uniformly magnetized sphere, to very complex models that seek to account for the full physical magnetic anomaly response of the actual geometry of a UXO target. The most useful models for practical UXO applications are modifications to the simple dipole model, e.g., a double-dipole model, or the magnetic field response of a prolate spheroid. The prolate spheroid (a special case of a general ellipsoid of revolution that is characterized by the orthogonal major and minor axis lengths) is a good geometrical model for many UXO shapes and captures much of the phenomenology of UXO magnetic anomalies. While the magnetic anomaly response of a prolate spheroid can be calculated analytically (Altshuler, 1996), it is most often implemented in a multipole expansion, where the first two terms in the expansion are a dipole and an octupole term (McFee, 1989; Altshuler, 1996; Butler et al., 1998; Billings, 2004; Billings et al., 2002, 2006). The multipole expansion solution for the prolate spheroid accounts for the size (length, diameter, volume), magnetic susceptibility, and orientation and aspect ratio influences on the induced magnetic field (i.e., accounts for demagnetization affects and the fact that the induced magnetization vector will follow, but always lag behind the spheroid long axis orientation relative to the earth's magnetic field vector (e.g., Altshuler, 1996); except for the special cases of spheroid orientation along or perpendicular to the earth's field direction). The octupole component of the expansion falls off as $1/r^5$ compared to $1/r^3$ for the dipole component, where r is the distance from an observation point to the "center of the spheroid," so the octupole component can have significant effects for small values of r.

The primary objective of magnetic modeling of the ordnance items and scenarios of the GMR measurements is a reality check. Do the magnitudes of the modeled and measured responses compare approximately? Do the modeled and measured orientations of the anomalies (i.e., the angle between the line through the maximum and minimum anomaly values and magnetic north) agree approximately and track the orientation of the ordnance item and spheroid model as predicted theoretically and as commonly observed? This effort is one of few documented cases when modeling has been compared to measurements for such small offset distances and exclusively for the smaller ordnance sizes, i.e., 20 mm to 81 mm.

There are several caveats to the modeling process that should be mentioned:

1. the length and diameter used for the spheroid model may not match the actual ferrous metal volume of the measured target (see Table 1 and Billings et al., 2006);
2. the value chosen for relative magnetic permeability for the model may not be correct for the actual measurement target, although variations from 100 to 1000 will change the response by nominally only 5%;

3. small errors in the measured distance from the magnetometer to center of UXO target can result in significant differences from the modeled response because of the inverse cube fall-off in magnitudes, for example, a 0.5 cm error in distance measurement can result in modeled differences of 5-20% for the cases shown in Table 1;
4. for small distances between measurement location and target center (distance (r) < characteristic target dimension), the spheroid octupole component may become quite significant and even higher order components might be needed to better replicate the measured response, or the prolate spheroid model may no longer be appropriate; in all cases modeled below, inclusion of the octupole component would decrease the magnitudes of the model responses by 10-15%; for larger ordnance sizes, e.g., 105-mm projectiles and larger, *and* for larger distances from observation point to ordnance, r > characteristic target dimension, the application of prolate spheroid dipole modeling has been quite successful in replicating all aspects of measured magnetic anomaly signatures: magnitudes, azimuth and dip response changes, spatial characteristics (wavelengths) (e.g., Butler et al., 1998; Billings et al., 2002; Billings, 2004).

When initially modeling the ordnance response, some significant discrepancies were observed between the strength of the model response and the GMR response. Upon inspection of the various ordnance, it was noted that all of the munitions used in this study have some component made of a non-ferrous metal. After accounting for the actual ferrous length of each ordnance type in the modeling program, there was a significant improvement between the modeled and acquired data results. Table 5 lists the ordnance, their length, and ferrous length. The ferrous length was used in the model results presented below. The program UXOLab (UXOLab developed by University of British Columbia Geophysical Inversion Facility; http://eos.ubc.ca/ubcgif/) was used to generate the forward models. The model data were generated using an earth's field of 49,600 nT and relative magnetic permeability of 500. Both model and test stand data are shown for azimuths of 0° and 60°, dip 0°, and a depth of 1.0L. In all cases, inclusion of the octupole component would decrease the magnitude differences.

Table 5. Actual length and ferrous length of ordnance studied.

Target	Length (cm)	Fe Length (cm)	Diameter (cm)	Fe Aspect Ratio
20-mm Projectile	7.5	5.5	2.0	0.36
40-mm Projectile	18.0	13.0	4.0	0.31
60-mm Mortar	24.5	18.0	6.0	0.33
81-mm Mortar	49.0	24.0	8.1	0.34

20-mm projectile. A comparison of the measurement data with the modeled data for the 20-mm projectile is shown in Fig. 24. The peak-to-peak magnitudes differ by approximately 25%, while the magnetization vector surface projecting angle agrees within 5° (24° for measurements compared to 29° for model). Distance errors for this case will have a larger effect than other cases.

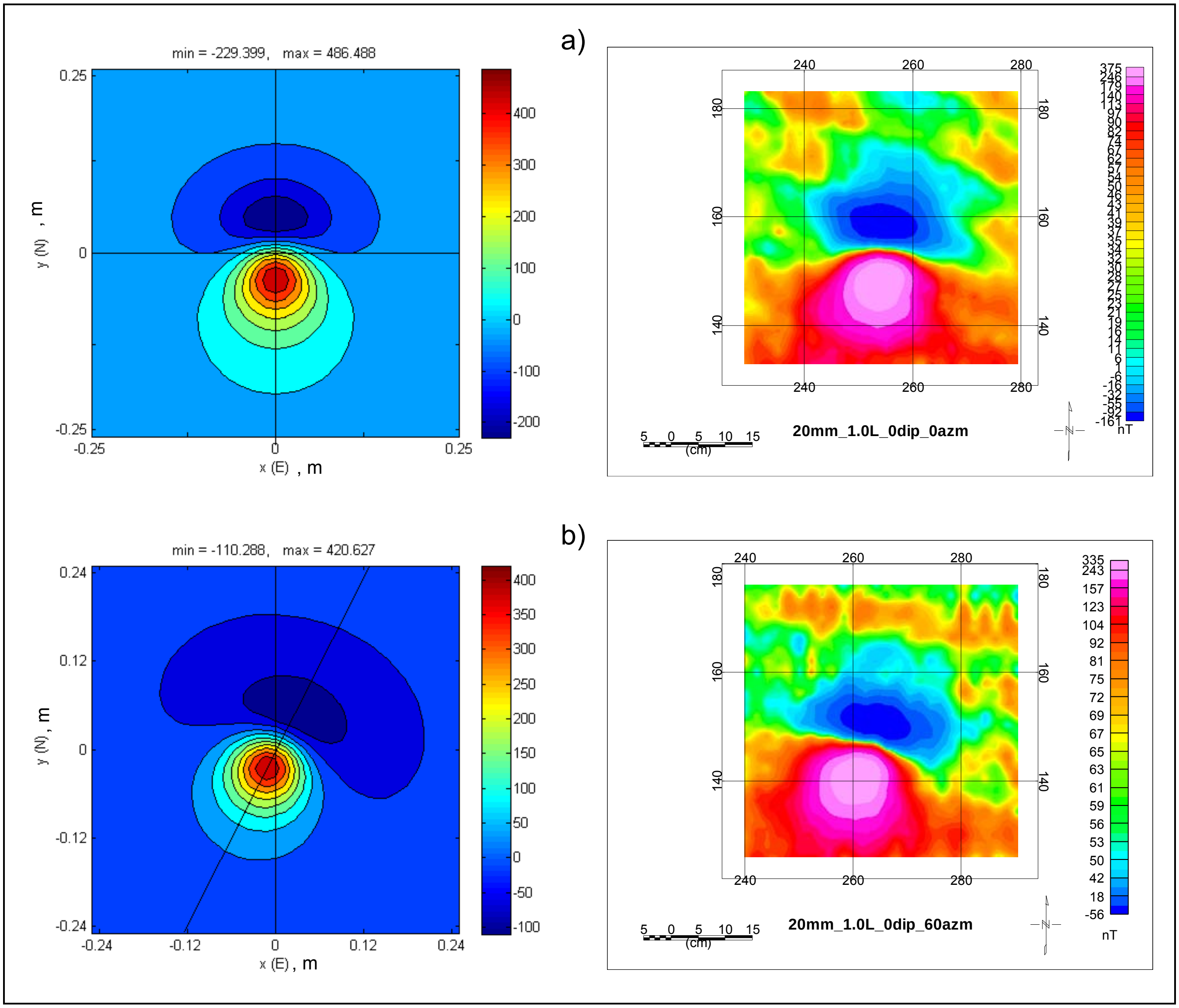

Figure 24. Model (left) and GMR sensor (right) plots of the 20-mm projectile at a depth of 1.0L (7.5 cm) oriented along (a) magnetic north (azimuth 0º) and parallel to the ground surface (dip 0°), and (b) 60° east of magnetic north (azimuth 60°) and parallel to the ground (dip angle of 0°).

40-mm projectile. A comparison of the measurement data with the modeled data for the 40-mm projectile is shown in Fig. 25. The rotation of the surface projection of the magnetization vector for an azimuth of 60º is quite close for this case (approximately 32º for each). Anomaly magnitudes agree to within about 14%.

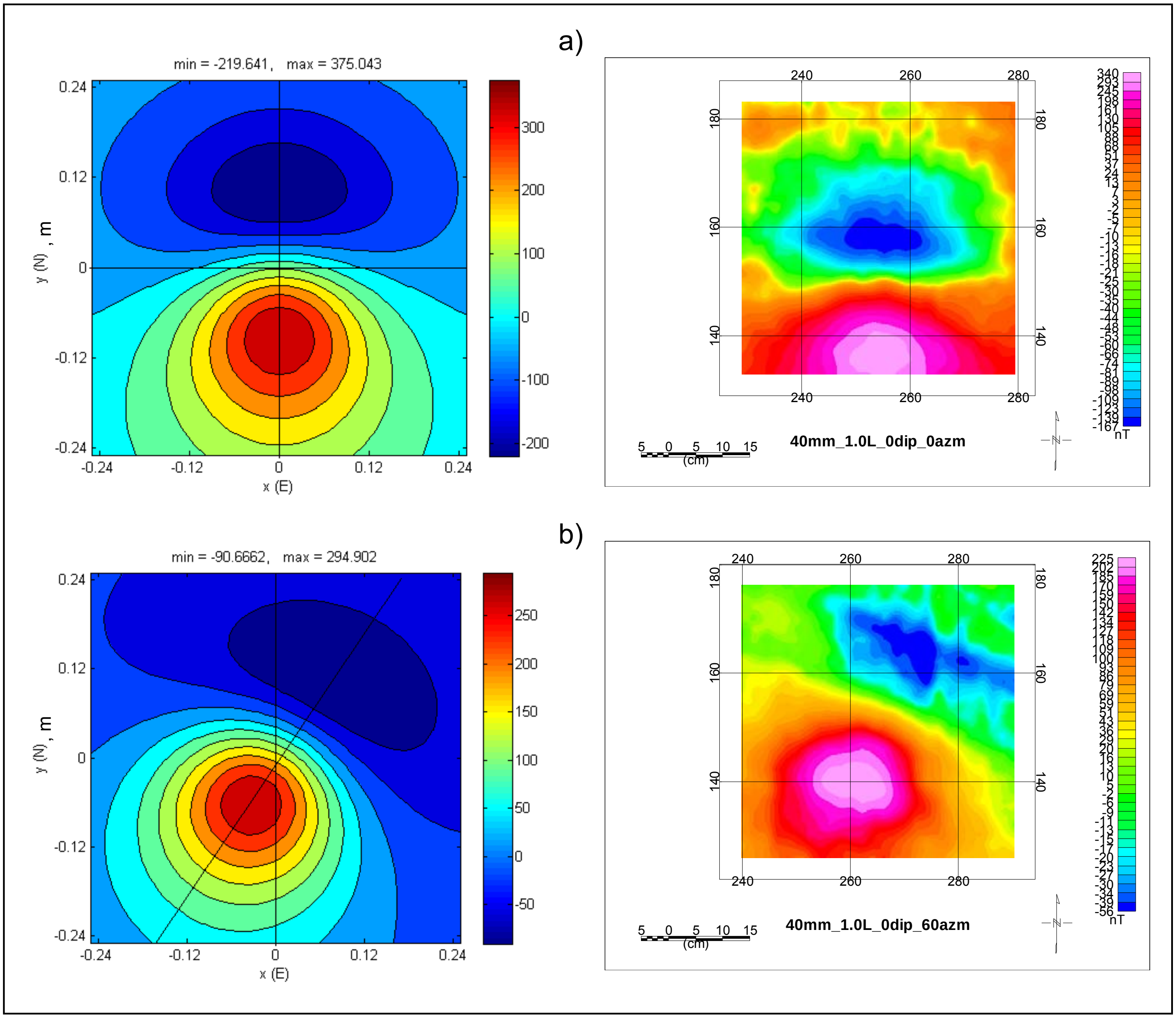

Figure 25. Model (left) and GMR (right) plots of the 40-mm projectile at a depth of 1.0L (18 cm) oriented along (a) magnetic north (azimuth 0°) and parallel to the ground surface (dip 0°), and (b) 60° east of magnetic north (azimuth 60°) and parallel to the ground (dip angle of 0°).

60-mm mortar. A comparison of the measurement data with the modeled data for the 60-mm mortar is shown in Fig. 26. Both data sets exhibit almost exactly the same angle (~30°) of rotation of the magnetization vector for an azimuth of 60°, while the peak-to-peak magnitudes differ by about 25%.

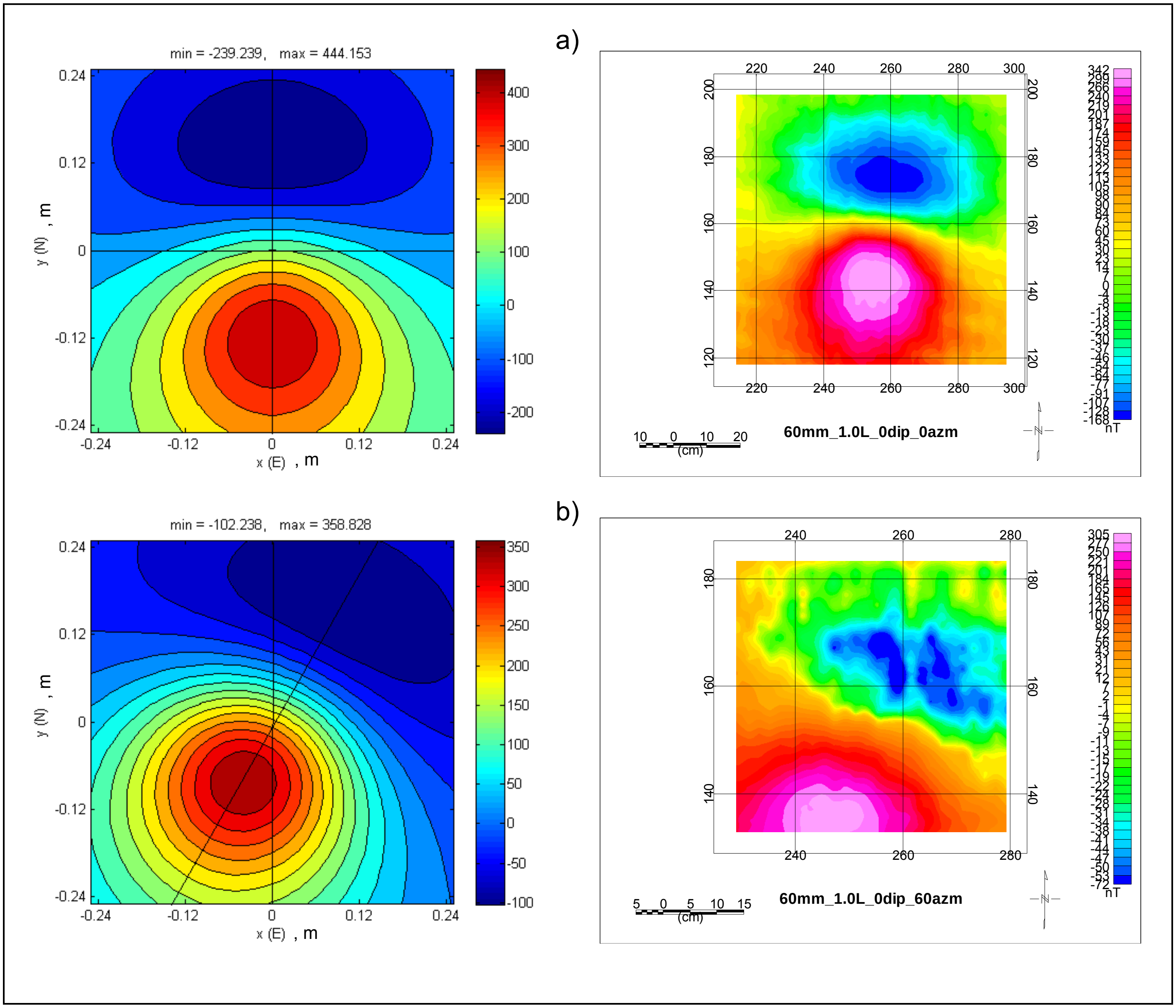

Figure 26. Model (left) and GMR (right) plots of the 60-mm mortar at a depth of 1.0L (24.5 cm) oriented along (a) magnetic north (azimuth 0°) and parallel to the ground surface (dip 0°), and (b) 60° east of magnetic north (azimuth 60°) and parallel to the ground (dip angle of 0°).

81-mm mortar. A comparison of the measurement data with the modeled data for the 81-mm mortar is shown in Fig. 27. The rotation of the surface projection of the magnetization vector for an azimuth of 60° is comparable (~31° modeled, ~33° measured). There is a greater difference in peak-to-peak magnitudes (about 50%), but this is attributed to a shorter sensor-target separation (< 0.5L) and the exclusion of the octupole component in the modeled data.

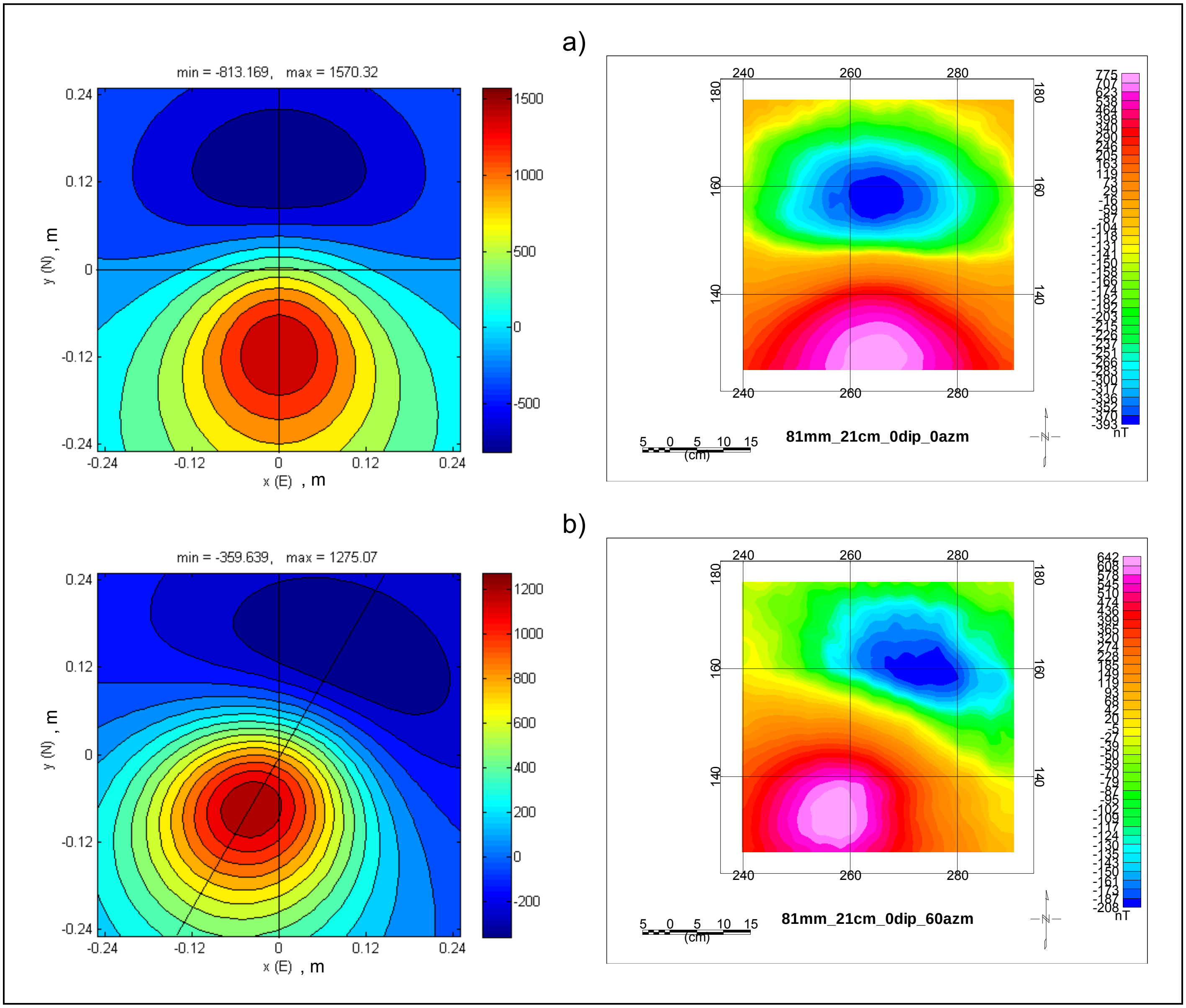

Figure 27. Model (left) and GMR (right) plots of the 81-mm mortar at a depth of 21 cm oriented along (a) magnetic north (azimuth 0^o) and parallel to the ground surface (dip 0^o), and (b) 60^o east of magnetic north (azimuth 60^o) and parallel to the ground (dip angle of 0^o).

Resolution of Proximal Targets

The 20-mm projectile was used to study the ability of the GMR sensor to resolve proximal targets. Two 20-mm projectiles were positioned both horizontally and vertically to determine the minimum separation required to detect the presence of a second target. The photographs in Fig. 28 show how the horizontal and vertical spacing between the projectiles was maintained. The affect of horizontal spacing on the GMR magnetic signature of two 20-mm projectiles is shown in Fig. 29. The sensor-target separation is 1.0L. At a separation of one-half the actual 20-mm length (0.5L=3.75 cm), the magnetic signature shows little indication that there

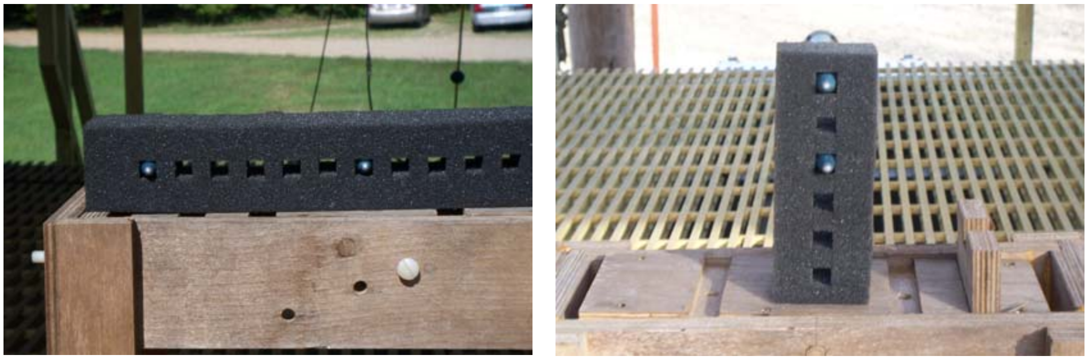

Figure 28. Photographs showing the hard foam forms used to maintain the various horizontal and vertical spacing of the two 20-mm projectiles.

are two targets contributing to the signature. At 1.0L (7.5 cm), the magnetic signature suggests the possibility of two peaks in the positive portion of the signature. At a separation of 1.5L, both the positive and negative parts of the dipole response are beginning to show the presence of two targets. As the horizontal separation increases, two distinct dipole responses are observed.

The sensor-target separation was decreased to 0.5L to determine if a smaller separation would improve the resolution of the horizontal targets (Fig. 30). The 0.75L horizontal separation exhibits a change in shape from the 0.5L separation, however if it was unknown that two targets are present, one would probably not suspect two targets. The 1.0L horizontal separations are similar for both the 0.5L (Fig. 30) and 1.0L (Fig. 29) sensor-target separations, where the positive dipole suggests the presence of a second target. As the horizontal target separation increases beyond 1.0L, the resolution of the two targets is better at the 0.5L sensor-target separation.

GMR sensor plots of the two 20-mm projectiles positioned one directly over the other at separations of 0.5L (3.75 cm) and 1.0L (7.5 cm) are shown in Fig. 31. The sensor-target separation to the upper projectile is 1.0L. Both projectiles are oriented at 0º azimuth and 0ºdip. As expected, there is no indication that a second target is present, although the magnitudes are larger than for the single 20-mm case (Fig. 24).

Comparison of GMR and G-858 Sensor Data

The G-858 data were obtained under SERDP project UX-1380, "Advanced UXO Discrimination Using Magnetometry: Understanding Remanent Magnetization." As mentioned previously, it was intended to use the same ordnance orientations as those used for project UX-1380, however the orientations differ for the G-858 and GMR sensor except for data collected at (azimuth 0º, dip 0º). Besides characterizing the GMR sensor, this will provide a valuable comparison of the two sensor types.

Data from the 60-mm and 81-mm mortars are used to compare the signatures obtained using the GMR sensor and the G-858 cesium vapor magnetometer. These targets were selected because they are the only common ordnance that were studied in this project and project

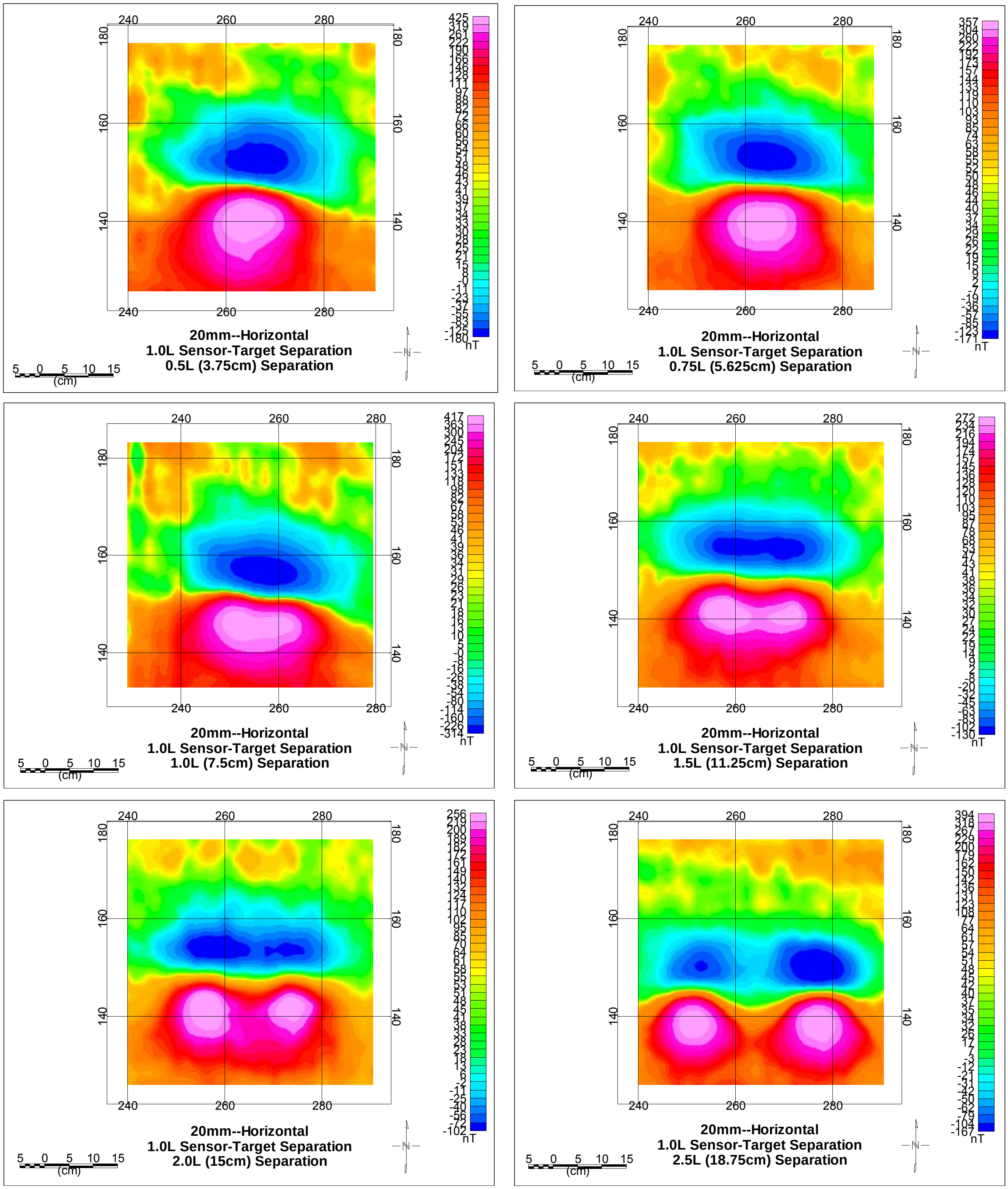

Figure 29. Plots of two 20-mm projectiles placed at horizontal spacings of 0.5L (3.75 cm), 0.75L (5.625 cm), 1.0L (7.5 cm), 1.5L (11.25 cm), 2.0L (15 cm), and 2.5L (18.75 cm) oriented along magnetic north (azimuth 0°) and parallel to the ground (dip 0°). The sensor-target separation is 1.0L.

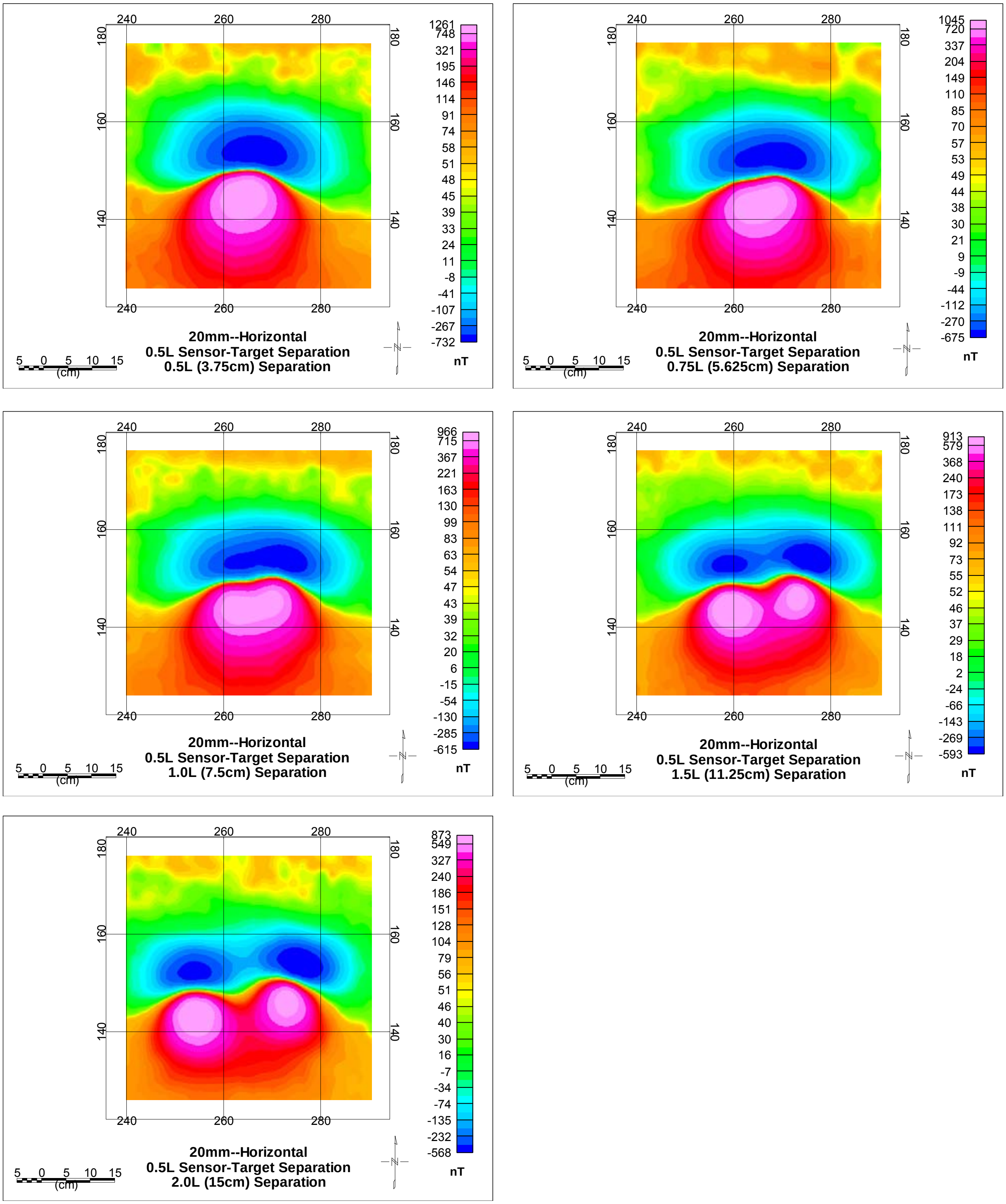

Figure 30. Plots of two 20-mm projectiles placed at horizontal spacings of 0.5L (3.75 cm), 0.75L (5.625 cm), 1.0L (7.5 cm), 1.5L (11.25 cm), 2.0L (15 cm), and 2.5L (18.75 cm) oriented along magnetic north (azimuth 0^{o}) and parallel to the ground (dip 0^{o}). The sensor-target separation is 1.0L.

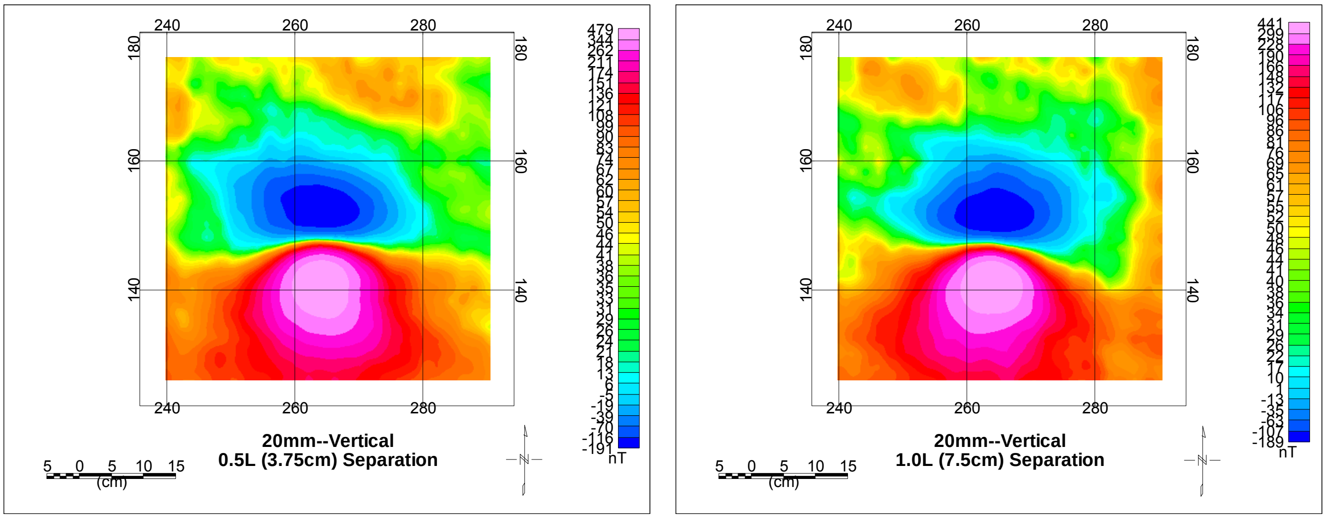

Figure 31. GMR sensor response of two 20-mm projectiles positioned directly over one another with vertical separations of 0.5L (3.75 cm) and 1.0L (7.5 cm). The projectiles are oriented at 0º azimuth and 0ºdip, with a 1.0L separation between the sensor and upper target.

UX-1380. Only the general behavior of the responses can be compared, and not the magnitudes, because the sensor-target separation distance varied for the two sensors. The GMR sensor-target separation was 24.5 cm for the 60 mm, whereas the G-858 sensor-target separation was 59 cm. For the 81 mm, the GMR sensor-target separation was 21 cm, while the G-858 separation was 59.75 cm.

A comparison of the test stand signatures for the GMR sensor and G-858 shows that the basic shape of the two signatures is similar (Fig. 32). The primary difference in magnitude is attributed to the difference in target depths. It is interesting to note that the inverse cube scaling can be used to show that the 60-mm example scales almost exactly in magnitude. The 81-mm example is not comparable because of the small sensor-target separation.

In general, the GMR sensor response is similar to the G-858 cesium vapor magnetometer, although there is a significant difference in resolution of the two sensors; 7 nT for the GMR sensor compared to 0.01 nT for the G-858. Often times the background (geologic/clutter/natural) noise level at a site is not less than 5 nT (Butler et al., 1998; Butler et al., 1999; Butler, 2001; Butler et al., 2001; Butler, 20003; Butler et al., 2003), in which case a sensor having 7 nT resolution is acceptable. At low noise sites and for stationary measurements, change detection measurements and low-flying (1.5-2 m above ground surface) airborne magnetic applications, where the higher spatial frequency noise is "filtered" because of distance from the source, the greater resolution of the cesium vapor sensor is desirable.

An example demonstrating the usefulness of a small magnetometer sensor, such as a GMR, is given in Fig. 33 for a 20-mm projectile. The maximum positive anomaly amplitude is plotted for a sensor passing directly over (0-cm offset) the target, and 10-cm and 25-cm laterally offset. Compare the detection capability of a multi-sensor cesium vapor magnetometer array, which requires a minimum 25-cm sensor separation (Bob Selfridge, personnel communication), and a GMR sensor array having a 5-cm sensor separation. For a 20-mm projectile buried several centimeters deep, it is possible that a more sensitive magnetometer (such as the cesium vapor) array, with a greater sensor separation, could miss the projectile because of the reduced anomaly amplitude from lateral offset. However, the less sensitive GMR sensor array, with a smaller sensor separation, is likely to detect the higher amplitude anomaly resulting from a shorter lateral offset. The GMR sensor should be adequate for detecting the small, shallow munitions (under typical magnetic backgrounds) in this study.

Conclusions and Implications for Future Research

This study addressed the fundamental operating characteristics of commercially available GMR sensors manufactured by Honeywell and NVE. It was determined that the Honeywell HMC100x series and NVE AA00x series GMR sensors have comparable performance characteristics relative to operating range, sensitivity, and noise levels. The HMC100x series GMR sensors have desirable features that are not available on the NVE sensors, therefore the Honeywell GMR sensors are the sensor of choice. The HMC100x series sensors are incorporated into the HMR2300 Smart Digital Magnetometer, which is a compact three-component magnetometer suitable for *passive* magnetic field measurements. The HMR2300 has a resolution of less than 10 nT.

GMR sensors have certain operating characteristics that must be addressed to ensure successful operation. It is important to understand the tradeoff between sensitivity and dynamic range so that the proper GMR sensor can be chosen for a particular application; as sensitivity increases, linear operating range decreases. Furthermore, latch-up in GMR sensors can render the sensor useless, but latch-up can be corrected with proper electronic design.

Measurements were presented with the GMR sensor used as both a static magnetic field sensor (magnetometer) and a dynamic magnetic field sensor. In the later case (dynamic field sensor), the GMR sensor was evaluated both as a continuous wave (CW) sensor and in a pulsed mode of operation. The GMR sensors have less sensitivity than standard coils, but they are able to make much higher resolution measurements. In either static or dynamic mode of operation, it was demonstrated that, with proper signal conditioning, GMR sensors have sufficient sensitivity and dynamic range to be useful for purposes of detecting small, shallow buried munitions. We envision no insurmountable difficulties in developing a high-resolution array of GMR sensors.

For array applications, GMR sensors can be placed millimeters apart as opposed to tens of centimeters (Bob Selfridge, personal communication) for the G-858 cesium vapor sensors. A practical issue is how best to acquire data from a dense array of GMR sensors. Every sensor must have power (plus and ground) and, if we assume all three axes of the magnetic field are measured by each sensor, each sensor must have 4 additional wires (three signal and one ground) brought out to the A/D converter. Alternatively, each sensor could have its own microcontroller and the three-axis data from each sensor could be wirelessly transferred to a host computer (laptop). The wired solution would be less expensive, but cumbersome in comparison with the wireless solution.

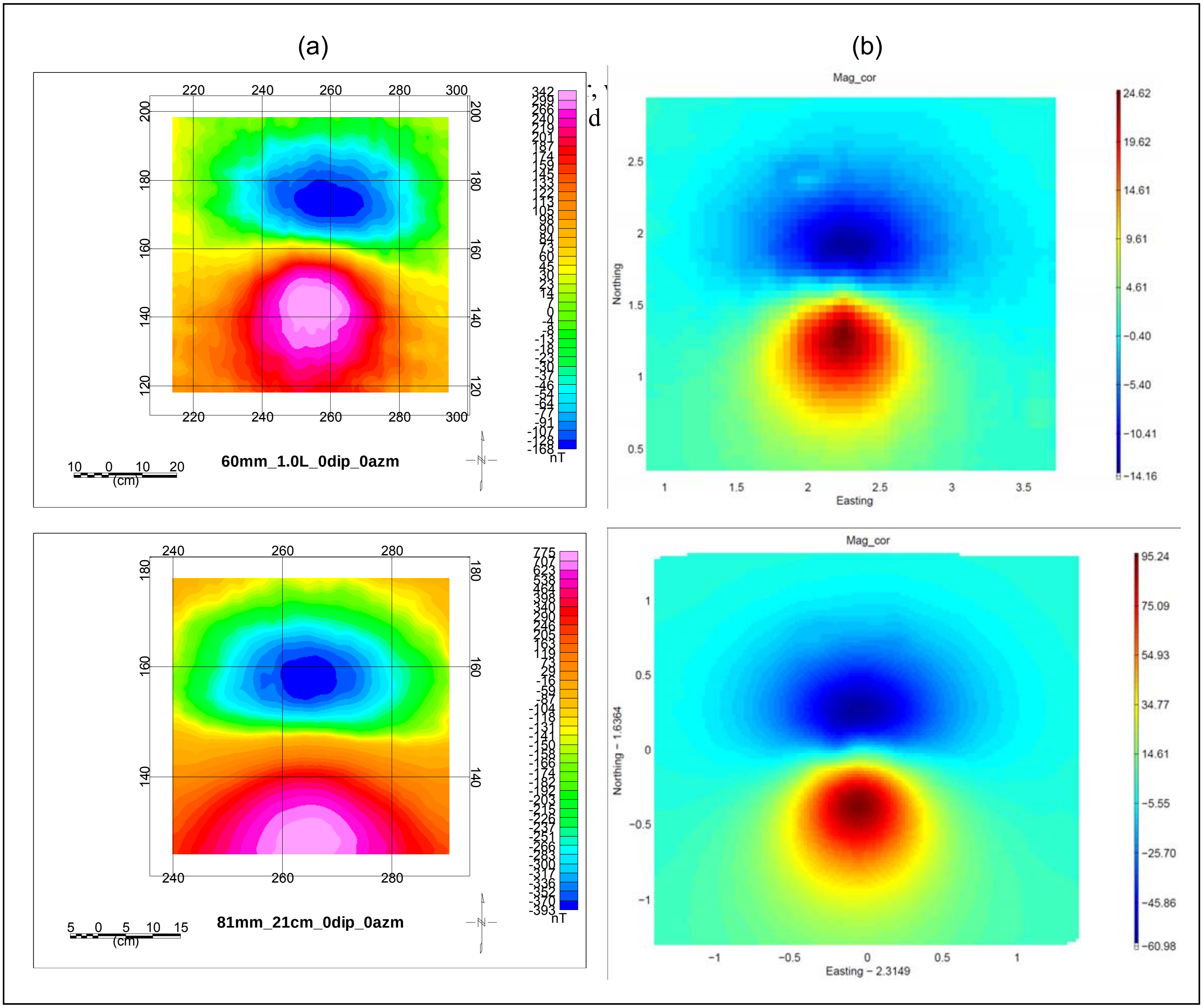

Figure 32. Plots of the 60-mm (top) and 81-mm (bottom) mortars acquired using a (a) GMR sensor with a sensor-target separation of 1.0L (24.5cm) (60 mm) and 21 cm (81 mm) oriented along magnetic north (azimuth 0^{o}) and parallel to the ground (dip angle of 0^{o}), and (b) G-858 cesium magnetometer with a sensor-target separation of 59 cm (60 mm) and 59.75 cm (81 mm) oriented along magnetic north (azimuth 0^{o}) and parallel to the ground (dip 0^{o}). The right-hand plot axis units are in meters.

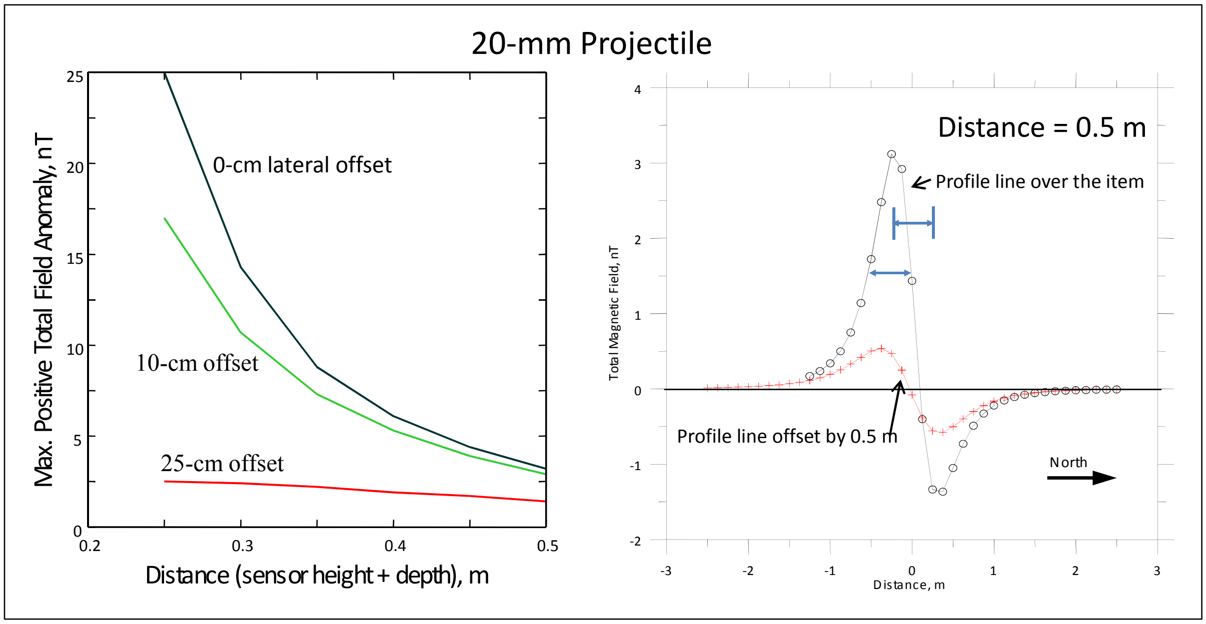

Figure 33. Effect of lateral offset on anomaly amplitude for a total field magnetometer.

The HMC2300 uses three precision low-noise instrumentation amplifiers with 1 kHz low pass filters to reject unwanted noise. If the envisioned array is to measure both static and dynamic fields simultaneously, then the 3 dB frequency of the low pass filter would need to be increased to at least 10 kHz. This can probably be accomplished by modifying the feedback capacitors on the HMC2300 circuit board.

Cost is also an important issue. The Honeywell HMC2300 is a three-axis analog sensor hybrid (20-pin wide DIP footprint (2.5 cm by 1.9 cm) that includes all signal conditioning electronics) that can be easily interfaced with an A/D converter and sells for approximately $200 per unit. (This unit integrates an HMC1001 and HMC1002, and has 40 µGauss (4 nT) resolution). A 1-m × 1-m array with 10-cm spacing between sensors would cost approximately $20,000 not including interface electronics. Some cost savings could be achieved by combining a one- and two-axis sensor on a single small PC board using in-house interface components (instrumentation amplifier, etc.). In this case, the Honeywell HMC1002 and HMC1001 would be used with a cost of $27 and $21, respectively, for a total cost of $45 per unit for the GMR sensors alone. One would need to add the cost of the interface electronics, which would probably be less than $50, for a per unit savings (over the HMC2300) of $100 (50%). Labor costs might well erode savings to the point where the HMC2300 would be economically a better choice than integrating the HMC1002 and HMC1001 on a single PC board with all the required interface electronics. For comparison, a single sensor cesium vapor magnetometer system might cost $20,000.

As a passive magnetic sensor, the GMR sensor performs similarly to a G-858 cesium vapor magnetometer. The resolution of the GMR sensor is two orders of magnitude less than the G-858, approximately 7 nT for the GMR compared to 0.01 nT for the G-858. Generally, a resolution within 10 nT is sufficient for UXO applications involving shallow, small munitions.

The ability of the GMR sensor to resolve two proximal horizontal 20-mm projectiles showed only a slight improvement at a horizontal separation of 0.75L when the sensor-target separation was reduced from 1.0L to 0.5L. At horizontal target separations of 1.0L and greater, resolution of the two targets was similar at 0.5L and 1.0L sensor-target separations, although the resolution was better at 0.5L for horizontal target separations greater than 1.0L. When the 20-mm projectiles were placed vertically over another, the GMR sensor was unable to resolve two targets. However, the magnitude of the total magnetic field was greater than when only one target was present.

The GMR sensor has potential applications for near-surface geophysical studies. It was shown that non-ferrous targets exhibited distinct decay curves when their responses were measured in dynamic mode. Impromptu tests at the test stand suggest that ferrous targets should also exhibit distinct decay curves, however further research is needed to study the GMR sensor response in dynamic mode to ferrous-based targets. Additional research is required to determine the feasibility and practicality of using a GMR sensor simultaneously in passive and dynamic modes. It is also necessary to study the implementation of GMR sensors in separate passive and dynamic array configurations.

Literature Cited

Altshuler, T.W., 1996, Shape and orientation effects on magnetic signature prediction for unexploded ordnance, Proceedings of the UXO Forum ’96, Williamsburg, VA, 282-291.

Billings, S. D., 2004, Discrimination and classification of buried unexploded ordnance using magnetometry, IEEE Transactions on Geoscience and Remote Sensing, Vol. 42, 1241-1251.

Billings, S.D., Pasion, C., Walker, S., and Beran, L., 2006, Magnetic models of unexploded Ordnance, IEEE Transactions on Geoscience and Remote Sensing, Vol. 44, 2115-2124.

Billings, S., Pasion, L., and Oldenburg, D., 2002, Discrimination ad identification of UXO by geophysical inversion of total-field magnetic data, ERDC/GSL TR-02-16, US Army Engineer Research and Development Center, Vicksburg, MS.

Butler, D. K., Cespedes, E. R., Cox, C. B., and Wolfe, P. J., 1998, Multisensor methods for buried unexploded ordnance detection, discrimination and identification, SERDP-98-10, US Army Engineer Waterways Experiment Station, Vicksburg, MS.

Butler, D.K., Llopis, J.L., and Simms, J.E. 1999, Phenomenological investigations of the Jefferson Proving Ground UXO Technology Demonstrations, Technical Report GL-99-7, U.S. Army Engineer Waterways Experiment Station, Vicksburg, MS.

Butler, D.K., 2001, Potential fields methods for location of unexploded ordnance,” The Leading Edge, Vol. 20, 890-895.

Butler, D.K., Wolfe, P.J., and Hansen, R.O., 2001, Analytical modeling of gravity and magnetic signatures of unexploded ordnance, Journal of Environmental and Engineering Geophysics, Vol. 6, No. 1, 33-46.

Butler, D.K., 2003, Magnetic backgrounds implications for UXO detection, Journal of Applied Geophysics, Vol. 54, Issues 1-2.

Butler, D.K., Pasion, L.R., Billings, S., Oldenburg, D., and Yule, D., 2003, Model-based inversion for enhanced UXO detection and discrimination, Proceedings of the Detection of Mines and Mine-like Targets Conference, AeroSense 2003, Society of Profession Optical Engineers (SPIE), Orlando, FL.

Dalichaouch, Y., Whitecotton, B., Trammel, H., Shelby, R., and Carin, L., 2003, Broadband frequency-domain magnetic system for landmine/UXO detection and discrimination, Detection and Remediation Technologies for Mines and Minelike Targets VIII, Russell S. Harmon, John H. Holloway Jr. J. T. Broach, Editors, Proceedings of SPIE Vol. 5089 (2003).

Dalichaouch, Y., Whitecotton, B., McManus, T., Kuhn, S., Tramel, H., Shelby, R., and Carin, L., 2004, Wideband frequency response of low metal mines, Detection and Remediation Technologies for Mines and Minelike Targets IX, Russell S. Harmon, J. Thomas Broach, John H. Holloway Jr. Editors, Proceedings of SPIE Vol. 5415 (2004).

Honeywell, 2004, Smart Digital Magnetometer HMR2300, Honeywell International, http://www.magneticsensors.com/datasheets/hmr2300.pdf , 900139 02-04 Rev.H.

Horowitz, P., and Hill, W., 1999, The Art of Electronics, second edition, Cambridge University Press, ISBN 0 521 37095 7 (hardback).

McFee, J., 1989, Electromagnetic remote sensing: Low frequency electromagnetics, DRES-SP-124, Defense Research Establishment Suffield, Canada.

McGlone, D.T., 1998, Magnetometer Comparison Smoke Creek Instruments' GMR SCIMAG-01 & Bartington Fluxgate MAG-03MC70, A Report on Recent Comparison Results, Ineel Subsurface Science Initiative, Idaho Falls, ID, December 2002 Under INEEL SOW-468.

Ott, H.W., Noise Reduction Techniques in Electronic Systems, John Wiley and Sons, ISBN: 0-471-65726-3. (Copyright 1976 by Bell Telephone Laboratories, Incorporated)

SERDP UX-1327, Advanced magnetic system for UXO detection and discrimination, Quantum Magnetics, Inc.

Simms, J.E., Smithhart, L.B., and Butler, D.K., 2000, Evaluation of three-component magnetic sensors for delineation and identification of UXO, ERDC TR-00-6, U.S. Army Engineer Research and Development Center, Vicksburg, MS.

Appendix A - GMR Sensor Total Magnetic Field Plots for the 20 mm, 40 mm, and 81 mm Ordnance

20-mm, L=0.5

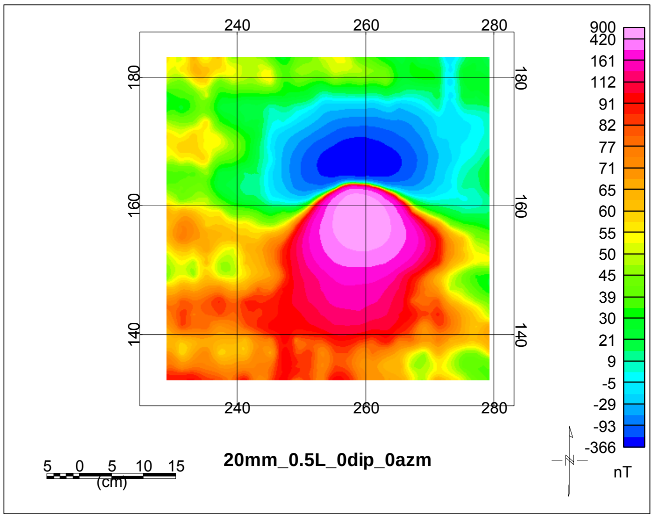

20mm_0.5L_0dip_0azm

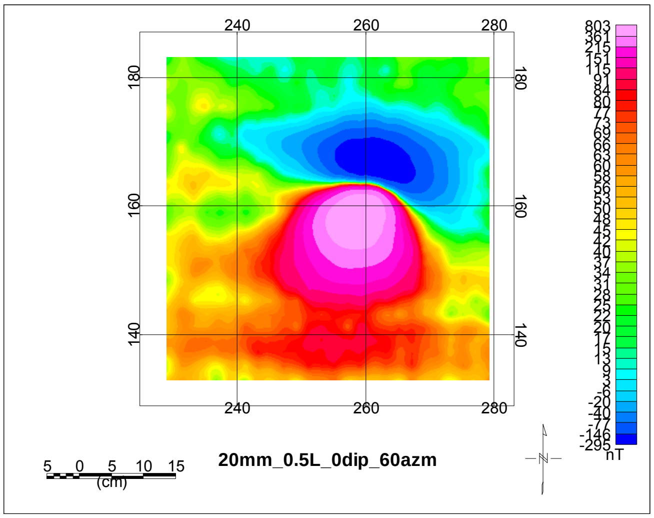

20mm_0.5L_0dip_60azm

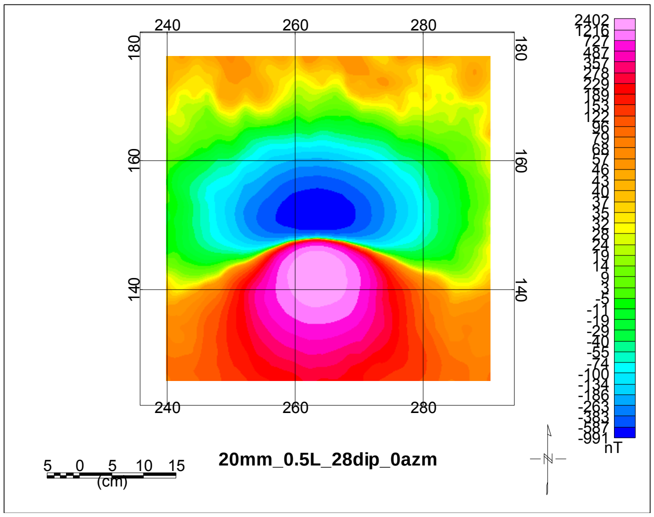

20mm_0.5L_28dip_0azm

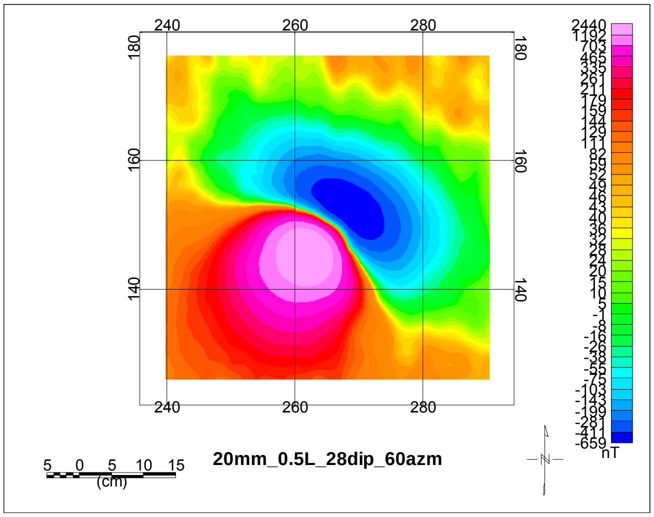

20mm_0.5L_28dip_60azm

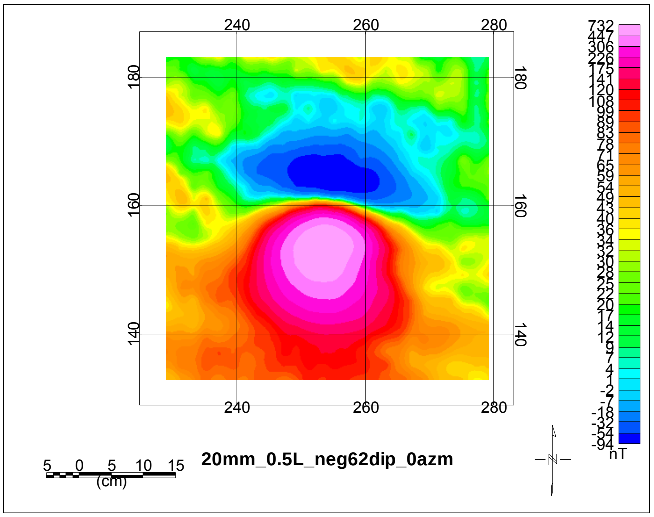

20mm_0.5L_neg62dip_0azm

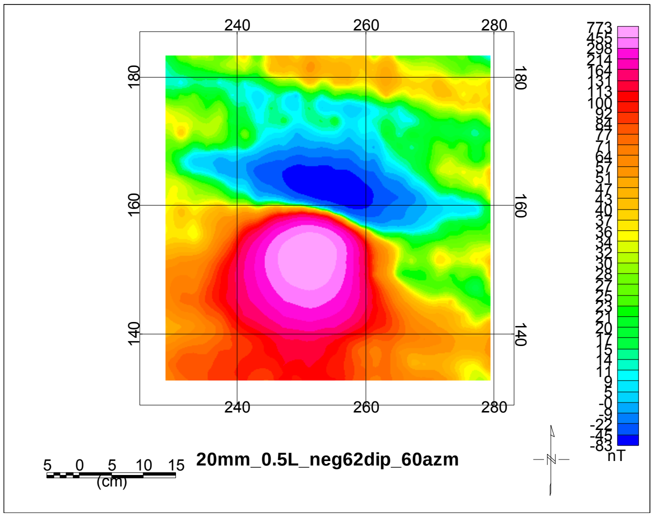

20mm_0.5L_neg62dip_60azm

20 mm, L=1.0

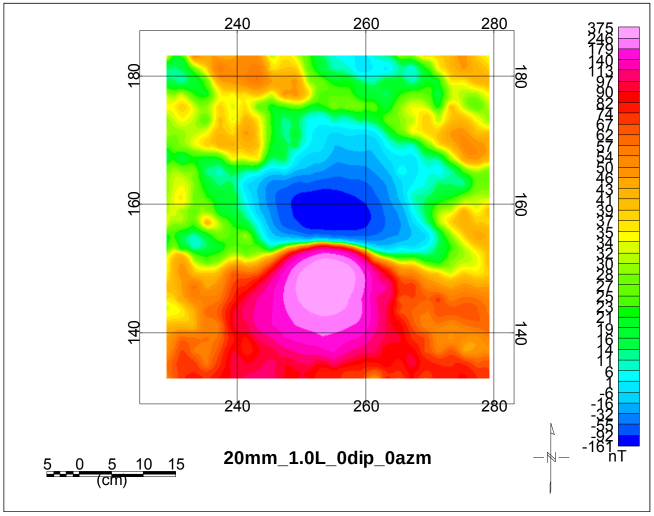

20mm_1.0L_0dip_0azm

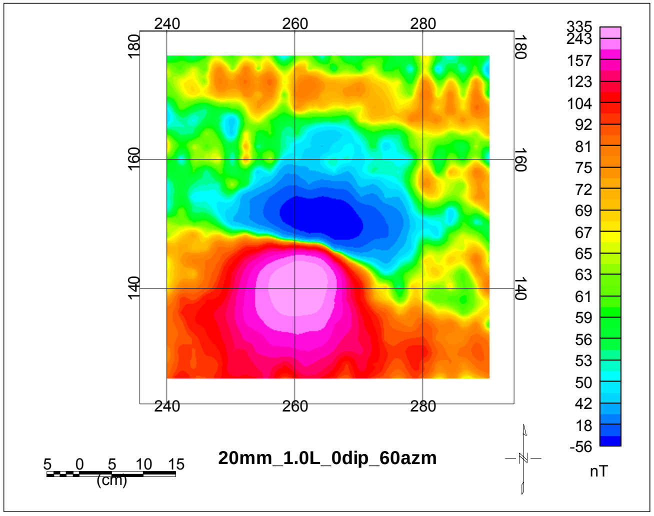

20mm_1.0L_0dip_60azm

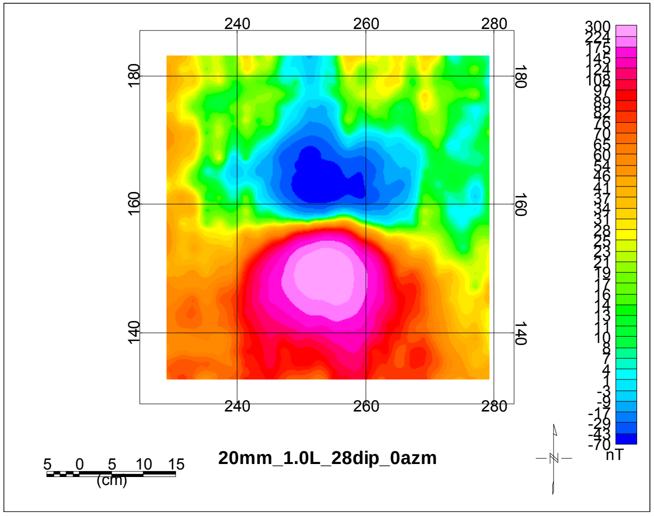

20mm_1.0L_28dip_0azm

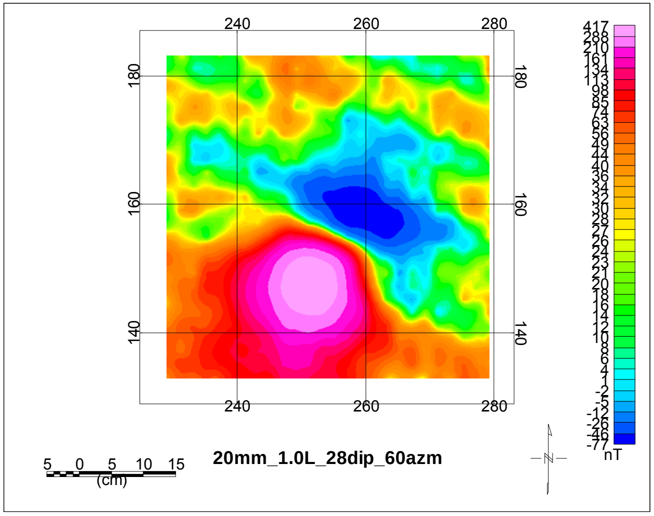

20mm_1.0L_28dip_60azm

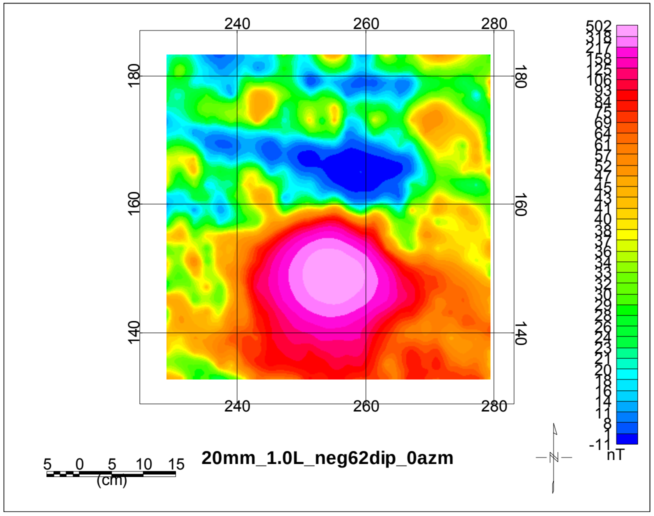

20mm_1.0L_neg62dip_0azm

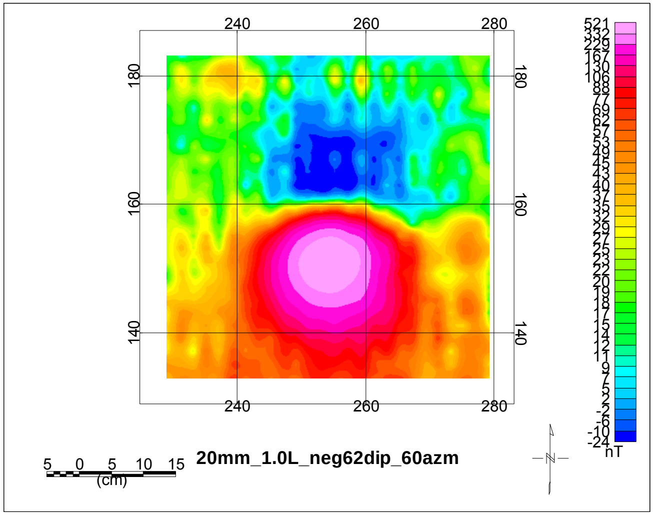

20mm_1.0L_neg62dip_60azm

40 mm, L=0.5

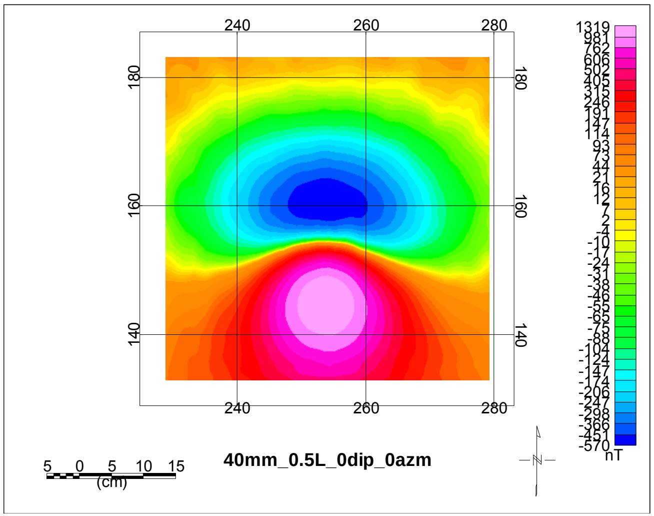

40mm_0.5L_0dip_0azm

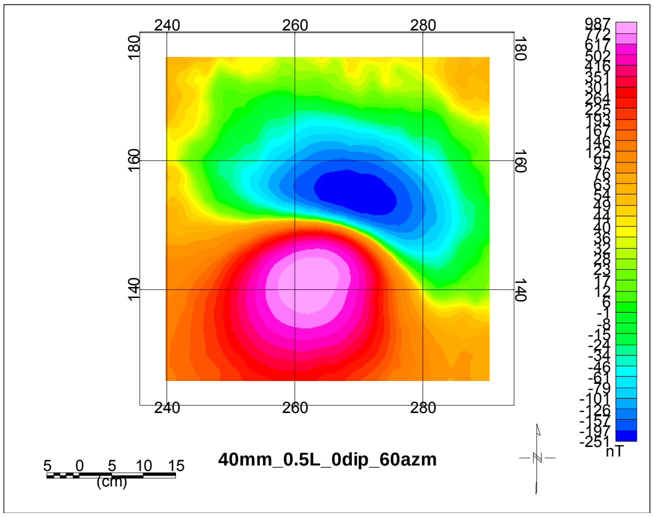

40mm_0.5L_0dip_60azm

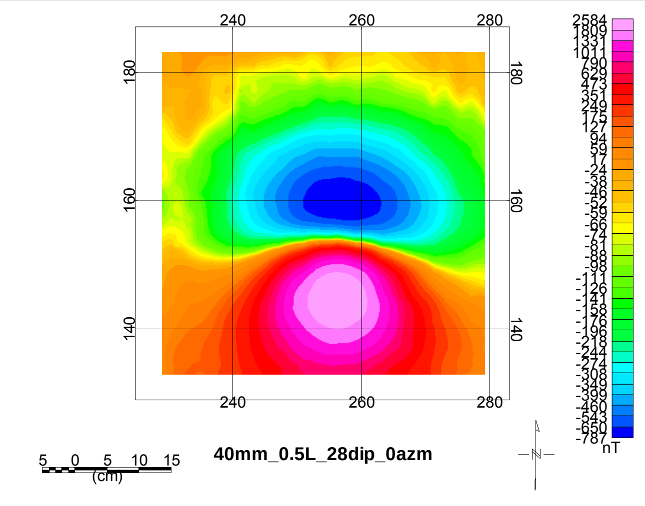

40mm_0.5L_28dip_0azm

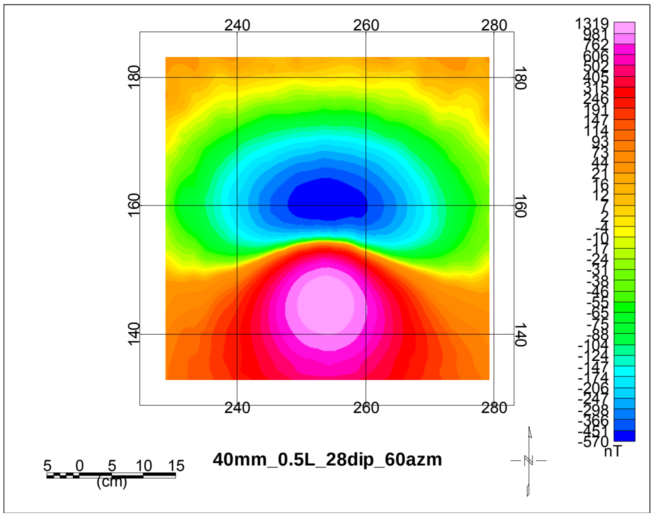

40mm_0.5L_28dip_60azm

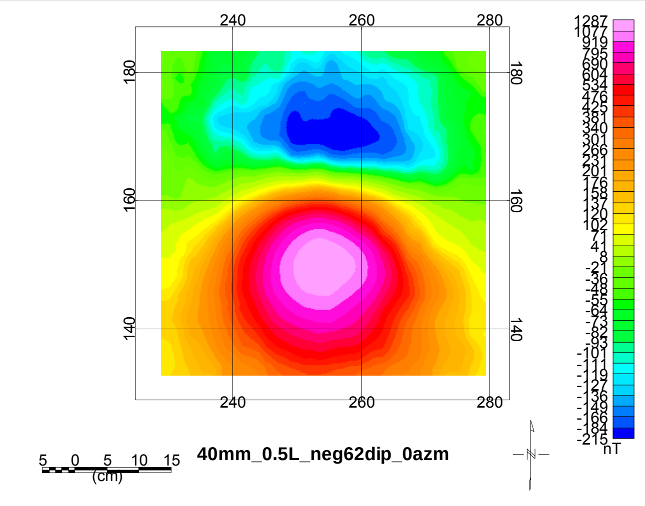

40mm_0.5L_neg62dip_0azm

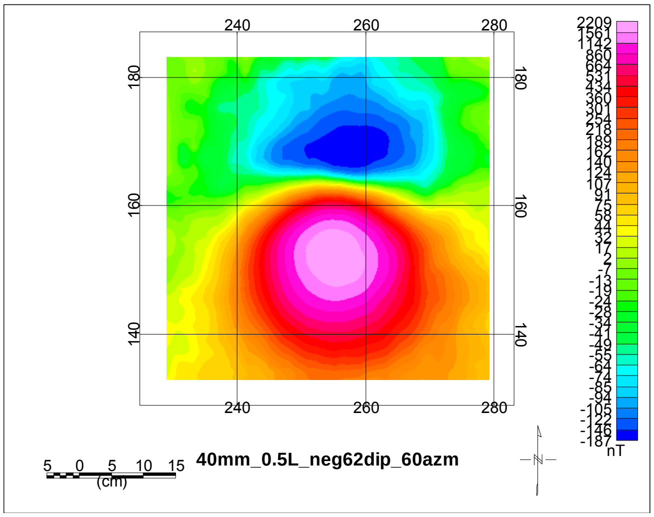

40mm_0.5L_neg62dip_60azm

40 mm, L=1.0

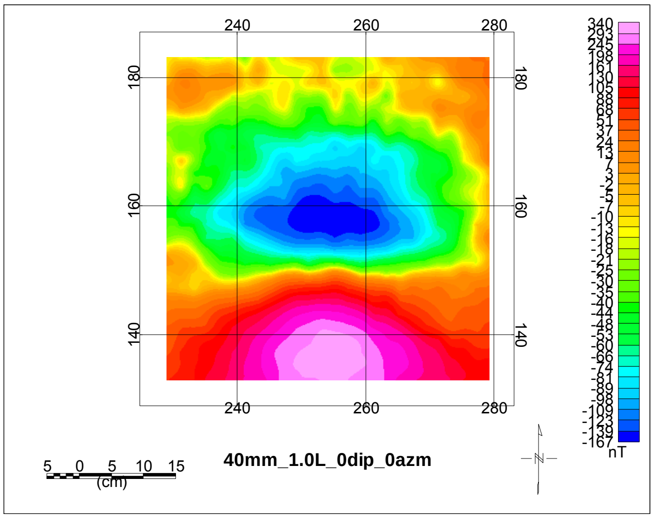
40mm_1.0L_0dip_0azm

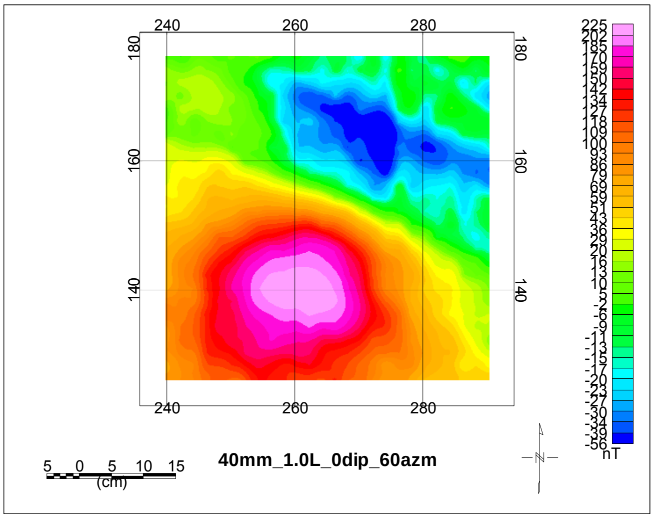
40mm_1.0L_0dip_60azm

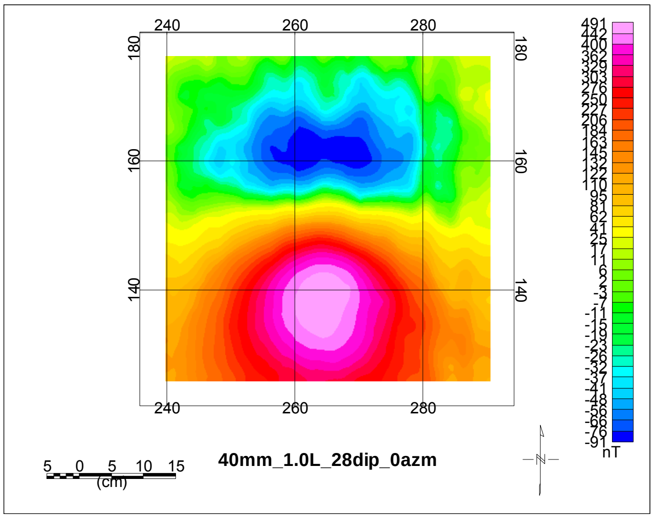
40mm_1.0L_28dip_0azm

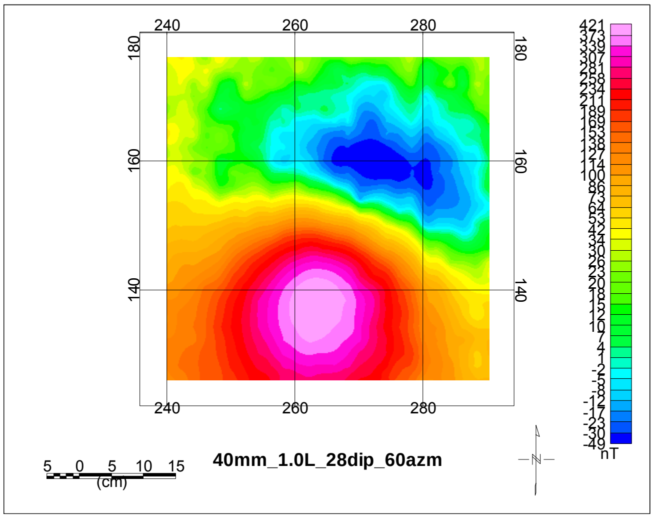
40mm_1.0L_28dip_60azm

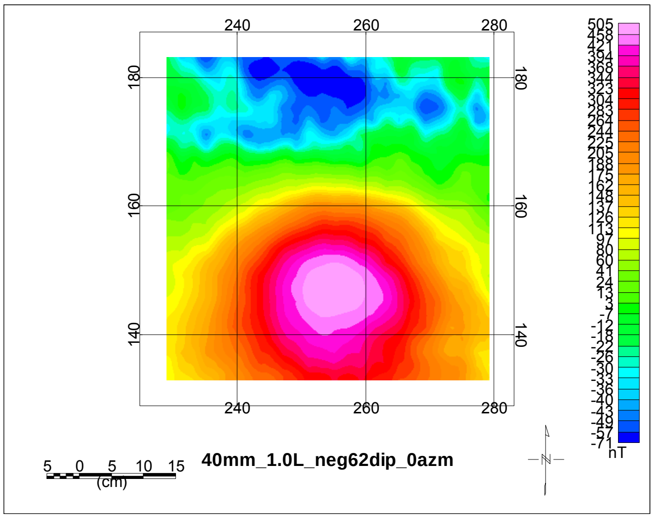
40mm_1.0L_neg62dip_0azm

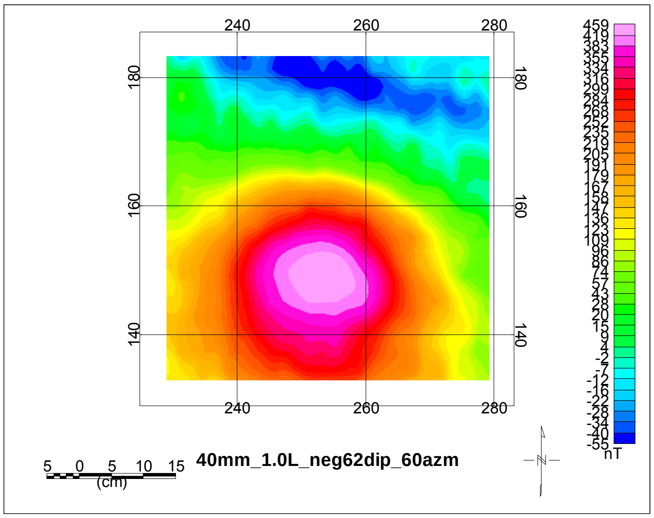
40mm_1.0L_neg62dip_60azm

81 mm, L=10 cm and 15 cm

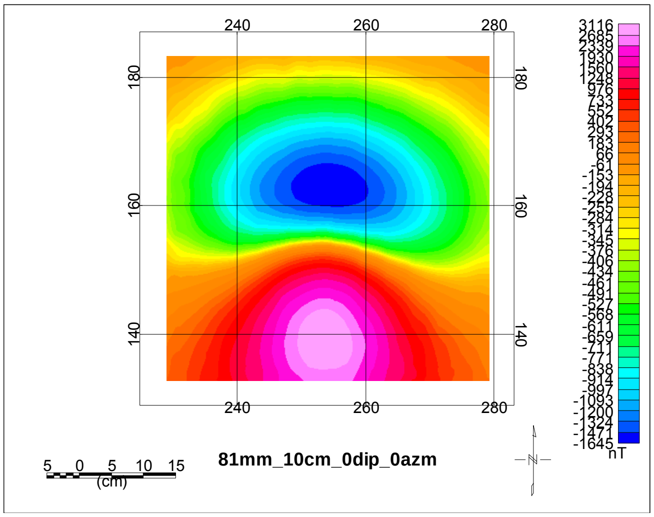
81mm_10cm_0dip_0azm

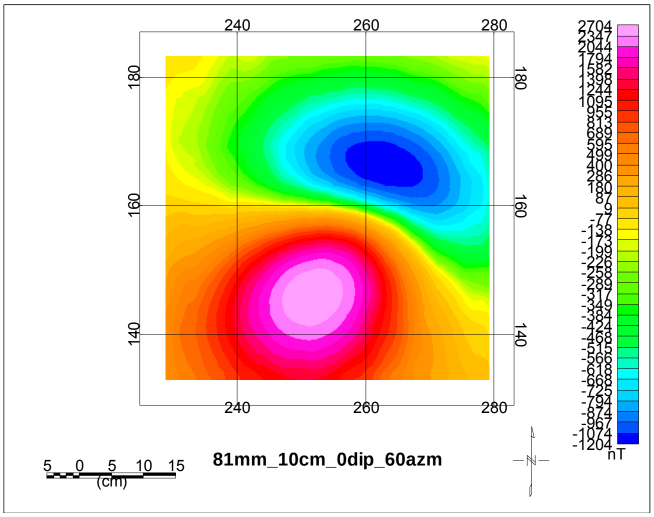
81mm_10cm_0dip_60azm

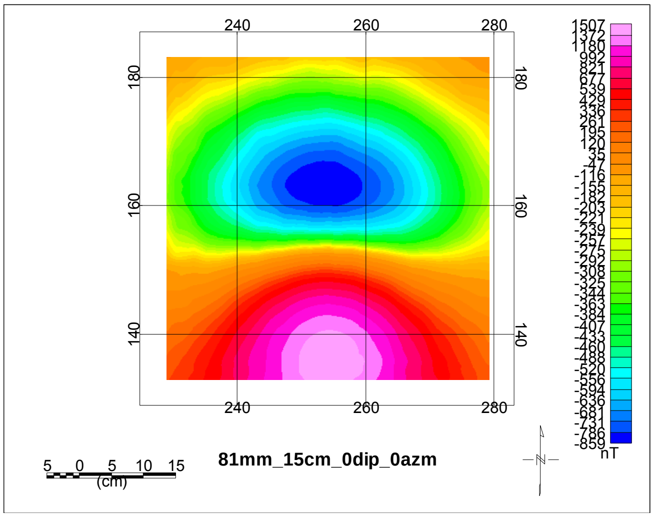
81mm_15cm_0dip_0azm

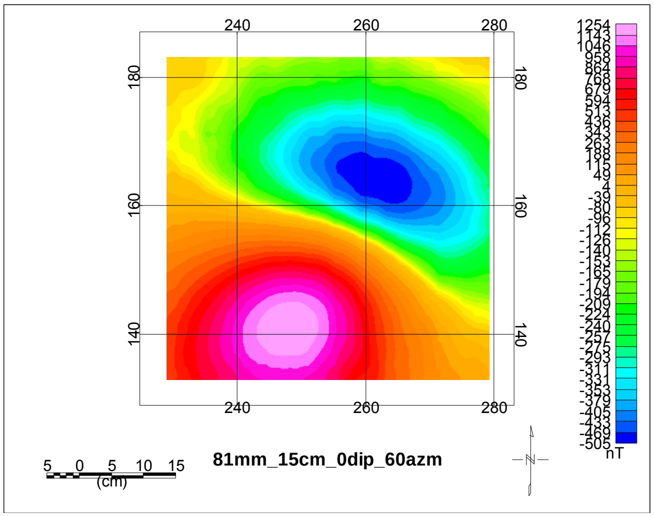
81mm_15cm_0dip_60azm

81 mm, L=21 cm

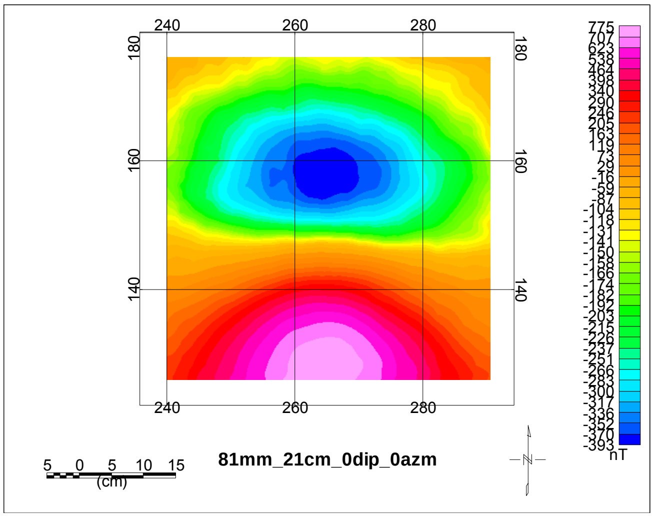

81mm_21cm_0dip_0azm

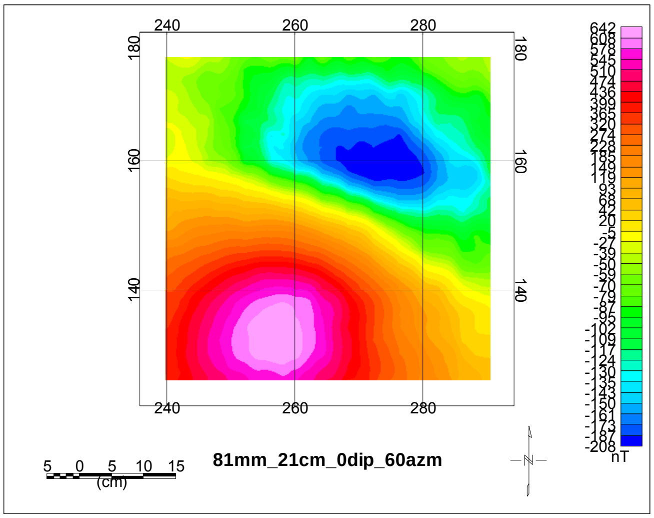

81mm_21cm_0dip_60azm

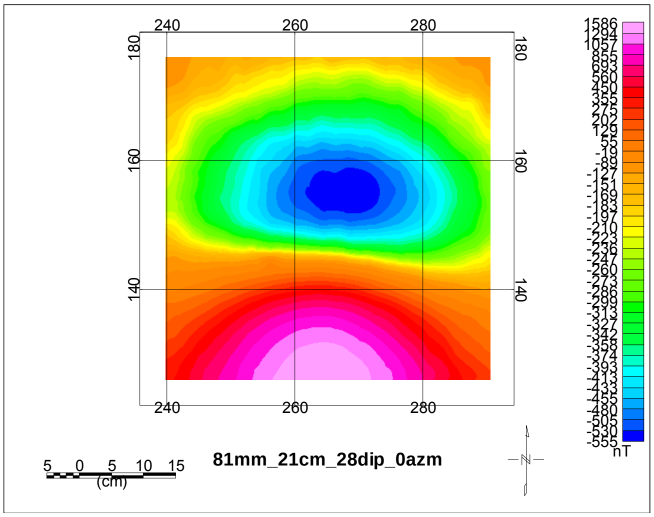

81mm_21cm_28dip_0azm

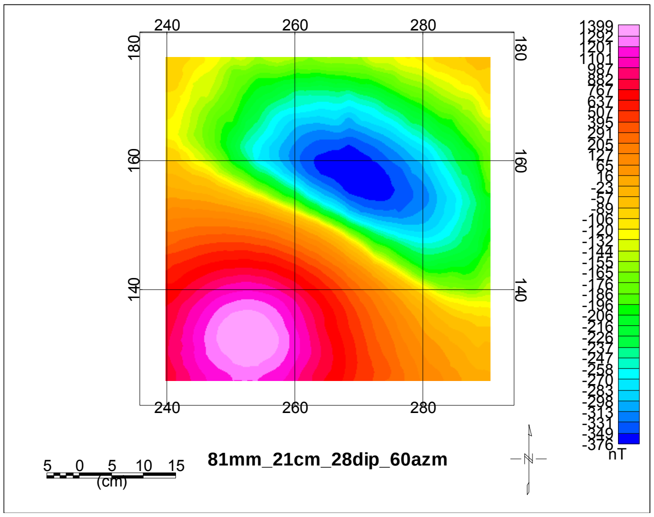

81mm_21cm_28dip_60azm

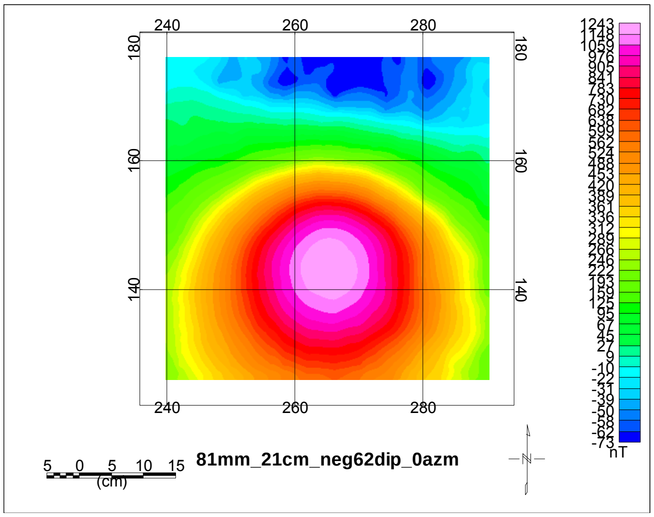

81mm_21cm_neg62dip_0azm

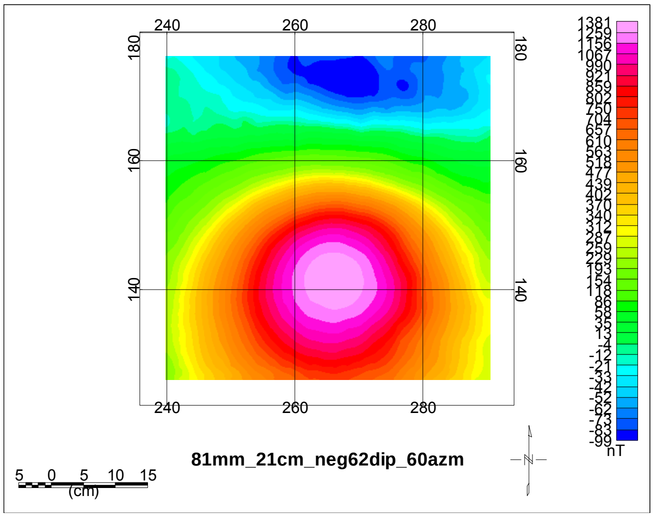

81mm_21cm_neg62dip_60azm

Appendix B - GMR Sensor Total Magnetic Field Plots for the Clutter

Clutter1, 0.5L

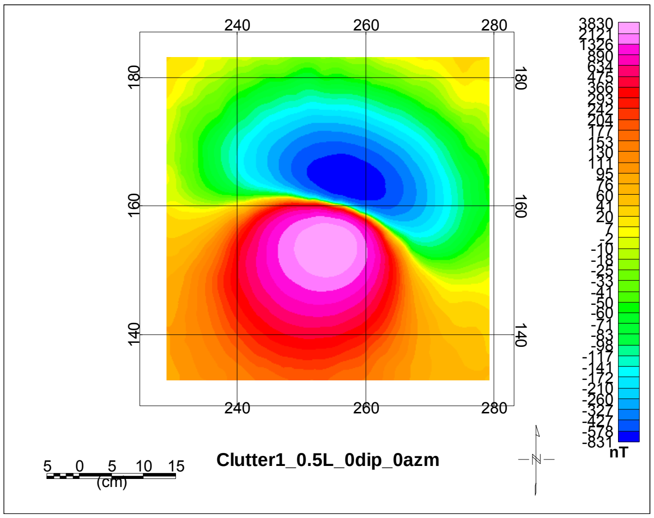

Clutter1_0.5L_0dip_0azm

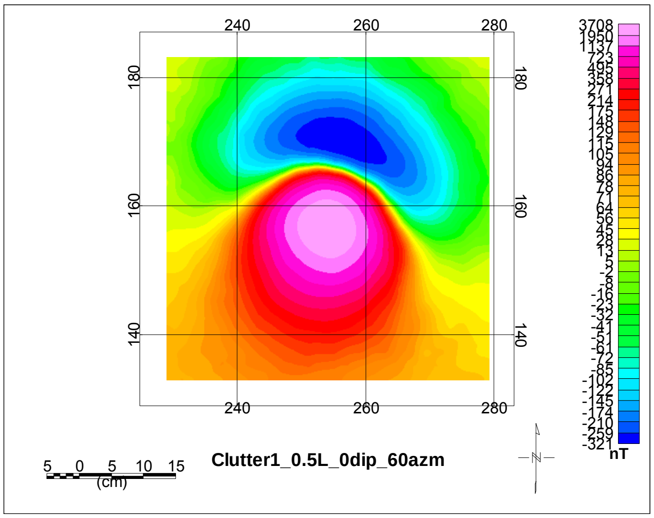

Clutter1_0.5L_0dip_60azm

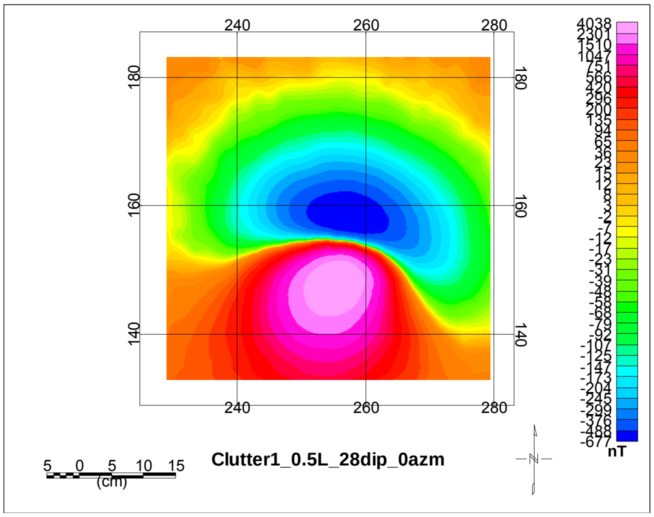

Clutter1_0.5L_28dip_0azm

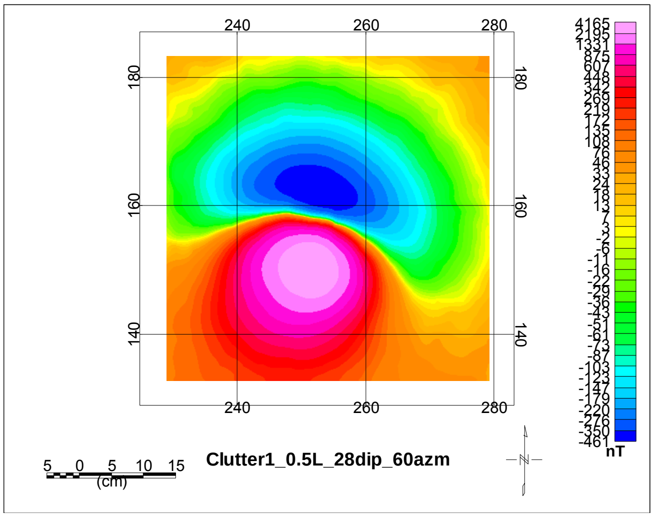

Clutter1_0.5L_28dip_60azm

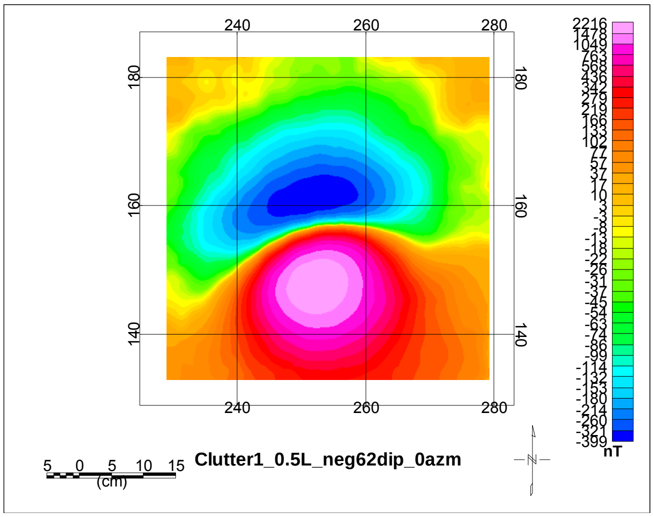

Clutter1_0.5L_neg62dip_0azm

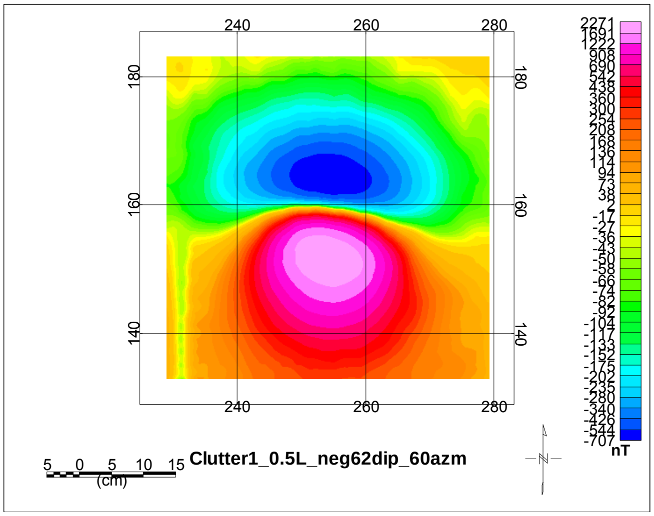

Clutter1_0.5L_neg62dip_60azm

Clutter1, 1.0L

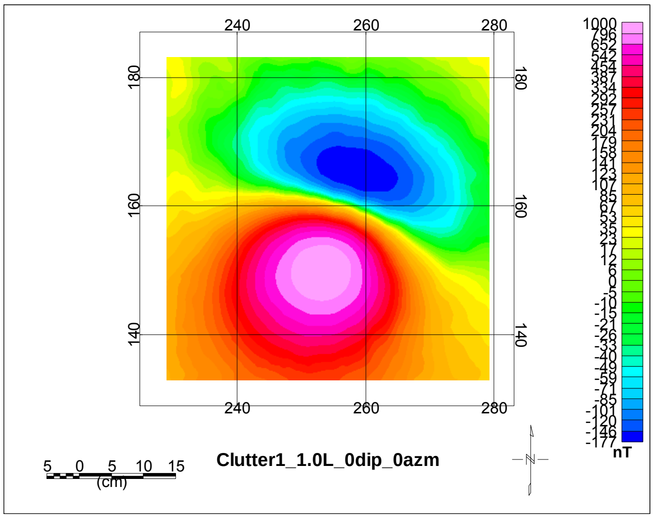

Clutter1_1.0L_0dip_0azm

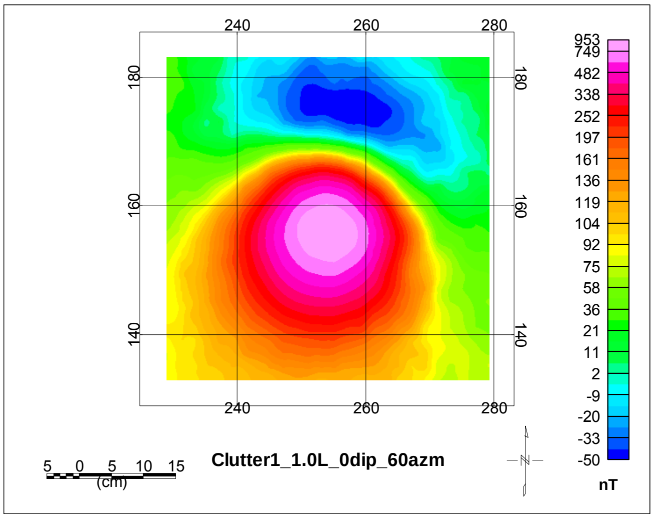

Clutter1_1.0L_0dip_60azm

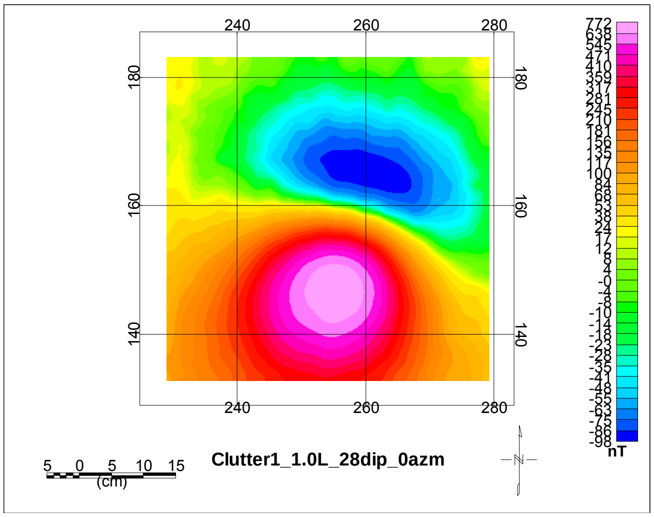

Clutter1_1.0L_28dip_0azm

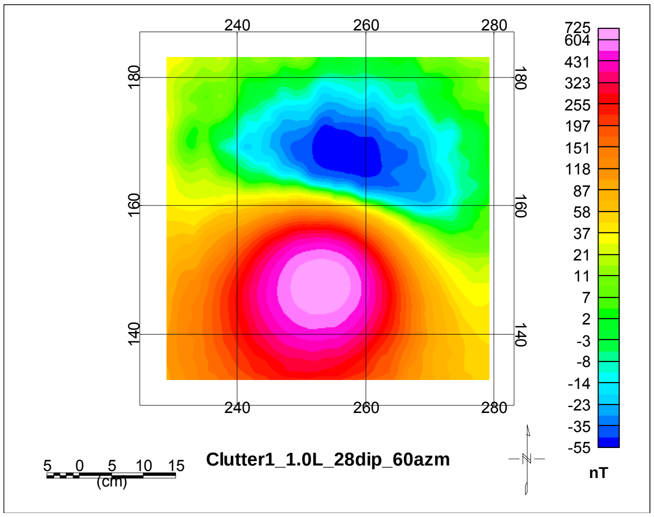

Clutter1_1.0L_28dip_60azm

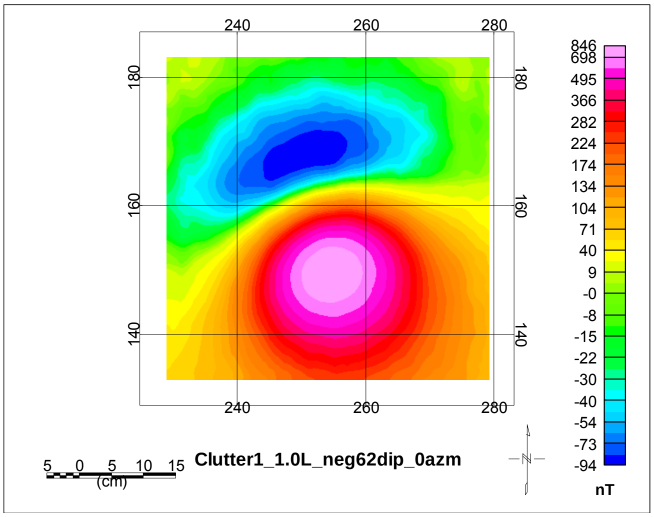

Clutter1_1.0L_neg62dip_0azm

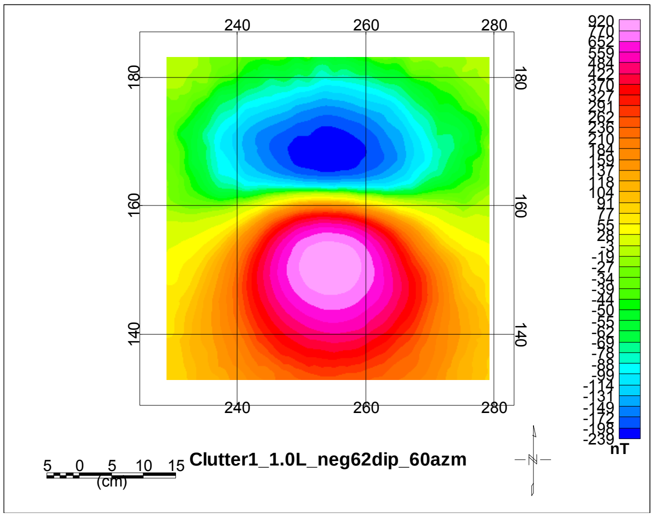

Clutter1_1.0L_neg62dip_60azm

Clutter2, 0.5L

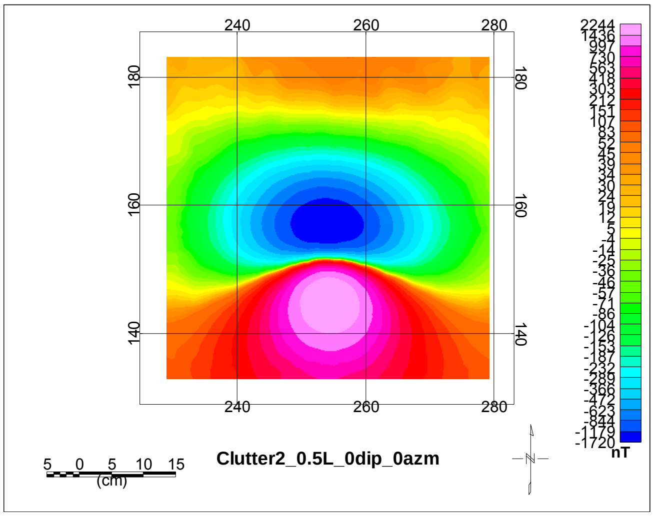

Clutter2_0.5L_0dip_0azm

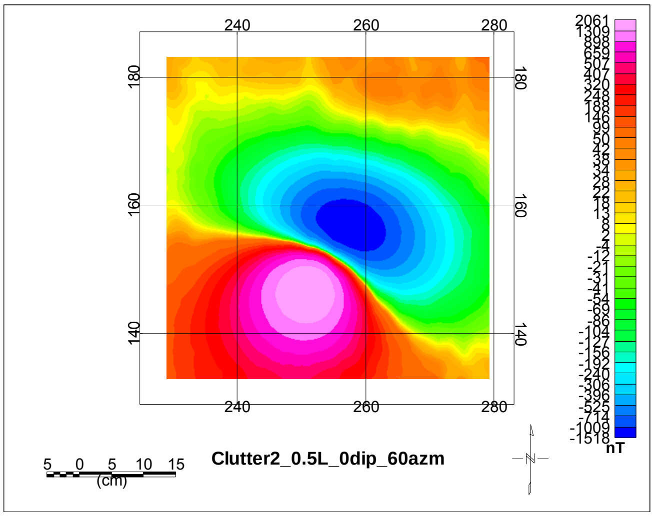

Clutter2_0.5L_0dip_60azm

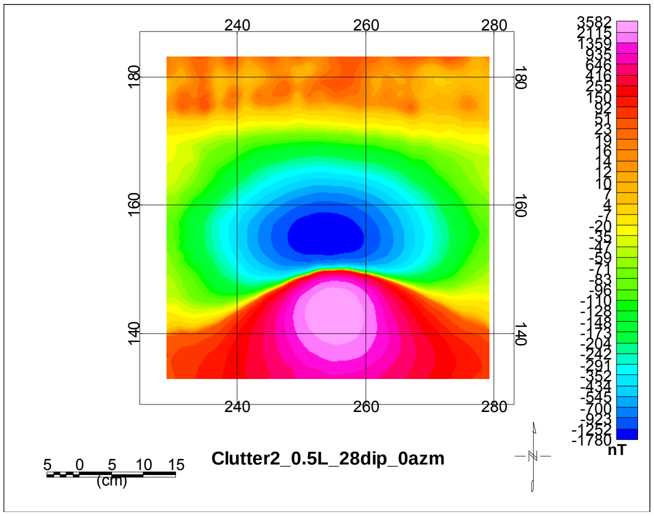

Clutter2_0.5L_28dip_0azm

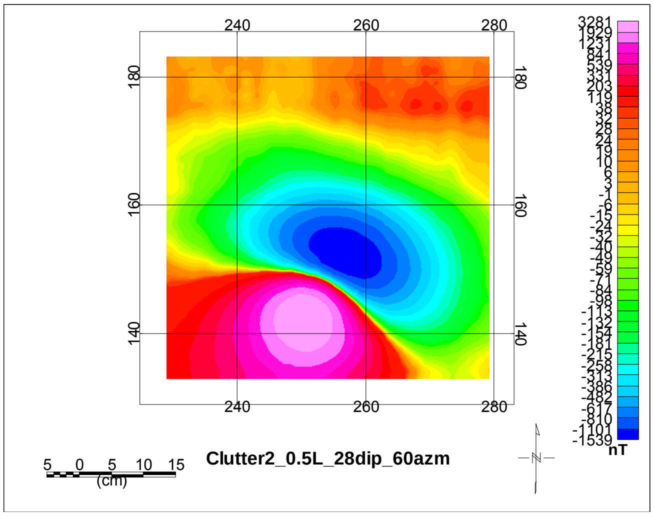

Clutter2_0.5L_28dip_60azm

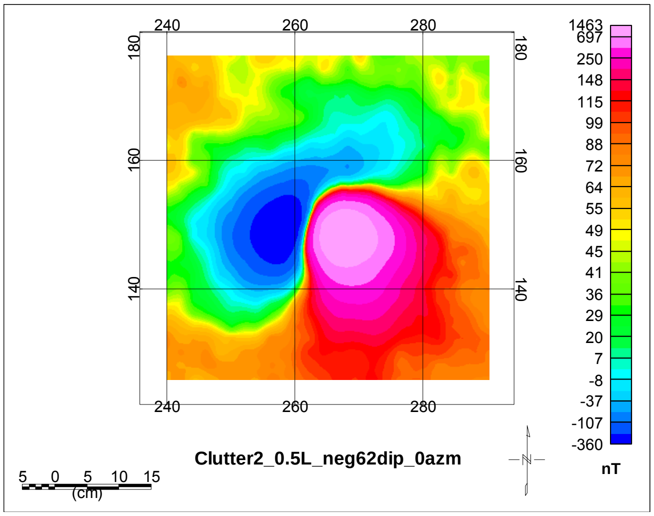

Clutter2_0.5L_neg62dip_0azm

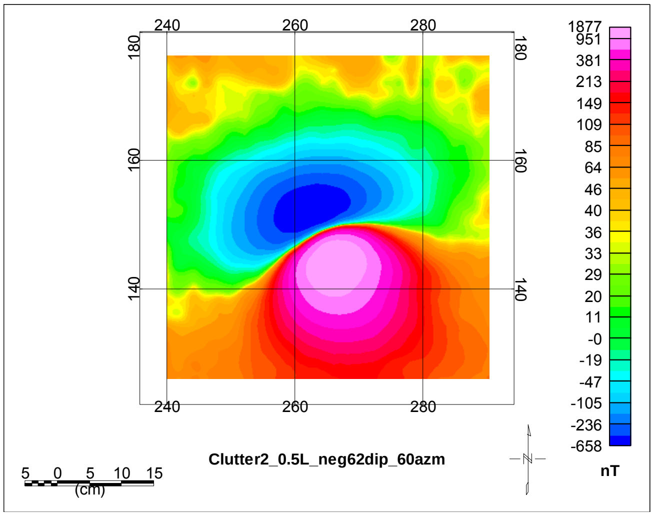

Clutter2_0.5L_neg62dip_60azm

Clutter2, 1.0L

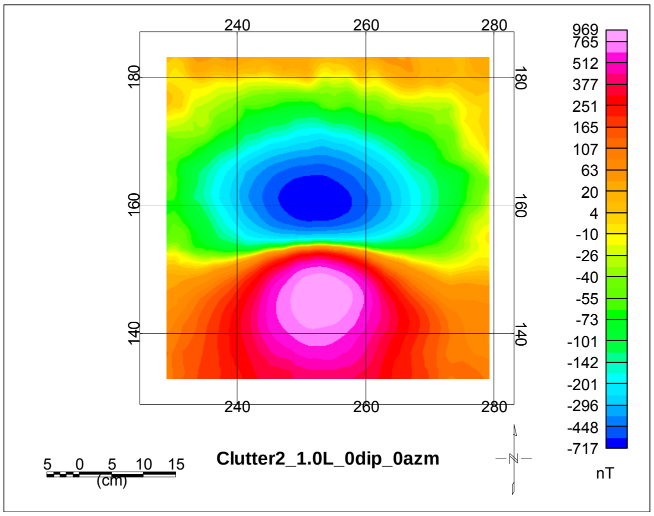

Clutter2_1.0L_0dip_0azm

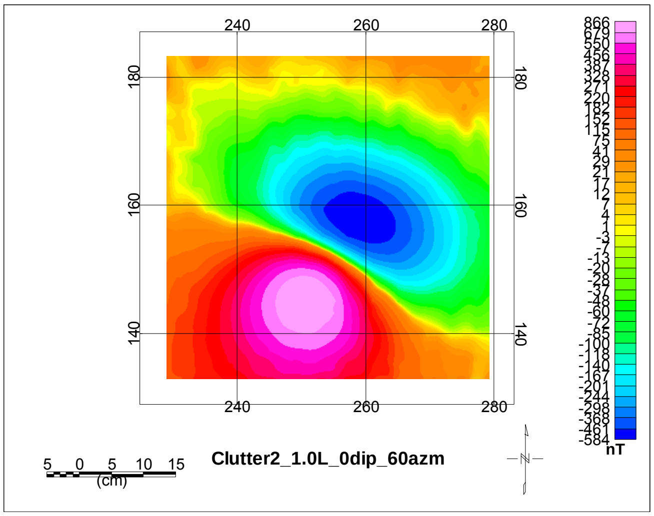

Clutter2_1.0L_0dip_60azm

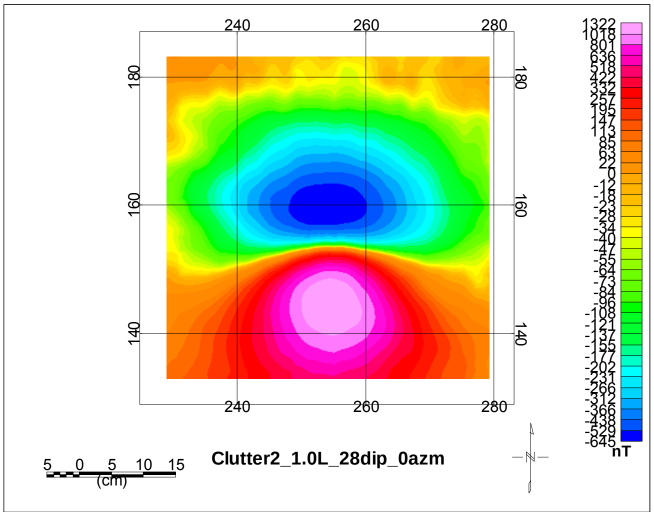

Clutter2_1.0L_28dip_0azm

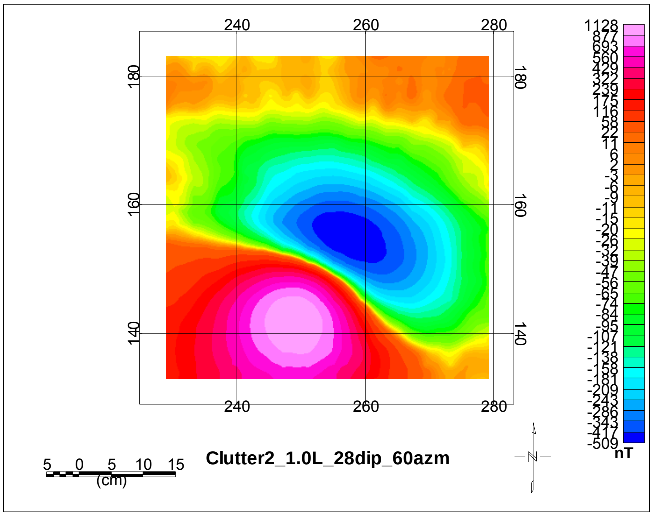

Clutter2_1.0L_28dip_60azm

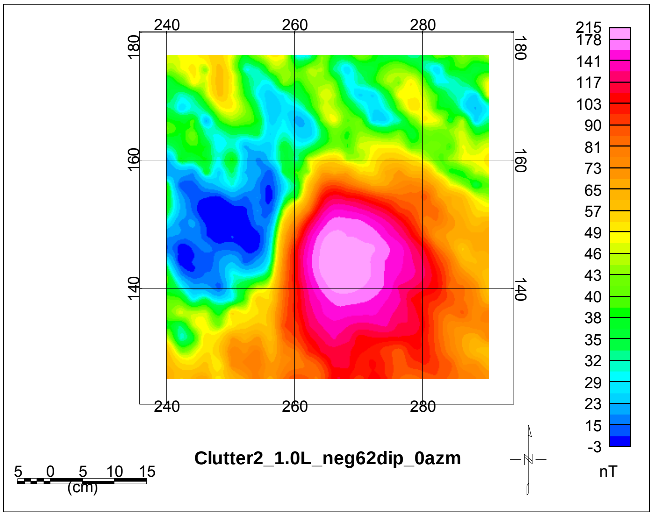

Clutter2_1.0L_neg62dip_0azm

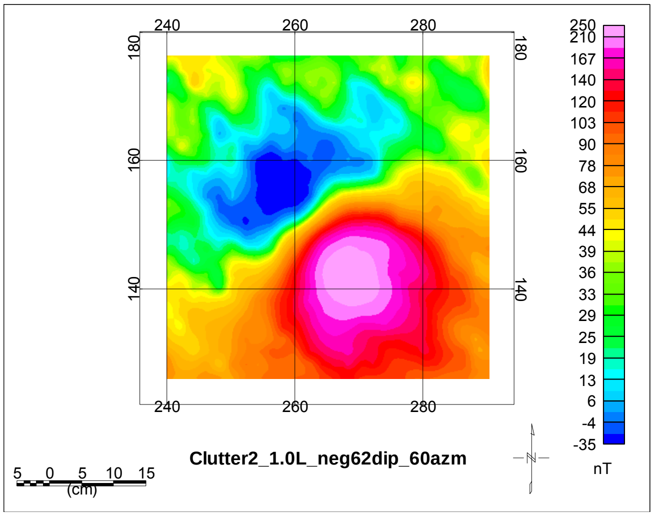

Clutter2_1.0L_neg62dip_60azm

Clutter3, 0.5L

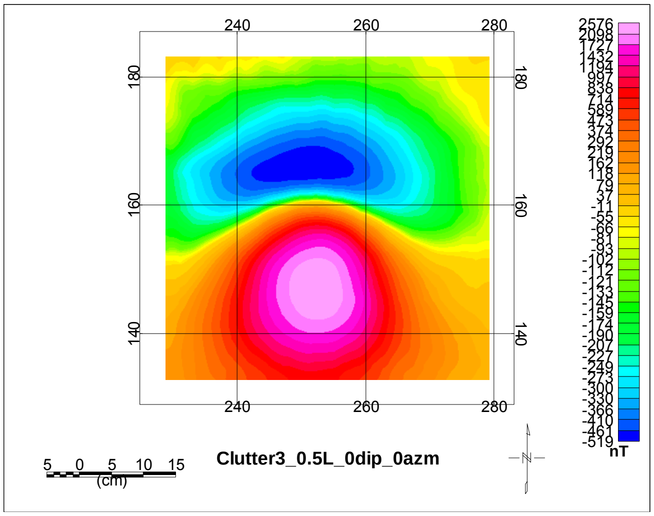

Clutter3_0.5L_0dip_0azm

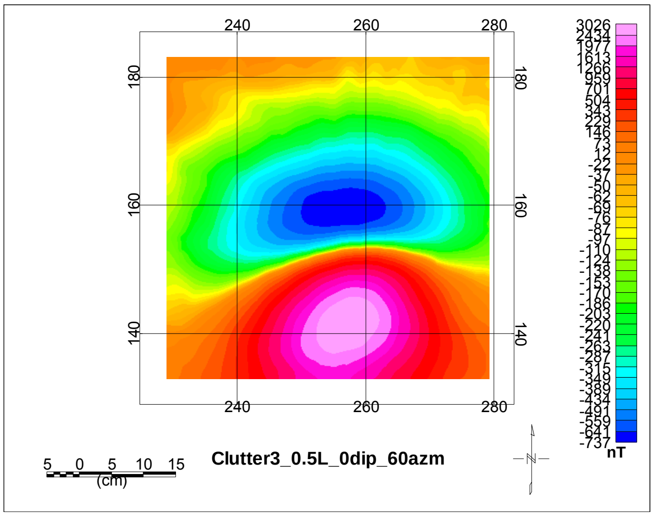

Clutter3_0.5L_0dip_60azm

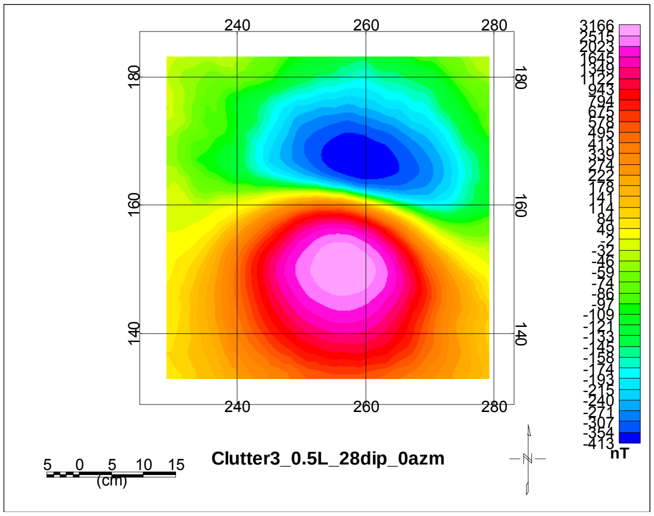

Clutter3_0.5L_28dip_0azm

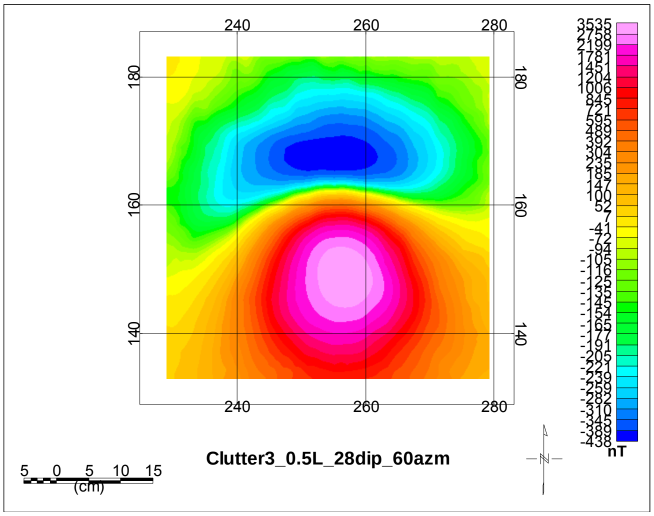

Clutter3_0.5L_28dip_60azm

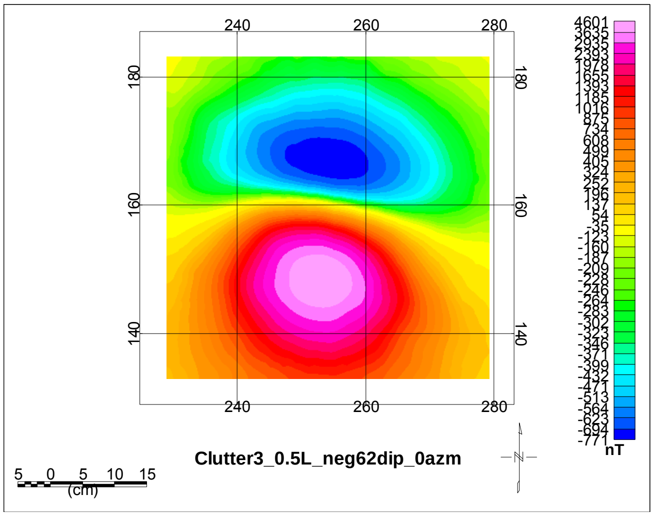

Clutter3_0.5L_neg62dip_0azm

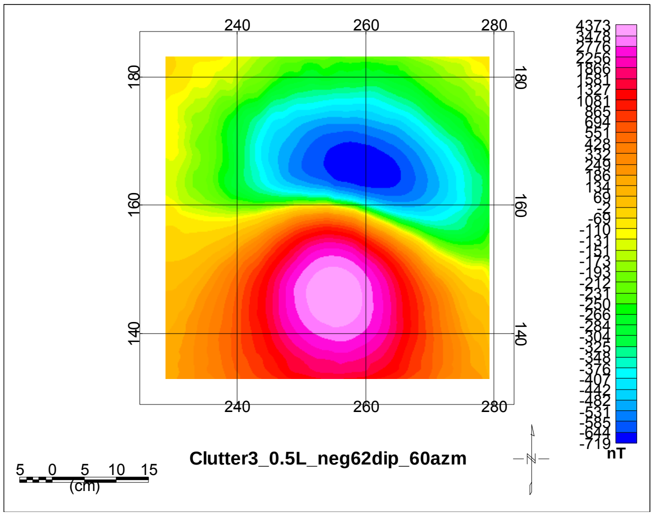

Clutter3_0.5L_neg62dip_60azm

Clutter3, 1.0L

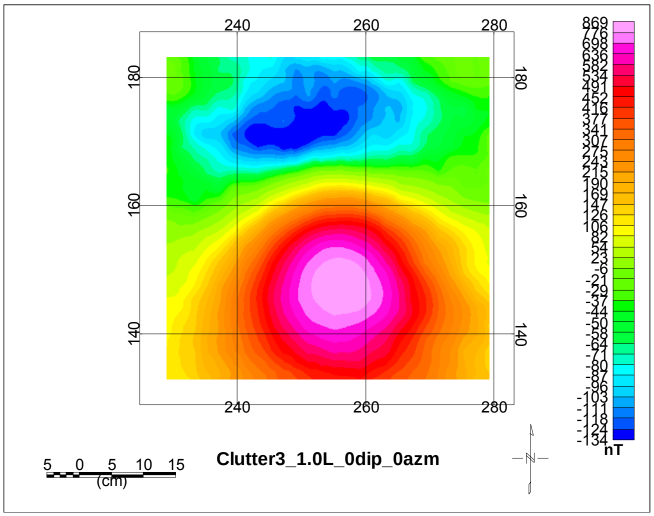

Clutter3_1.0L_0dip_0azm

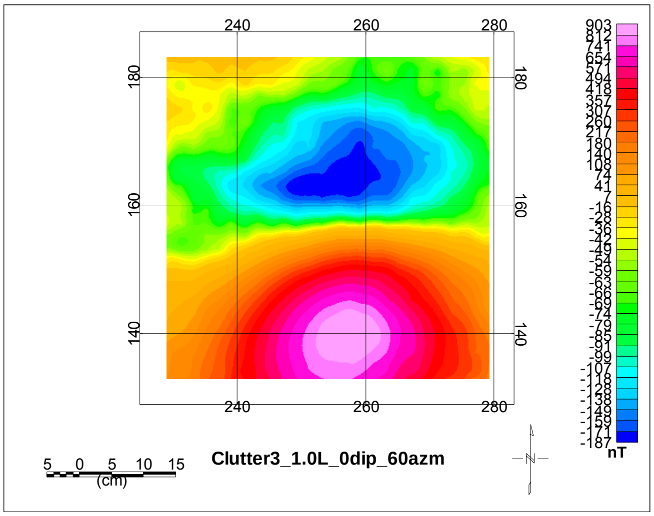

Clutter3_1.0L_0dip_60azm

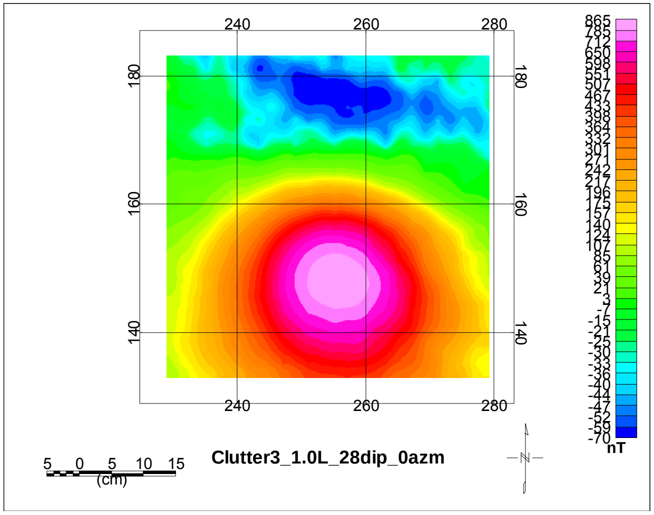

Clutter3_1.0L_28dip_0azm

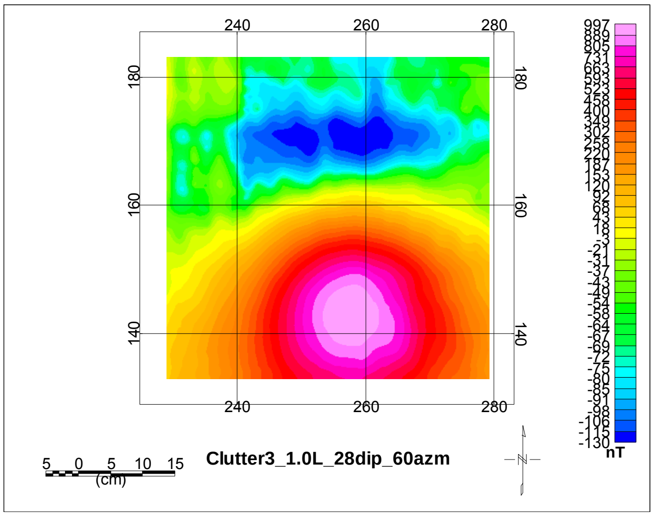

Clutter3_1.0L_28dip_60azm

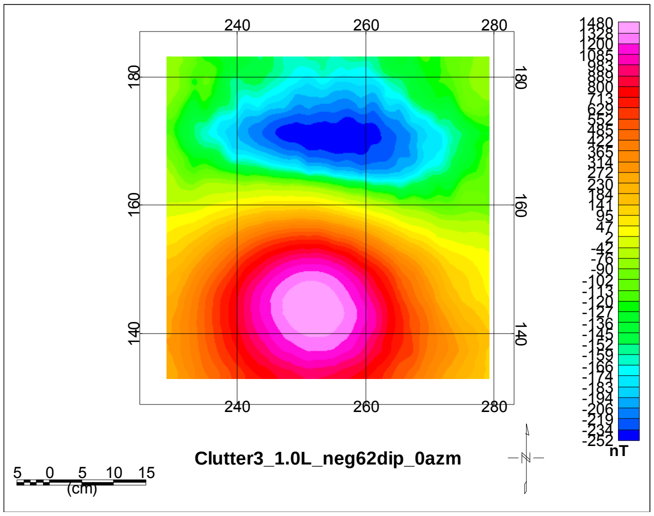

Clutter3_1.0L_neg62dip_0azm

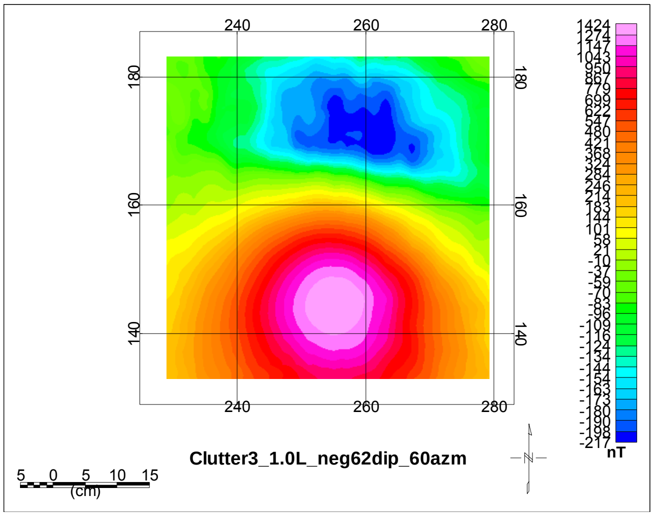

Clutter3_1.0L_neg62dip_60azm